Department of Precision and Microsystems Engineering

Simultaneous optimization of multi-part structure topologies and connection points

Ines Molina Ramírez

Report no : 2023.042
Coach : -
Professor : L. Noel and M.Langelaar
Specialisation : SOM
Type of report : Master Thesis
Date : 17 July 2023

Simultaneous optimization of multi-part structure topologies and connection points

MSc Thesis

Ines Molina Ramirez

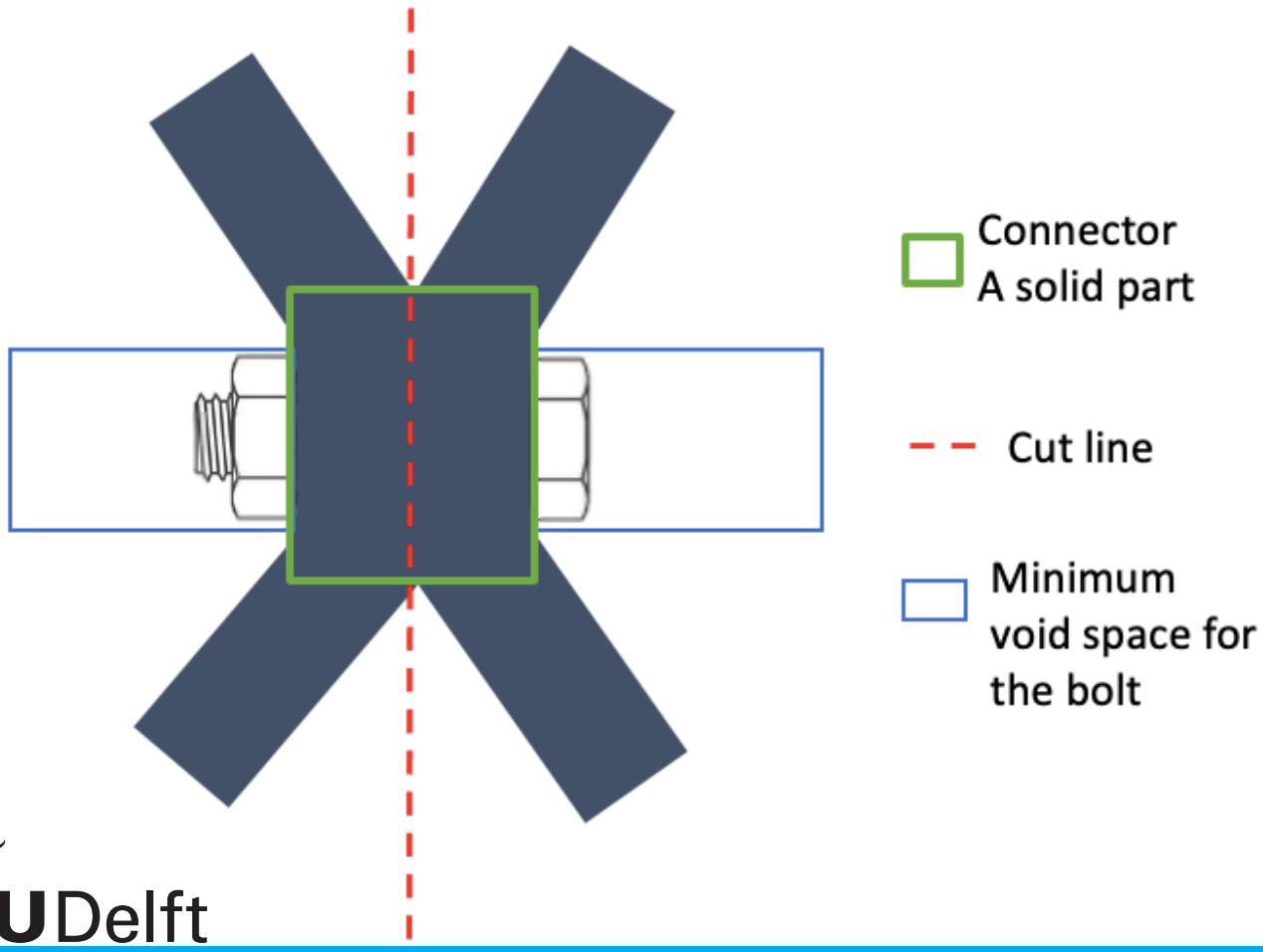

TU Delft

Simultaneous optimization of multi-part structure topologies and connection points

by

to obtain the degree of Master of Science
at the Delft University of Technology.

Student number: 5352681
Supervisors: L. Noel M. Langelaar

TU Delft

Preface

This master's thesis concludes my studies at TU Delft. In my master's thesis, I was able to include a topic I am passionate about, and I think it has great importance in the future. Hopefully, this report can inspire people to future work.

Firstly, I would like to thank my supervisors, Lise Noel and Matthijs Langelaar, for all the meetings and all the help they always gave. Thank you for all the guidance, feedback and ideas shared at the meetings.

To my parents who do not speack english; Muchas gracias de verdad por todo lo que me habeis dado y por apostar por mi fufuro. Thank you also to my family and brothers for always being there. I would also like to thank all my amazing friends who helped me through tough times and made my master the most enjoyable years of my life with all the adventures, even in COVID times. Thank you for all the laughs and coffee breaks at uni.

I am really excited about what the future holds!

Inés Molina Ramírez
Delft, July 2023

Abstract

Given the growing number of environmental and societal concerns we confront today, the idea of sustainability has gained importance. At the same time, new strategies for improving the performance of structures and systems have been developed due to developments in engineering and computational design. This research aims to generate a sustainable design using topology optimization by focusing on design for disassembly. One advantage of design for disassembly is that when a product can be disassembled, the parts can be reused, repaired, recycled, and remanufacture. This facilitates other aspects of product sustainability, such as the product's life cycle and end-of-life. A structure is divided into two parts and attached by a connection point, this connection point is called the connector. Due to sustainability, the connection method needs to be a non-destructive method, which in this case is the bolts. Next to the connector, two voids are required to insert, tighten and remove the bolts. Therefore, in this research, a structure is optimized using topology optimization and simultaneously optimizing the position of cut lines and connectors. The approach taken uses level set functions to model the cut of the structure, as well as the connectors and the voids. Then, they are converted into a density field using a smoothed Heaviside function. A Solid Isotropic Material with Penalization (SIMP) motivated method is used to join all the different density fields into an equation for the interpolated elasticity modulus. The optimization aims to minimize compliance with volume and no-overlap constraints. The non-overlap constraint is applied to the connectors. The structure and the position of the cut line and the connectors are optimized using the Method of Moving Asymptotes (MMA) method. A gradient based sensitivity analysis is used in the MMA. Afterwards, the influence of the cut line, the connector and the voids are observed individually. After optimizing the parts individually, the full optimization was performed, where the structure, the cut lines and the connectors with the voids were optimized. Furthermore, a parameter study was done to observe their influence on the final layout. The optimizer's behaviour was observed by looking at the optimization results and the parameter study. For example, how the optimizer tends to stack some connectors together to create a member of the structure or the influence of the voids.

With the approach presented, the main idea of optimizing a structure using topology optimization and simultaneously dividing it and optimizing the connector's position is obtained. However, the optimization has some limitations, as some assumptions and design considerations are not accurate, further research is needed to get accurate results.

Contents

List of Figures

List of Tables

1

Introduction

The importance of sustainability has grown over the past years. The concept of sustainability had its origins as a policy concept. It was first introduced in the Brundtland Report 1987 (Imperatives, 1987). In this report, the United Nations Brundtland Commission defines sustainability as:

"Sustainable development is a development that meets the needs of the present without compromising the ability of future generations to meet their own needs" (Imperatives, 1987).

However, over the years, the definition has evolved. Regarding sustainability and design, there is a concept called Design for X (DFX), sometimes called Design for Excellence. This concept has been developed to help with the design in the product development phase. Some benefits are reduced product cost, shorter launch time, reduced product risk, improved product quality, enhanced testability, improved production, customer satisfaction, and improved operational efficiency (Usmani, 2021). This concept aims for the designers and engineers to improve a product during the design phase by focusing on one aspect. For example, if a designer is trying to design a product, the designer could use one of these techniques to focus on and improve the product in the chosen direction.

Figure 1.1: Design for sustainability (Mayyas et al., 2012)

DFX has a wide range of techniques. One of these techniques is design for sustainability (DFS). Fig.1.1 shows an overview of all the design aspects DFS can be involved in.

It is estimated that over 80% of all product-related environmental impacts are determined during the design phase of a product (Querol, 2021).

Topology optimization is a computational design method that creates optimized structures based on mathematical optimization algorithms. The algorithm optimizes the material layout by maximizing the performance and efficiency of the design. It was first introduced in a seminal paper by Bendsøe and Kikuchi, 1988, and is currently widely used in industry.

Topology optimization is used to create high-performance structures that meet specific design requirements. It distributes material in a design domain by minimizing an objective function and fulfilling a set of constraints. To use topology optimization, certain initial conditions are required and defined by the user, including a defined initial domain, a set of loads, conditions, and constraints. Some people might think that topology optimization is already sustainable due to the reduction of material usage. This is different from the approach that will be taken here, which is to generate a sustainable design by not only reducing the material used.

Design for disassembly was chosen as the focused DFS technique in the previous literature study. Brennan et al., 1994 defined disassembly as the systematic removal of desirable parts from an assembly while ensuring that parts are not impaired due to the process. Nowadays, designers aim to be able to disassemble a product to recycle, remanufacture, or repair the broken product. Disassembly can be categorized into destructive and non-destructive disassembly (Battaia et al., 2018 Chang et al., 2017). Destructive disassembly focuses on the material and non-destructive focuses on the recovery of the parts. Regarding sustainability, a non-destructive disassembly is preferred. A product will need to be divided into parts and assembled to be later able to disassemble it. A division line, also called a cut line, is needed to separate the product into different parts. The different sections will be connected using a non-destructive method. The connector is where the structure is assembled together. Looking at further research on design for the division of a topology optimized structure, the connection method between the separate parts used is primarily welding, which is a destructive method for disassembly. Therefore, the research question is:

How can a structure be divided into different parts by optimizing the position of the cut lines and the connection points simultaneously while optimizing the structure using topology optimization?

The remainder of this report is organized as follows. Chapter 2 introduces design for disassembly and an idea of the initial approach to solve this research question. Chapter 3 introduces the methods used for modelling connectors, cut lines, and voids and Chapter 4 shows the optimization problem and the sensitivity analysis. The results are shown in Chapter 5 and the discussion in Chapter 6. Finally, the conclusion and future work is found in Chapter 7.

2

State of the art

Design for disassembly is mentioned in the introduction as the sustainable approach to use with topology optimization. This section introduces the topic of design for disassembly and the connection methods. At the end of this section, the idea on how to answer the research question is proposed.

2.1. Design for disassembly

How can design for disassembly and topology optimization be used to make a design sustainable? A possible solution is to have a structure that needs to be divided to disassemble by optimizing the division line and the connection points simultaneously while optimizing the structure using topology optimization.

One advantage of design for disassembly is that when a product can be disassembled, the parts can be reused, repaired, recycled, and remanufacture. This facilitates other aspects of product sustainability, such as the product's life cycle and end-of-life.

Designing for disassembly additionally includes designing for assembly. However, the main difference is their focus. Design for assembly only focuses on the assembly of the part, not the steps after, and design for disassembly focuses on how easily the pieces can be taken apart after the assembly. There are two types of disassembly: destructive and non-destructive disassembly (Battaia et al., 2018). Although to be able to disassemble the product quickly and be able to reuse or repair the parts, the disassembly must be non-destructive. This makes the design focus on the part rather than the material.

Literature research was done on how this topic and topology optimization are related in previous studies. It was found that most studies which include a focus on both topics focused on the connection mechanism, for example, a compliant mechanism as in Li et al., 2004, a snap-fit pressure-based fasteners as in Shalaby and Saitou, 2008 and Willems et al., 2007 or the concept of one-to-many fasteners as in Willems et al., 2006. However, there was little research on dividing and connecting the structure while optimizing it using topology optimization.

When looking for the objective of having a structure, dividing and connecting it while optimizing it using topology optimization, some research was found in terms of topology optimization and design for assembly. Most studies as Pollini and Amir, 2020, Yi and Saitou, 2021, and Saeed et al., 2021 have welding as the connection method. Welding leads to a destructive disassembly procedure, which is not desired. However, the idea of dividing the structure used in this report is based on the methodology proposed by Pollini and Amir, 2020. The part is divided with a 1-D profile, a piece-wise linear geometric entity composed of a chain of piece-wise linear segments. One of the coordinates nodes is fixed in the segments, and the other is a variable. However, as mentioned, the connection method needs to be changed. The following section introduces connection methods.

2.2. Connection methods

How the connections will be modelled is an essential aspect of the project. In this section, there is one clear goal: non-destructive connections. Non-destructive connections typically have a specific size and lower strength than the complete structure or the destructive connection methods such as welding.

In the previous literature research, different studies on how the position of the connectors is optimized are done (Chickermane and Gea, 1996, Chickermance et al., 1999 and Oinonen et al., 2010). These studies have different criteria for their optimization and have the bolt inserted perpendicular to the structure. However, the main idea is to connect it parallel to the structure.

Non-destructive connection methods are the types of connections that are easy to remove and do not damage the structure, they are also called temporary connectors. Some examples are snaps-fits, retaining rings (circlip), quick-release devices (clip/lock/latch/clamp), pins, tapered keys, magnetic devices, threaded fasteners and adhesives. For retaining rings, it needs to be a circular connection point. The quick-release devices are similar to threaded fasteners. For pins, the connection shape should be adapted to be able to put a tapered key. The magnetic devices and the adhesive have a similar connection to welding. For easy disassembly, threaded fasteners such as bolts and screws and snap-fits are looked into.

There are three types of snap-fits, annular, cantilever and torsional. They must have the same orientation to be able to disassemble it. If the snap-fit breaks, it is hard to repair. Moreover, it is a fast method to assemble and disassemble pieces. However, the threaded fasteners are chosen as the non-permanent connection method. However, they need some space to be able to insert them.

2.3. Proposed idea

As mentioned, the main idea is to optimize a structure and simultaneously optimize the cut lines and the connection points. In term of the connection point, the idea is that it will be divided in half, where each half is part of the divided structure and it is the point where the bolt will be inserted to join the structure together.

One requirement to join two surfaces with a bolt is to be bolted perpendicular to the connection surface. Another critical requirement is space for the bolt to be inserted, fastened and removed.

To ensure these requirements are met, the connection point consists of a void-solid-void fixture, which position will be optimized. Fig. 2.1 visualises the main idea. The dark grey area is the structure which is optimized. The red dashed line is the cut line, which divides the structure and the connector. The connector is the part which is inside the green borders. In the optimizations, the connector will not be divided, it is optimized a solid piece. As mentioned, the bolts need to have a minimum space around them to insert and remove them. Therefore, the blue boxes represent two voids, which are the minimum required spaces. This is the initial idea on how to approach the aim of this paper.

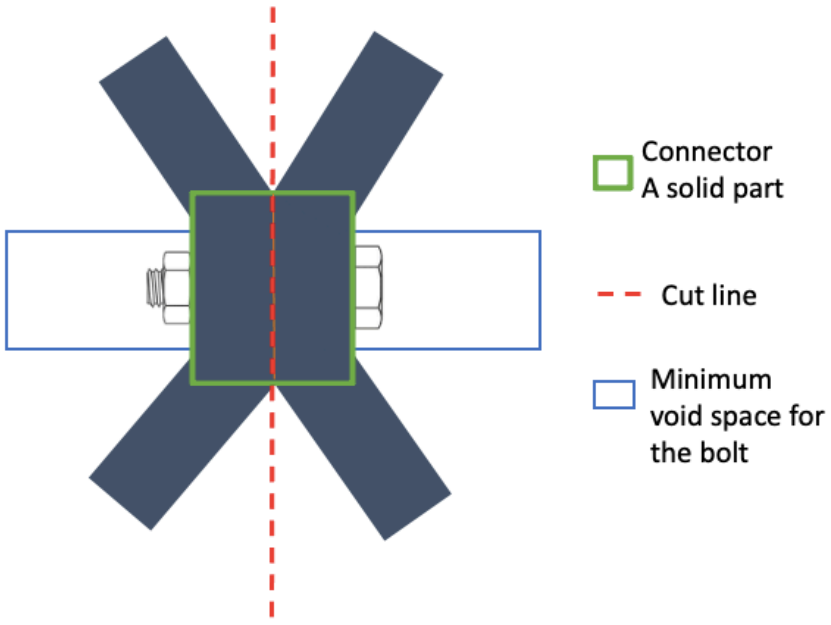

Figure 2.1: Main idea of the cut and the connector and how it will be bolted.

3

Methodology

In this chapter, the methodology used to complete the aim of dividing a structure into different parts and joining them together by a connection point similar to the one shown in Fig. 2.1 is presented. The methodology chapter includes the introduction and modelling of the connectors, cut lines and voids, and the next chapter includes the optimization problem with the sensitivity analysis.

The different topology methods used and other information needed are introduced. Followed by the modelling of the connector, voids and cut lines and how they are added to the interpolated elastic modulus.

3.1. Topology optimization approaches

There are different methods for topology optimization. One method is the Solid Isotropic Microstructure with Penalization (SIMP) (Bendsøe, 1989, Zhou and Rozvany, 1991, Mlejnek, 1992). The initial idea of this method was to reduce the complexity of the homogenisation approach and improve convergence. Bendsøe and Sigmund, 1999 stated the power law gave a relation between the density design variable and the material property. The material distribution is seen by the SIMP approach as a continuous density field with a range of 0 (void or empty space) to 1 (completely solid material). The proportion of material existing at each location within the design domain is represented by the density field. Greater density values denote areas with more material concentrated in them, whilst lower density values denote areas with less material concentrated in them.

Another method is the level-set, which is the most used alternative to the density-based approach. Introduced and developed by Osher and Sethian, 1988. The boundaries are represented as zero-level curves of a scalar function (Deaton and Grandhi, 2014). The level-set approach was first applied to topology optimisation by Sethian and Wiegmann, 2000.

3.2. Introduction to the modelling part

Fig.2.1 shows that the connection consists of two voids and a solid connection over the cut line. There are different ways to approach modelling a solid movable component and movable voids. In topology optimization, there are two approaches called the Moving Morphable Component (MMC) and the Moving Morphable Void (MMV) (Guo et al., 2014), which are part of the feature mapping method (Wein et al., 2020) . This provides a different solution framework which can be achieved explicitly and geometrically. In MMC, a set of components are adopted as the building blocks of topology optimization, and for MMV, a set of voids is used to optimize the structural topology. However, these methods are not used as the modelling approach in this research.

Zhu et al., 2016 reviews different ways to optimize multi-component structure systems, integrated component layout, and structural topology optimization. In the paper Wang et al., 2020, the optimization of the layout of continuum structures embedded with movable parts and holes using a SIMP-based optimization to maximize the overall stiffness. This paper uses a level-set method to model the embedded voids and the embedded components, and it is then converted into a density field. The modelling used for the connector, cut lines and voids is based on this paper.

Fig. 3.1 shows the schematic to understand the problem better. The grey area is the design domain as well as the structure, which will be optimized using the density variable, the red lines are the cut lines which will be used to divide the structure. For the cut line, the red points are the coordinates which will be optimized. The green area is the connectors, they will be on the top of the cut line as they will connect the structure, this represents the connection point for the bolt as in Fig. 2.1. Their position is optimized by optimizing the green dots, the mid-point of the connector. On both sides of the connector is a void, represented as the blue area. They represent the area needed to insert, tighten and remove the bolt, therefore, they need to be on the side of the connector. Due to their dependency, the position of the voids is not optimized, they depend on the position of the connector.

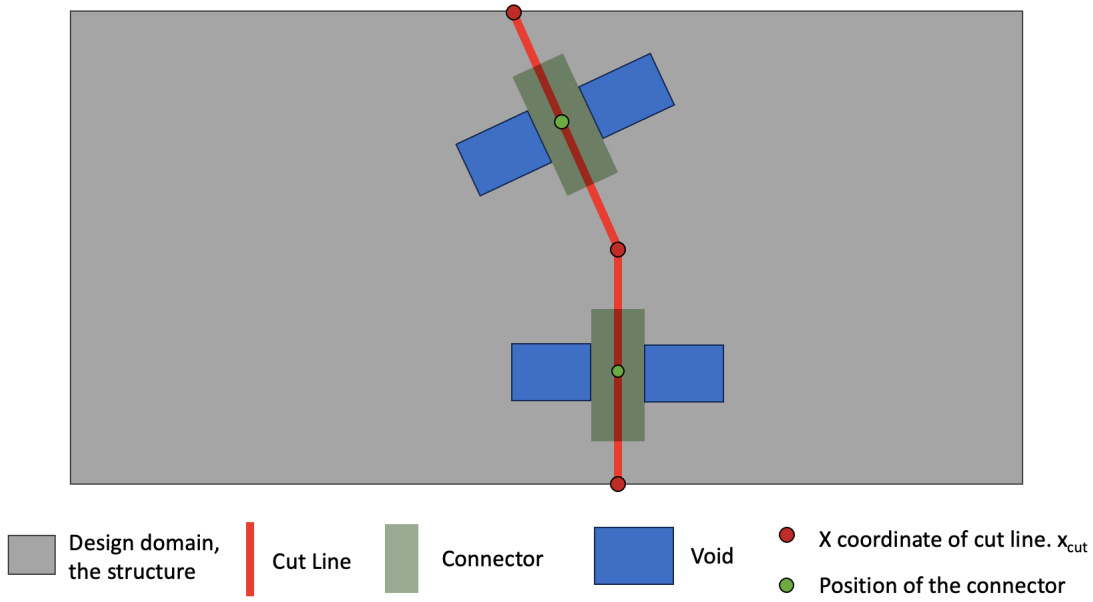

Figure 3.1: Schematic graph to understand idea showing the starting point of the optimization and which ones are the variables to optimize on the cut line and the connectors. The voids are dependent on the connector and their position is not optimized.

3.3. Density as a design variable

The SIMP method is used for topology optimization. It is a density-based approach. Each element has a density ρ_i for i = 1 to the number of elements (Nelx x Nely), where Nelx is the number of elements in the x direction and Nely is the number of elements on the y direction. ρ_i has 0-1 values. When $\rho_i = 0$, there is a void and no material, and when $\rho_i = 1$, there is a solid material for the i^{th} element.

As the design variables must be continuous, the density values can be $0 \leq \rho_i \leq 1$. There are more design variables in the optimization, this will be introduced in the modelling section.

The density-based method often suffers from well-known numerical instabilities due to finite element discretization. This is also known as the checkerboard pattern (Diaz and Sigmund, 1995). To avoid it, filters are used. The most common filters are the density filter (Bruns and Tortorelli, 2001) and the sensitivity filter (Sigmund and Petersson, 1998). The primary function of the sensitivity filter is to filter the sensitivities after they are calculated before using them in the optimization method. The aim is to smooth the sensitivities values to improve the optimization performance, as it uses the filtered sensitivities instead of the real ones. The density filter averages the element densities over the number of elements in a circular region with the r_{min}. Both filters use r_{min}, which is the filter size/radius.

In this part, a density filter is applied. Therefore, $\rho \rightarrow \widetilde{\rho_e}$. The density filter is applied by using the equation:

$$\widetilde{\rho_e} = \frac{1}{\sum_{i=1}^{N_e} H_{ei}} \sum_{i=1}^{N_e} H_{ei}\rho_i, \tag{3.1}$$

where, $\widetilde{\rho_e}$ are the filtered densities, and ρ_e are the non filtered, the design variable. N_e is the number of elements, $\widetilde{\rho_e}$ are referred to as physical densities due to the filter causing the initial density to lose its physical meaning (Andreassen et al., 2011) H_{ei} is weight factor defined as:

$$H_{ei} = max(0, r_{min} - \Delta(e,i)), \tag{3.2}$$

where r_{min} is the filter radius and $\Delta(e,i)$ is the centre-to-centre distance.

The filtering affects the sensitivity analysis of the objective function and the volume constraint concerning the density. They are calculated with the filtered $\widetilde{\rho_e}$. The sensitivities with respect to the design variable ρ_e are calculated in the following chain rule:

$$\frac{\delta\psi}{\delta\rho} = \sum_{e\in N_j} \frac{\delta\psi}{\delta\widetilde{\rho}}\frac{\delta\widetilde{\rho}}{\delta\rho} = \sum_{e\in N_j} \frac{1}{\sum_{i\in N_e} H_{ei}} H_{je}\frac{\delta\psi}{\delta\widetilde{\rho}} \tag{3.3}$$

where ψ represents the objective function (J) or the volume constraint (g_v).

3.4. Modelling introduction

As mentioned, the aim is to divide a structure into different parts and join them by a connection point similar to the one shown in 2.1 and simultaneously optimize the structure using topology optimization. From now on, this section focuses on the modelling aspect of the division of the structure with cut lines, the connection point, referred to as the connector and the two voids needed on each side of the connector as a bolt requirement. The approach taken here is based on the paper Wang et al., 2020, where level set functions are used to model the components and holes and mapped into density fields to optimize it using SIMP method.

Firstly, the modelling of the connector and the voids are shown, followed by the modelling of the cut lines and lastly, how all the previous ones, the connectors, the voids and the cut lines, are added together.

3.5. Modelling of the connection

In this section, the connectors are modelled first, followed the addition of the voids. The new design variable introduced for the connector is $c_k = \{x_{con_k}, y_{con_k}, \theta_{con_k}\}$, which determines its positioning for the k^{th} connector. The term θ_{con_k} is also called θ_{c_k}. For the addition of the voids, their coordinates are not optimized as they need to be next to the connector, thus the position is determined with the coordinates of the connector, and their sizes are determined by the minor and major lengths a_{con} and b_{con} for the connector and a_{void} and b_{void} for the voids. The coordinates of the connector are $z_k = \{x_{void_t}, y_{void_t}, \theta_{voids_t}\}$, and as the voids must have the same orientation as the connector, then $\theta_{con_k} = \theta_{voids_t}$ is also called θ_{c_k}.

3.5.1. Modelling of the connector

As mentioned, the initial idea of how the connectors are added into the design field is based on Wang et al., 2020. Furthermore, changes and additions to the methodology presented in this paper are made. For example, using a density filter, a new equation for the material interpolation scheme, a new equation for the volume constraint, and a different optimization problem. Some of these changes are due to the change to a density filter, the structure and the connector were not joining, this is explained in more details on Appendix. A.1.

3.5.1.1 Topology description of the connectors

The topology description function φ describes the shape and topology of the connector. This is based on previous work from J. Zhang et al., 2012 and Kang and Wang, 2013. It can be expressed as follows:

$$\begin{cases} \phi(x) > & \text{if} \quad x \in (D \backslash \Omega) \\ \phi(x) = & \text{if} \quad x \in (\delta\Omega \cap D) \\ \phi(x) < & \text{if} \quad x \in (\Omega \backslash \delta\Omega) \end{cases} \tag{3.4}$$

Where D is the fixed design domain, Ω and $\delta\Omega$ are the sub-domain occupied by the connector or void and its boundary. If a point x lies inside the connector, then the corresponding value of the topology description function will be less than zero. The value of x is calculated with $x_{con_{k_{in}}}$ multiplied by the scaling factor c_x, which corresponds to the number of elements on the x direction. $x_{con_{k_{in}}}$ is the input and the optimized value, which is a value between 0 and 1. For the y, the same case is applied. $y_{con_{k_{in}}}$ is the input and the optimized value, which is a value between 0 and 1, and it is multiplied by c_y, which is the number of elements on the y direction to obtain the scaled value for the y coordinate.

For an object, the corresponding topology description function can be expressed with the following function based on W. Zhang et al., 2015:

$$\phi(x, x_o, y_o, \theta, a, b) = \phi(\bar{x}, \bar{y}), \tag{3.5}$$

where:

$$\begin{Bmatrix} \bar{x} \\ \bar{y} \end{Bmatrix} = \begin{bmatrix} cos\theta & sin\theta \\ -sin\theta & cos\theta \end{bmatrix} \begin{Bmatrix} x - x_o \\ y - y_o \end{Bmatrix} \tag{3.6}$$

In this equation, $\bar{x}$ and $\bar{y}$ are the local coordinates on the object, and the rotation angle is θ, which is relative to the horizontal axis. x_o and y_o are the horizontal and vertical coordinates of a specified reference point on the object. These coordinates are calculated with the following equations.

$$x_{con_k} = x_{con_{k_{in}}} \cdot c_x, \qquad y_{con_k} = y_{con_{k_{in}}} \cdot c_y \quad \text{and} \quad \theta_{c_{k_{in}}} = 2\pi\theta_{c_k} - \pi \tag{3.7}$$

These values are used to calculate the topology description function (TDF) representing an object is obtained with the following formula:

$$\phi = \left(\frac{\bar{x}}{a}\right)^6 + \left(\frac{\bar{y}}{b}\right)^6 \tag{3.8}$$

Where a and b are the semi-major and semi-minor lengths of the object, respectively. The equation is based on the superellipse equation, also known as the Lamé curve (Gielis et al., 2021), and has an exponential of 6, creating a rectelliptical shape, a rectangle with rounded corners. This function will not be used only for the connectors, it will also be used later with the cut line and the voids. Therefore, each one will have different values of a and b. For the connector, the notation a_{con} and b_{con} will be used in the remainder of the text.

Fig.3.2a shows the TDF representing a rectelliptical object with a value of $a_{con} = 2$ and $b_{con} = 1$.

The TDF is a level-set function that needs to be mapped to the mesh to perform the analysis. The level set function needs to be converted into a 0-1 field to be able to combine it with the density field and use the SIMP method. A smoothed Heaviside function projects the TDF of the connectors into a density field (Saxena, 2011; Kumar and Saxena, 2015;Hoang and Jang, 2017 ; Wang et al., 2018) with the following equation:

$$\eta_e = 1 - \prod_{k=1}^{N_c} \frac{1}{1 + exp(-\beta\phi_{con_k}(x_e))} \tag{3.9}$$

ϕ_{con_k} is the TDF corresponding to the k^{th} connector. N_c is the number of connectors. x_e represents the centroid coordinate of element e in the Cartesian coordinate system. $\phi_{con_k}(x_e)$ represents the value of TDF calculated at point x_e.

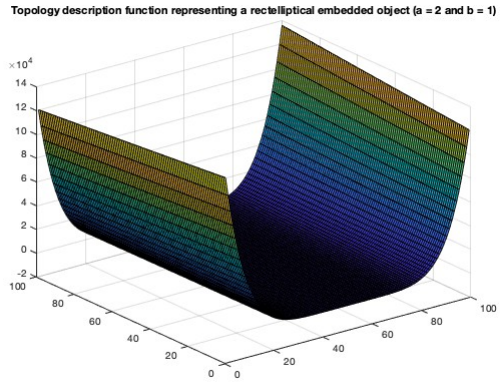

(a) The topology description function representing a rectelliptical object

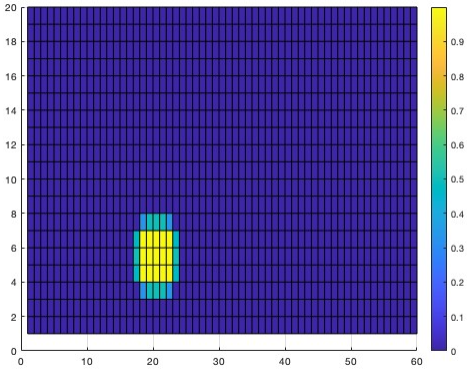

(b) The smoothed Heaviside function η_e

Figure 3.2: TDF of an object and its smoothed Heaviside function η_e

In Fig. 3.2b, the values of the center point are $x_{con} = 20, y_{con} = 5, \theta_c = 0.5$ and where $a_{con} = 3$ and $b_{con} = 2$, this is on a 60 by 20 element domain. It can be appreciated that the obtained field η_e is set to 1 for the connector and 0 for the rest of the domain.

3.5.1.2 Material interpolation scheme

The material interpolation scheme is based on the discrete material optimization (DMO) developed in Stegmann and Lund, 2005, ensuring all elements have one material from a set of pre-defined ones. It is used to solve multi-material topology optimization problems. The SIMP-motivated material interpolation scheme is used. The new term η_e is the element density of the connectors. The structure has the elastic modulus of E_0, and E_c is the Young's modulus for the connector. The interpolated elastic modulus is based on the one introduced at Wang et al., 2020. However, this was changed. One of the reasons for this modification is the filter. Now a filtered density is used ($\widetilde{\rho_e}$). A p-norm is also added to obtain the smooth maximum between the density and the solid connector. This was added due to the connector and the structure not joining. This is explained in Appendix. A.1. The equation for the interpolated elastic modulus is the following:

$$E_e(\widetilde{\rho_e}, \eta_e) = \left(\mathrm{E_{min}} + \left((\mathrm{E_c}\, \eta_e{}^{p_2})^p + \left(\epsilon + \mathrm{E_o}\, \widetilde{\rho_e}^{p_1} \right)^p \right)^{1/p} \right) \tag{3.10}$$

3.5.2. The addition of the voids

As shown in Fig. 2.1, the desired connection consists of an connector with two voids, one on each side. The connector represents the bolt connection, and the voids are free spaces with a density of zero, which is needed to offer the necessary clearance to be able to put the bolt and the nut in place.

This section will explain how the voids are modelled and their dependency on the connectors. The position of the voids will not be optimized.

3.5.2.1 Topology description of voids

As in Eq. 3.8 for the connectors, the horizontal and vertical coordinates of a specified reference point on the voids are needed. The voids are dependent on the position of the connectors. Thus, their coordinates are obtained with the connector's coordinates. A visualisation of how how the voids depend on the position of the connectors is shown in Fig. 3.3. It shows .

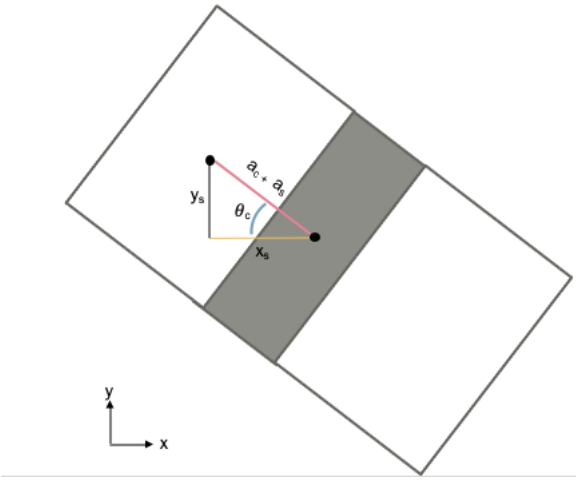

Figure 3.3: Visualization of the how the coordinates of x and y are calculated

Simple trigonometry is used with the coordinates of the solid connector for the relation. This uses sine and cosine operations. The values of z_{void_t} = (x_{void_t}, y_{void_t} and θ_{void_t}), which represent the variables of the voids for the t^{th} void. The angle θ_{c_k} is equivalent in solids and voids as the voids must have the same orientation as the connector, and therefore,$\theta_{void_t} = \theta_{void_{t+1}} = \theta_{c_k}$ for $t = 2k - 1$. Furthermore, each connector needs to have two voids, one void at each side.

They are values of z_{void_t} are calculated:

$$\begin{aligned} x_{void_t} &= x_{con_k} + ((a_{con} + a_{void}) \cdot cos(\theta_{c_k})), & x_{void_{t+1}} &= x_{con_k} - ((a_{con} + a_{void}) \cdot cos(\theta_{c_k})) \\ y_{void_t} &= y_{con_k} + ((a_{con} + a_{void}) \cdot sin(\theta_{c_k})), & y_{void_{t+1}} &= y_{con_k} - ((a_{con} + a_{void}) \cdot sin(\theta_{c_k})) \end{aligned} \tag{3.11}$$

for $t = 2k - 1$, where k is the number of the connector.

These values are used to calculate the TDF φ, used to describe the shape and topology of the voids in Eq. 3.6 and then Eq. 3.5. For the voids, the notation a_{void} and b_{void} are used in the equations as the semi-major and semi-minor lengths.

Similarly to the connector, the voids are projected from the level set function onto a 0-1 field using a smoothed Heaviside function. This new field is called ζ_e, which represents a zero field used to describe the presence of the holes:

$$\zeta_e = \prod_{t=1}^{N_h} \frac{1}{1 + exp(-\beta \phi_{void_t}(x_e))} \tag{3.12}$$

ϕ_{void_t} is the TDF corresponding to the t^{th} void. N_h is the number of voids. $\phi_{void_t}(x_e)$ represents the value of the TDF calculated at the centroid of element e.

In Fig. 3.4a, the values of the center point are $x_{void} = 12, y_{void} = 7, \theta_c = 0.5$ and where $a_{void} = 2$ and $b_{void} = 2$, this is on a 60 by 20 element domain. It can be appreciated that the obtained field ζ_e that is set to 0 for the void and 0 for the rest of the domain.

3.5.2.2 Material interpolation scheme

Now, E_e is a function of $E_e = E(\rho_e, \eta_e, \zeta_e)$. As the E_e is now also a function of ζ_e, the Eq. 3.10 is modified to the following equation:

$$E_e(\widetilde{\rho_e}, \eta_e, \zeta_e) = {\zeta_e}^{p_3} \left(\mathrm{E_{min}} + \left((\mathrm{E_c}\, {\eta_e}^{p_2})^p + \left(\epsilon + \mathrm{E_o}\, \widetilde{\rho_e}^{p_1} \right)^p \right)^{1/p} \right) \tag{3.13}$$

This equation prioritizes the void, if there is an overlap of the position of the voids and connectors, and they overlap each other, the void will overwrite the connector. Fig. 3.4b shows the plot of E_e using Eq. 3.13, with a $\rho_e = 0.5$ and a connector and two voids.

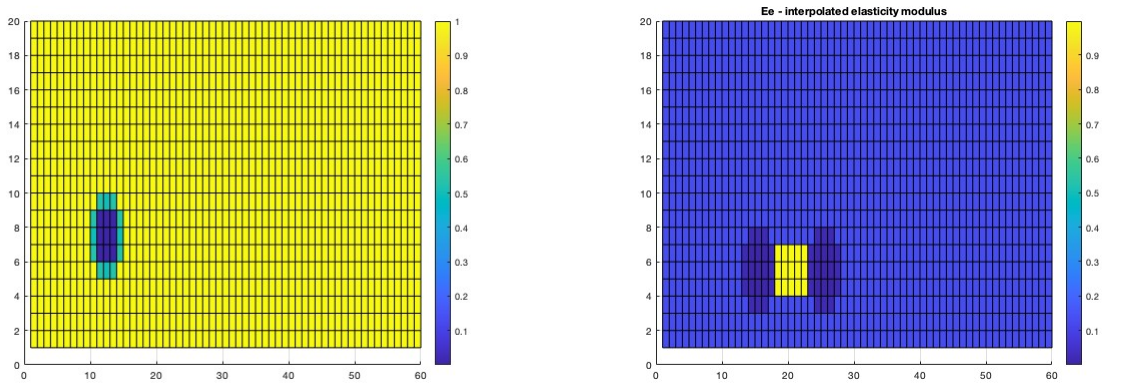

(a) The smoothed Heaviside function ζ_e

(b) Plot of E_e in EQ. 3.13 with two voids, a connector and $\rho = 0.5$

Figure 3.4: TDF of an object and its smoothed Heaviside function η_e

3.6. Modelling the division of the structure, the cut line

To model the division of the structure, cut lines are needed. The idea of the optimization of the cut lines is based on the paper Pollini and Amir, 2020.

To divide the structure, a division line with a zero density field is needed. How the cut line is modelled is the same as the voids, ζ_e. The main difference is that the points optimized in the cut line are endpoints of the line instead of the mid-point, as it is in the voids and connectors.

The new design variable introduced in this part for the optimization is x_{cut_i}. It is a column vector, $x_{cut} = (x_{cut_1}, x_{cut_2}, ..., x_{cut_{n_c+1}})$, where n_c is the number of cut lines. Each cut segment has two values of x, as can be appreciated in Fig. 3.5. The coordinate y_{cut_i} is not optimized; it is a user input. This will determine how many cut lines there are.

The following figure, Fig. 3.5, visualises the cut lines with their coordinates on the MBB beam. The MBB beam is introduced in more detail in section 5.1. The cut line on the figure is not optimized, it is manually added to have a visual idea of how it will work.

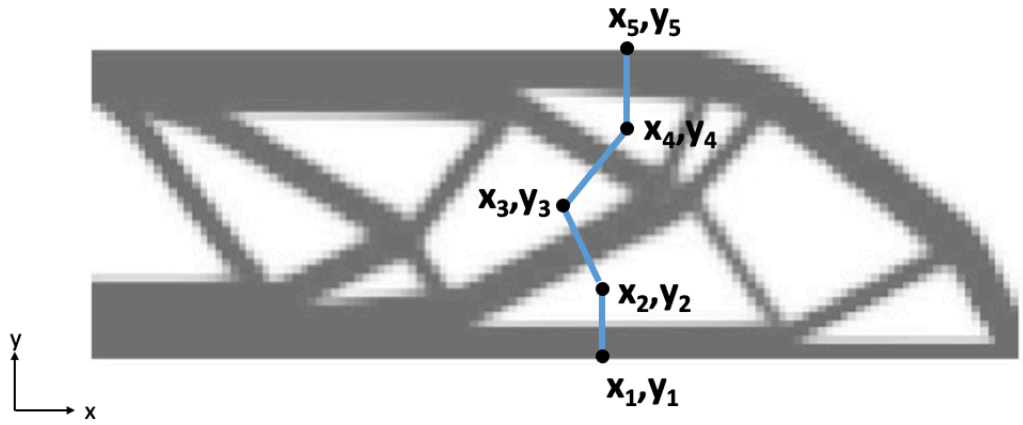

Figure 3.5: Cut line visualisation on the MBB beam

As mentioned, changing the x coordinates will optimise the cut line. In the case of a single cut line, the values to optimize are x_{cut_1} and x_{cut_2}.

y_{cut} is a parameter chosen by the user and not optimized. The thickness of the cut line is determined by the variable b_{cut}. This is also determined by the user and not optimized. As in the previous parts, the inputs and outputs for the optimization method will range from 0-1. Therefore, the coordinates of the cut lines are:

$$x_{cut_i} = x_{cut_{i_{in}}} \cdot c_x \tag{3.14}$$

where $x_{cut_{i_{in}}}$ are the optimized values and as mentioned, they have a range from 0-1. However, x_{cut_i} will be the values used in the following formulation.

The formulation used is the same as before. The topology description function, as shown in Eq. 3.5 is ($\phi(\bar{x}, \bar{y})$), where the local coordinates $\bar{x}, \bar{y}$ are calculated in Eq.3.6. In this equation, the values of x and y used are the mid-points of the cut line. The mid points are presented by $x_{cut_{lmid}}$, for the l^{th} cut line. Each cut line has two coordinates. For example, a single cut line will have a mid point $x_{cut_{1mid}}$ and the x coordinates x_{cut_1} and x_{cut_2}. The mid-points of the cut lines are calculated with the following equations:

$$x_{cut_{lmid}} = \frac{x_{cut_i} + x_{cut_{i+1}}}{2} \qquad y_{cut_{l_{mid}}} = \frac{y_{cut_i} + y_{cut_{i+1}}}{2} \qquad (i = 2l - 1) \tag{3.15}$$

The angle of rotation θ_{cut_l} for the l^{th} line will be the same as the angle θ_{c_k} as there will only be one connector per cut line, therefore $\theta_{cut_l} = \theta_{c_k}$ as $l = k$. From now, the angle of rotation notation for the cut line is θ_{c_k} .The rotation angle is used in Eq.3.6, is determined by the endpoints of the cut line, therefore, is dependent on the values x_{cut_i} and $x_{cut_{i+1}}$ for $i = 2k - 1$. It is calculated with the following equation:

$$\theta_{c_k} = tan^{-1}\left(\frac{y_{cut_{i+1}} - y_{cut_i}}{x_{cut_{i+1}} - x_{cut_i}}\right) \qquad (i = 2k - 1) \tag{3.16}$$

For the TDF of the cut line (ϕ_{cut_l}) the values of a_{cut_l} and b_{cut} are needed. As mentioned, the b_{cut} value is constant in the optimization, this value is constant as it is the thickness of the cut line, which is used to ensure the structure is divided. However, the value of a_{cut_l} is also determined by the endpoints of the cut. The value of a_{cut_l} determines the vertical length from the mid-point to the endpoints. Therefore, for each l^{th} cut line it differs.

$$a_{cut_l} = \frac{\sqrt{\left(x_{cut_{i+1}} - x_{cut_i}\right)^2 + \left(y_{cut_{i+1}} - y_{cut_i}\right)^2}}{2} \qquad (i = 2l - 1) \tag{3.17}$$

As with the connector and the voids, the cut line has to be converted from a level set function into a 0-1 field to combine it on the equation of the interpolated elastic modulus. Therefore, ϕ_{cut_l} are projected onto a density field γ_e using the following smoothed Heaviside function:

$$\gamma_e = \prod_{l=1}^{N_l} \frac{1}{1 + exp(-\beta \phi_{cut_l}(x_e))} \tag{3.18}$$

where ϕ_{cut_l} is the TDF corresponding to the l^{th} cut line and N_l is the number of cut lines. $\phi_{cut_l}(x_e)$ represents the value of the topology description function calculated at the centroid of element e.

The γ_e is obtained separately and not in the same function as ζ_e due to the equation of the material interpolation (E_e). The void ζ_e multiplies the density ($\tilde{\rho}_e$) and the connector η_e in the equation. Therefore it overwrites both of them, leading to the cut over the connector. A new equation for the E_e is used to avoid this problem where the connector is over the cut line.

3.6.0.1 Material interpolation scheme

In this part, the equation for E_e in Eq. 3.13 is changed to add γ_e. A new equation for the E_e is used where the connector is over the cut line.

$$E_e(\widetilde{\rho_e}, \eta_e, \zeta_e, \gamma_e) = \mathrm{E}_{\min} + {\zeta_e}^{p_3} \left((\mathrm{E}_c \, {\eta_e}^{p_2})^q + \left(\epsilon + \mathrm{E}_o \, \widetilde{\rho}_e^{p_1} \, {\gamma_e}^{p_4} \right)^q \right)^{1/q} \tag{3.19}$$

ϵ is a constant value to avoid the undercuts. Due to the p-norm, small values tend to give an error in the calculation of the sensitives of the objective function. The term ϵ is added, with a value of 1e-10, which will give a minimum value and avoid low values when multiplying the density and the cut line field. There is an addition of a minimum value for the Young's modulus (E_{min}). To prevent the stiffness matrix from becoming singular, void areas are given an extremely low stiffness E_{min}.

3.7. Modelling of the combination of the cut the connectors

In the previous sections, the modelling of cut lines, components and voids are introduced. This part explains how the cut line and the connector with the voids are combined and their dependencies.

3.7.1. Modelling of the cut line with movable connector

The position of the connector must lie in the cut line. Previously, when modelling the positioning of the connector, the variables of c_k were optimized, assuming c_k represented the design variable $c_k = \{x_{con_k}, y_{con_k}, \theta_{con_k}\}$ for the k^{th} connector. However, as the connector is now dependent on the coordinates of the cut line, the optimized variables will be different.

A new variable is introduced. This variable ensures that the x_{con_k} and y_{con_k} are in the cut line. As the connector will have the same orientation as the cut line, the θ_{con_k} will be the same as θ_{cut_l} in Eq. B.47, which both are equal to θ_{c_k}. The variable to ensure the connector position on the cut line is s_{con_k}, introduced in Eq. 3.20.

The new equations are:

$$x_{con_k} = x_{cut_i} + s_{con_k}(x_{cut_{i+1}} - x_{cut_i}), \qquad y_{con_k} = y_{cut_i} + s_{con_k}(y_{cut_{i+1}} - y_{cut_i}) \tag{3.20}$$

for $i = 2k - 1$ for the k^{th} connector.

This has a limit of 0-1. Therefore, when s_{con_k} is 0, the connector will be at x_{con_i}, and when it is 1, then the connector will be at $x_{con_{i+1}}$ for $i = 2k - 1$. As mentioned, the decision was made to have a single connector in each cut line, the more connector needed, the more cut lines could be added, also allows each connector to have a different orientation. As there is one connector in each cut line, the number of cut lines, l, is the same as the number of connector k. The number of voids is double. For the first cut line, when the cut is $l = 1$, the x coordinates of the cut lines is x_{cut_1} and x_{cut_2}, the component number is $k = 1$, and the voids are $t = 1$ and $t = 2$. Therefore, $k = l$, and the relationship between k and cut lines x coordinates and the voids number for each component is $i = 2k - 1$ and $t = 2k - 1$.

3.7.2. Addition of the voids

The position of the void depends on the position of the connector. The dependency of the voids shown in Fig. 3.3 and Eq. 3.11 has to be changed due to the connectors are now dependant on the cut line. The new dependency is shown in Fig. 3.6. The main difference is the change between a_{con} and b_{con}.

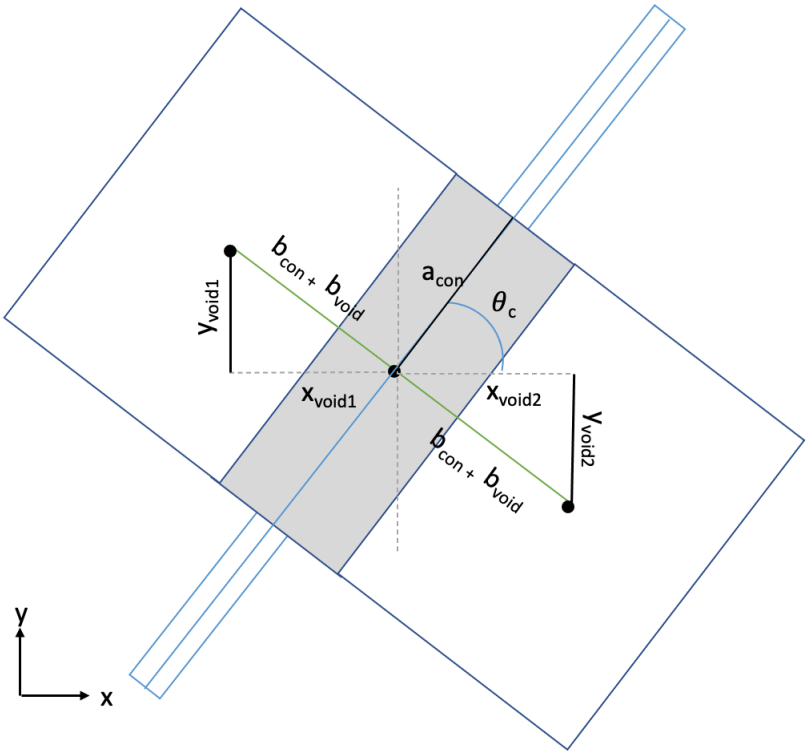

Figure 3.6: Visualization of how the voids are dependent on the connector

If Fig 3.6 is compared to Fig. 3.3, the relation of the voids with the angle θ_{c_k} has changed. Now, it is the angle of the cut line concerning the horizontal axis. The distance from the connector's mid-point to the void's mid-point is now calculated with the horizontal distance of the solid and the void. The variable used is the b_{con} and b_{void} instead of the values of a_{con} and a_{cut_l}, as the length a_{con} is parallel to the cut line. As the orientation of the voids are still the same as the connector, $\theta_{void_t} = \theta_{void_{t+1}} = \theta_{c_k}$ for $t = 2k - 1$. The new equations for the mid-point of the voids are:

$$\begin{aligned} x_{void_t} &= x_{con_k} + ((b_{con} + b_{void}) \cdot cos(-\theta_{c_k})), \quad & x_{void_{t+1}} &= x_{con_k} - ((b_{con} + b_{void}) \cdot cos(-\theta_{c_k})) \\ y_{void_t} &= y_{con_k} + ((b_{con} + b_{void}) \cdot sin(-\theta_{c_k})), \quad & y_{void_{t+1}} &= y_{con_k} - ((b_{con} + b_{void}) \cdot sin(-\theta_{c_k})) \end{aligned} \tag{3.21}$$

for $t = 2k - 1$.

3.7.2.1 Material interpolation scheme

As there is no new variable introduced from the last equation of E_e, the equation for the interpolated elastic modulus stays the same as in Eq. 3.19

4

Optimization problem and sensitivity analysis

This chapter shows the optimization problem and the sensitivity analysis needed for the optimizations.

All the optimizations are performed on the classic example of topology optimization, the MBB beam, which is explained in Section 5.1. Therefore, the topology optimization code combines the 88-line code for MATLAB from Andreassen et al., 2011 and the 99-line code from Sigmund, 2001. The density filter is used from the 88-line code, however, in both of these papers, the method used to optimize the structure is the Optimality Criteria (OC). Furthermore, this is modified to use the Method of Moving Asymptotes (MMA), which was first introduced by Svanberg, 1987. The MMA method has a better performance with multi-constrained and density-based topology optimizations.

4.1. Optimization problem

The position of the cut line, the position of the connectors on the cut line and the overall structure need to be optimised with the aim of maximizing the stiffness of the overall system. For this purpose, the structure's compliance is minimized. The formula for the layout optimization problem is the following:

$$Find: \begin{cases} \rho = (\rho_1, \rho_2, \dots, \rho_{N_e}) \\ \mathbf{s}_{con_k} = (\mathbf{s}_{con_1}, \mathbf{s}_{con_2}, \dots, \mathbf{s}_{con_N}) \\ \mathbf{x}_{cut_i} = (\mathbf{x}_{cut_1}, \mathbf{x}_{cut_2}, \dots, \mathbf{x}_{cut_{nc+1}}) \end{cases} \qquad min: J = \mathbf{F}^T\mathbf{U} \tag{4.1}$$

$$S.t. \begin{cases} \mathbf{KU} = \mathbf{F} \\ g_v = \sum_{e=1}^{N_e} E_e V_e - f_1 V_o \leqslant 0 \\ g_c = \sum_{e=1}^{N_e} (1-\zeta_e) V_e - (V_o - \sum_{N_c}^{c=1} V_c) \leqslant 0 \\ 0 \leqslant \rho_e \leqslant 1 \\ 0 \leqslant \mathbf{s}_{con} \leqslant 1 \\ 0 \leqslant \mathbf{x}_{cut_{in}} \leqslant 1 \end{cases} \tag{4.2}$$

where the objective function J is the following:

$$J = \mathbf{U}^T \mathbf{K} \mathbf{U} = \sum_{e=1}^{N_e} E_e \mathbf{u}_e^T \mathbf{k}_0 \mathbf{u}_e \tag{4.3}$$

where $\mathbf{K}$ is the global stiffness matrix, $\mathbf{F}$ is the load vector, and $\mathbf{U}$ is the displacement vector. $\mathbf{u}_e$ is the element displacement vector. N_e is the number of elements used to discretize the analysis domain. E_e is the interpolated elasticity modulus determined by 3.19.

In Eq. 4.2, there are two constraints. g_v is the volume constraint limiting the amount of material used. V_e is the volume of the element e, and V_0 is the volume of the entire design domain. f_1 is the volume fraction ratio of the available material in the design domain. In this case, the considered volume is the entire structure, including the voids, cut lines and connectors. It must be considered to ensure a connection between the structure part optimized by the density and the connectors. There is no penalisation on the volume constraint due to not being effective in preventing intermediate designs. The volume constraint is the following:

$$g_v = \mathrm{E}_{\min} + \zeta_e \left((\epsilon + \mathrm{V}_{\mathrm{eo}} \widetilde{\rho}_e \gamma_e)^q + (\mathrm{V}_{\mathrm{ec}} \eta_e)^q \right)^{1/q} \tag{4.4}$$

The constraint g_c is the non-overlap constraint for avoiding overlaps between the connectors and between each connector and the design domain boundary. V_c is the volume of the c^{th} connector. This is not the same as the sum of η_e; if not, the overlap constraint will not work. It is equal to the sum of each connector separately. Here the contribution of the void is not added as ζ does not contribute to the overlap constraint g_c.

4.2. Sensitivity Analysis

Sensitivity analysis discusses “how” and “how much” changes in the parameters of an optimization problem modify the objective function value and the point where the optimum is attained (Castillo et al., 2008). This section introduces the sensitivity analysis for the different design variables and the constraints.

The method used for the optimization is the MMA, which is a gradient-based algorithm. The sensitivities checks of these cases are in Appendix. A.2. The forward finite element method was used to check the derivations for all the numerical sensitivities. Some optimizations were performed with a tensile bar to try and optimize where there are fewer possible optimal solutions.

4.2.1. Dependencies

The dependencies are shown here for a better understanding of the sensitivity analysis.

$$J(E_e(\widetilde{\rho}, \eta_e(\phi_{con}), \zeta_e(\phi_{void}), \gamma_e(\phi_{cut}))) \tag{4.5}$$

where:

$$\phi_{con}(x_{con}(s_{con}(x_{cut}(x_{cut_{in}}))), y_{con}(s_{con}(y_{cut}(y_{cut_{in}}))), a_{con}, b_{con}, \theta_c(x_{cut}(x_{cut_{in}}))) \tag{4.6}$$

$$\phi_{void}(x_{void}(x_{con}(s_{con}(x_{cut}(x_{cut_{in}})))), y_{void}(y_{void}(y_{con}(s_{con}(y_{cut}(y_{cut_{in}})))), \theta_c(x_{cut}(x_{cut_{in}}))), a_{void}, b_{void}) \tag{4.7}$$

$$\phi_{cut}(x_{cut}(x_{cut_{in}}), y_{cut}(y_{cut_{in}}), a_{cut}(x_{cut}(x_{cut_{in}}), b_{cut}, \theta_c(x_{cut}(x_{cut_{in}})) \tag{4.8}$$

A visualization of the dependencies is shown in Fig. 4.1, the variables with a black box are not dependent on anything else, the coloured ones are dependent on the variables which the same coloured arrow leads to.

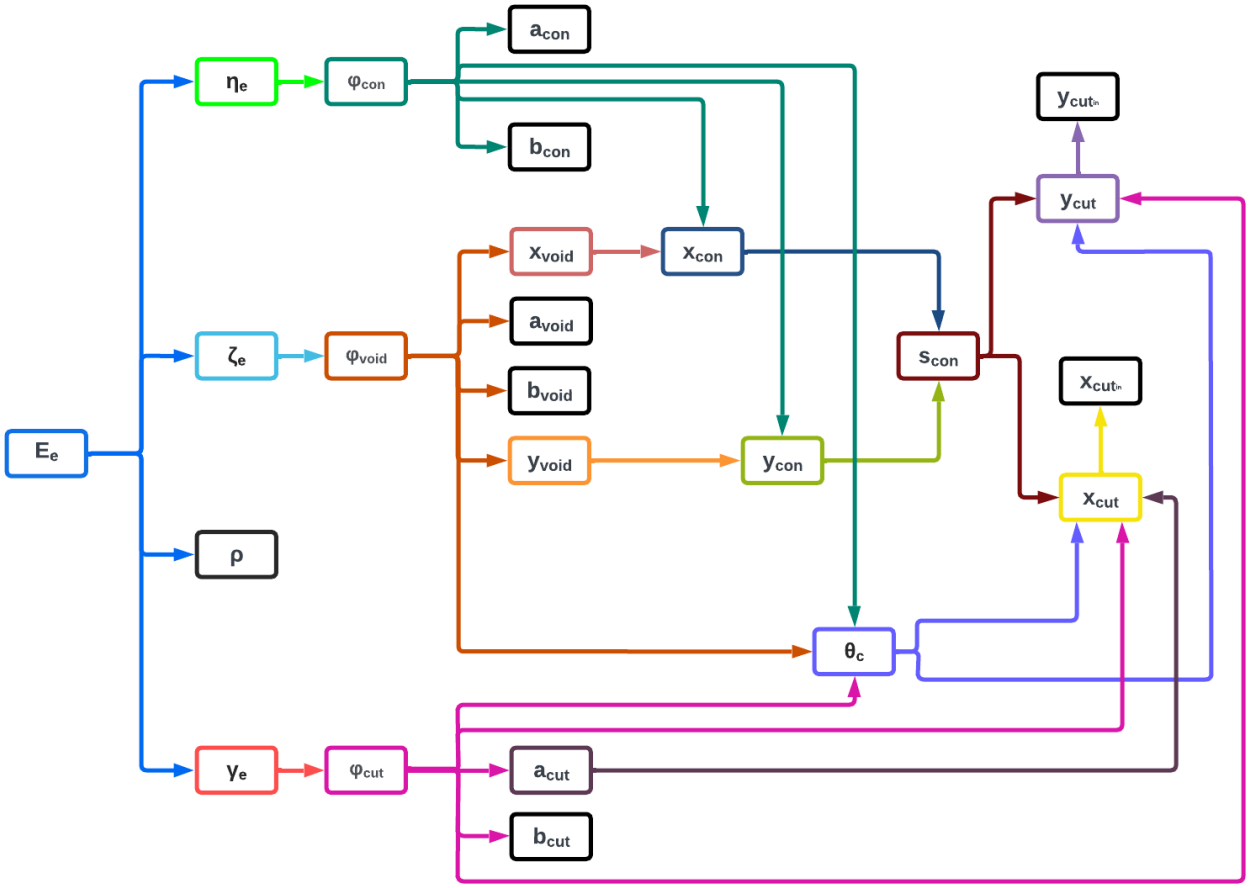

Figure 4.1: Flow chart of the visualization of the dependencies

4.2.2. Sensitivity analysis of the objective function with respect to the element density variable

The design sensitivities of the objective function with respect to the element relative density variable $\widetilde{\rho}_e$ can be written using the adjoint method as follows:

$$\frac{\delta J}{\delta \widetilde{\rho}_e} = -\frac{\delta E_e}{\delta \widetilde{\rho}_e} \cdot \mathbf{u}_e^T \mathbf{K}_o \mathbf{u}_e \tag{4.9}$$

The result of differentiating the equation E_e (Eq. 3.19) with respect to $\widetilde{\rho}_e$ is equal to:

$$\frac{\delta E_e}{\delta \widetilde{\rho}_e} = \mathrm{E_o}\, p_4\, \widetilde{\rho}_e^{p_1}\, \zeta_e^{p_3}\, \gamma_e^{p_4-1} \left((\mathrm{E_c}\, \eta_e^{p_2})^q + \left(\epsilon + \mathrm{E_o}\, \widetilde{\rho}_e^{p_1}\, \gamma_e^{p_4}\right)^q \right)^{\frac{1}{q}-1} \left(\epsilon + \mathrm{E_o}\, \widetilde{\rho}_e^{p_1}\, \gamma_e^{p_4}\right)^{q-1} \tag{4.10}$$

4.2.3. Sensitivity analysis of the objective function with respect to the cut line

When the cut lines move, the connector and the holes linked to that cut line are forced to move, therefore, they have a contribution to the sensitivity of that cut line, this is due to the connector and the voids' positions being dependent on the position of the cut line. The dependencies are shown in the section 4.2.1.

When there are different cut lines, they are connected. Therefore, the movement of one will influence the other cut line. The sensitivity on x_{cut_i}, where two lines have a common point, both cut lines' contribution needs to be added. For example, in Fig. 3.5, for x_{cut_2}, the sensitivities of line one and line two need to be added. This is added into Eq. 4.11 with the summation $\sum_{l=i-1}^{i}$. This means for the i^{th} x_{cut_i}, the contribution of the $l = i-1$ and $l = i$ are added, where l is the number of the cut line. For the initial point, x_{cut_1} and the last point, $x_{cut_{l+1}}$, the contribution is only a single line.

The design sensitivities of the objective function concerning the cut lines are:

$$\frac{\delta J}{\delta x_{cut_{i_{in}}}} = \sum_{e=1}^{N_e} \frac{\delta J}{\delta \gamma_e} \frac{\delta \gamma_e}{\delta x_{cut_{i_{in}}}} + \sum_{e=1}^{N_e} \frac{\delta J}{\delta \eta_e} \frac{\delta \eta_e}{\delta x_{cut_{i_{in}}}} + \sum_{e=1}^{N_e} \frac{\delta J}{\delta \zeta_e} \frac{\delta \zeta_e}{\delta x_{cut_{i_{in}}}} \tag{4.11}$$

As mentioned, the connectors and holes are forced to move when the cut lines move. They have a contribution to the sensitivity calculated for the cut lines. The second sum in Eq. 4.11 is the contribution of the connector, and the last sum is the contribution of the void. It is necessary to add the contribution of both voids on each cut line.

The gradient of the objective function over the cut lines field γ_e, the connectors field η_e and the void's field ζ_e are:

$$\frac{\delta J}{\delta \gamma_e} = -\frac{\delta E_e}{\delta \gamma_e} \cdot \mathbf{u}_e^T \mathbf{K}_o \mathbf{u}_e, \qquad \frac{\delta J}{\delta \eta_e} = -\frac{\delta E_e}{\delta \eta_e} \cdot \mathbf{u}_e^T \mathbf{K}_o \mathbf{u}_e, \qquad \frac{\delta J}{\delta \zeta_e} = -\frac{\delta E_e}{\delta \zeta_e} \cdot \mathbf{u}_e^T \mathbf{K}_o \mathbf{u}_e \tag{4.12}$$

Where the derivative of E_e with respect to the cut line field γ_e is the following:

$$\frac{\delta E_e}{\delta \gamma_e} = \mathrm{E_o}\, p_4\, \tilde{\rho}_e^{p_1}\, \zeta_e{}^{p_3}\, \gamma_e{}^{p_4-1} \left((\mathrm{E_c}\, \eta_e{}^{p_2})^q + \left(\epsilon + \mathrm{E_o}\, \tilde{\rho}_e^{p_1}\, \gamma_e{}^{p_4}\right)^q \right)^{\frac{1}{q}-1} \left(\epsilon + \mathrm{E_o}\, \tilde{\rho}_e^{p_1}\, \gamma_e{}^{p_4}\right)^{q-1} \tag{4.13}$$

and where Eq. 3.19 is derived over the connector's field η_e:

$$\frac{\delta E_e}{\delta \eta_e} = \mathrm{E_c}\, \eta_e{}^{p_2-1}\, p_2\, \zeta_e{}^{p_3} \left((\mathrm{E_c}\, \eta_e{}^{p_2})^q + \left(\epsilon + \mathrm{E_o}\, \tilde{\rho}_e^{p_1}\, \gamma_e{}^{p_4}\right)^q \right)^{\frac{1}{q}-1} (\mathrm{E_c}\, \eta_e{}^{p_2})^{q-1} \tag{4.14}$$

and where the derivative of E_e with respect to the voids field ζ_e is the following:

$$\frac{\delta E_e}{\delta \zeta_e} = p_3\, \zeta_e{}^{p_3-1} \left((\mathrm{E_c}\, \eta_e{}^{p_2})^q + \left(\epsilon + \mathrm{E_o}\, \tilde{\rho}_e^{p_1}\, \gamma_e{}^{p_4}\right)^q \right)^{1/q} \tag{4.15}$$

In Eq. 4.11, the gradient of the cut lines field γ_e over the input value for the cut line $x_{cut_{i_{in}}}$:

$$\frac{\delta \gamma_e}{\delta x_{cut_{i_{in}}}} = \frac{\delta \gamma_e}{\delta \phi_{cut_l}} \frac{\delta \phi_{cut_l}}{\delta x_{cut_i}} \frac{\delta x_{cut_i}}{\delta x_{cut_{i_{in}}}} \tag{4.16}$$

From Eq. 4.16, the derivative of ζ_{cut}, on Eq. 3.18 with respect to the topology description function for the cut ϕ_{cut_l} is:

$$\frac{\delta \gamma_e}{\delta \phi_{cut_l}} = \gamma_e \frac{\beta exp(-\beta \phi_{cut_l})}{(1 + exp(-\beta \phi_{cut_l}))} \tag{4.17}$$

The second term in Eq. 4.16, is the derivation of Eq. 3.5 with respect to the cut coordinates. Where $i = k$ due to the design decision of having a single component per cut line:

$$\frac{\delta \phi_{cut_l}}{\delta x_{cut_i}} = \sum_{l=i-1}^{i} \left(\frac{\delta \phi_{cut_l}}{\delta x_{cut_{l_{mid}}}} \frac{\delta x_{cut_{l_{mid}}}}{\delta x_{cut_i}} + \frac{\delta \phi_{cut_l}}{\delta \theta_{c_k}} \frac{\delta \theta_{c_k}}{\delta x_{cut_i}} + \frac{\delta \phi_{cut_l}}{\delta a_{cut_l}} \frac{\delta a_{cut_l}}{\delta x_{cut_i}} \right) \tag{4.18}$$

Where the topology description function with respect to the mid x coordinates of the cut line:

$$\frac{\delta \phi_{cut_l}}{\delta x} = 6 \left(\frac{\bar{x}}{a} \right)^5 \frac{-cos\theta_{c_k}}{a} + 6 \left(\frac{\bar{y}}{b} \right)^5 \frac{sin\theta_{c_k}}{b} \qquad (x = x_{cut_{l_{mid}}}) \tag{4.19}$$

for $a = a_{cut_l}$ and $b = b_{cut}$. The differentiation of the mid x coordinate position of the cut with the x coordinate is:

$$\frac{\delta x_{cut_{l_{mid}}}}{\delta x_{cut_i}} = 0.5 \qquad (i = l) \tag{4.20}$$

The derivative of the mid-point is the same for the cut's top and bottom x coordinates.
The topology description function with respect to the angle is:

$$\begin{aligned}\frac{\delta \phi_{cut_l}}{\delta \theta} = 6\left(\frac{\bar{x}}{a}\right)^5 \frac{-sin\theta_{c_k}(x - x_o) + cos\theta_{c_k}(y - y_o)}{a} \\ +6\left(\frac{\bar{y}}{b}\right)^5 \frac{-cos\theta_{c_k}(x - x_o) + sin\theta_{c_k}(y - y_o)}{b}\end{aligned} \tag{4.21}$$

for $a = a_{cut_l}$ and $b = b_{cut}$
The angle in Eq.3.16 with respect to the top and bottom x coordinates of a single cut is:

$$\begin{aligned}\frac{\delta \theta_{c_k}}{\delta x_{cut_i}} &= \frac{y_{cut_{i+1}} - y_{cut_i}}{(y_{cut_{i+1}} - y_{cut_i})^2 + (x_{cut_{i+1}} - x_{cut_i})^2} \qquad (\text{for} \quad i = k) \\ \frac{\delta \theta_{c_k}}{\delta x_{cut_i}} &= -\frac{y_{cut_i} - y_{cut_{i-1}}}{(y_{cut_i} - y_{cut_{i-1}})^2 + (x_{cut_i} - x_{cut_{i-1}})^2} \qquad (\text{for} \quad i = k + 1)\end{aligned} \tag{4.22}$$

The first term of the last sum in Eq. 4.18, is the length from the mid-point to the cut coordinates a_{cut_l}:

$$\frac{\delta \phi_{cut_l}}{\delta a_{cut_l}} = -\frac{6\,\bar{x}^6}{a_{cut_l}^7} \tag{4.23}$$

The derivative of a_{cut_l} is different with respect to the bottom ($i = l$) and top ($i = l + 1$) x of the cut line.

$$\begin{aligned}\frac{\delta a_{cut_l}}{\delta x_{cut_i}} &= \frac{2\,x_{cut_i} - 2\,x_{cut_{i+1}}}{4\sqrt{\left(x_{cut_i} - x_{cut_{i+1}}\right)^2 + \left(y_{cut_i} - y_{cut_{i+1}}\right)^2}} \qquad (\text{for} \quad i = l) \\ \frac{\delta a_{cut_l}}{\delta x_{cut_i}} &= -\frac{2\,x_{cut_{i-1}} - 2\,x_{cut_i}}{4\sqrt{\left(x_{cut_{i-1}} - x_{cut_i}\right)^2 + \left(y_{cut_{i-1}} - y_{cut_i}\right)^2}} \qquad (\text{for} \quad i = l + 1)\end{aligned} \tag{4.24}$$

The last term in Eq. 4.16, is the derivative of the actual value with respect to the input one. The scaling:

$$\frac{\delta x_{cut_i}}{\delta x_{cut_{i_{in}}}} = c_x \tag{4.25}$$

In Eq. 4.11, the gradient of the cut lines field γ_e over the input value for the cut line $x_{cut_{i_{in}}}$:

$$\frac{\delta \eta_e}{\delta x_{cut_{i_{in}}}} = \frac{\delta \eta_e}{\delta \phi_{con_k}} \frac{\delta \phi_{con_k}}{\delta x_{cut_i}} \frac{\delta x_{cut_i}}{\delta x_{cut_{i_{in}}}} \tag{4.26}$$

There is only one connector per cut line, then, for each cut line, the only connector contributing is the one on it, therefore, $k = i$ for the index.
The second term is the derivative of η_e with respect to ϕ_{con_i}. Giving the following equation:

$$\frac{\delta \eta_e}{\delta \phi} = -(1 - \eta_e)\frac{\beta exp(-\beta \phi)}{(1 + exp(-\beta \phi))} \qquad (\phi = \phi_{void_t}) \tag{4.27}$$

As the cut line moves, the connector is forced to, as it has to be on the cut line. Therefore, the x coordinate and the connector's angle, which is the same as the cut line, contribute to the cut line's sensitivities.

$$\frac{\delta \phi_{con_k}}{\delta x_{cut_i}} = \sum_{l=i-1}^{i} \left(\frac{\delta \phi_{con_k}}{\delta x_{con}} \frac{\delta x_{con}}{\delta x_{cut_i}} + \frac{\delta \phi_{con_k}}{\delta \theta_{c_k}} \frac{\delta \theta_{c_k}}{\delta x_{cut_i}} \right) \tag{4.28}$$

Where the derivative of ϕ_{con_i} with respect to x_{cut_i} is found in Eq. 4.19, when $x = x_{cut_i}$.
The differentiation of the connector's x coordinate over the cut line x coordinate is:

$$\frac{\delta x_{con_k}}{\delta x_{cut_i}} = 1 - s_{con_k} \quad (\text{for } i = k) \qquad \frac{\delta x_{con_k}}{\delta x_{cut_i}} = s_{con_k} \quad (\text{for } i = k+1) \tag{4.29}$$

The last term in the connector's contribution in Eq.4.11 is the same as calculated in Eq. B.46

In Eq. 4.11, the gradient of the cut lines field γ_e over the input value for the cut line $x_{cut_{i_{in}}}$:

$$\frac{\delta \zeta_e}{\delta x_{cut_{i_{in}}}} = \frac{\delta \zeta_e}{\delta \phi_{void_t}} \frac{\delta \phi_{void_t}}{\delta x_{cut_i}} \frac{\delta x_{cut_i}}{\delta x_{cut_{i_{in}}}} \tag{4.30}$$

The derivative of ζ_e over ϕ_{void_t} in Eq. 4.30, is equivalent to Eq. 4.17. However, using the values of the voids instead of the cut lines.

The second term in Eq. 4.30, is the differentiation of ϕ_{void_t} over the $x_{cut_{i_{in}}}$. It is calculated in the following equation:

$$\frac{\delta \phi_{void_t}}{\delta x_{cut_{i_{in}}}} = \sum_{l=i-1}^{i} \sum_{t=2l-1}^{2l} \left(\frac{\delta \phi_{void_t}}{\delta x_{void_t}} \frac{\delta x_{void_t}}{\delta x_{con_k}} \frac{\delta x_{k_{con}}}{\delta x_{cut_i}} + \frac{\delta \phi_{void_t}}{\delta y_{void_t}} \frac{\delta y_{void_t}}{\delta y_{con_k}} \frac{\delta y_{con_k}}{\delta x_{cut_i}} + \frac{\delta \phi_{void_t}}{\delta \theta_{void_t}} \frac{\delta \theta_{void_t}}{\delta \theta_{con_k}} \frac{\delta \theta_{con_k}}{\delta x_{cut_i}} \right) \tag{4.31}$$

There are two voids, one on each side of the connector, both contribute to the movement of that cut line. Therefore, both contribution needs to be added for each cut line.

Where the first term of each chain rule, ϕ_{void_t}, is derived over the coordinates of the connectors. The gradient of ϕ_{void_t} respect to x_{void_t} is equivalent to the one calculated on 4.19, where $a = a_{void}$ and $b = b_{void}$.

The term $\frac{\delta \phi_{void_t}}{\delta \theta_{void_t}}$ is also equivalent to Eq. B.42. With $a = a_{void}$ and $b = b_{void}$.

The differentiation of ϕ_{void_t} over the y_{void_t} is the following:

$$\frac{\phi_{con_k}}{\delta y} = 6\left(\frac{\bar{x}}{a}\right)^5 \frac{-sin\theta_{c_k}}{a} + 6\left(\frac{\bar{y}}{b}\right)^5 \frac{cos\theta_{c_k}}{b} \qquad (y = y_{void_t}) \tag{4.32}$$

where $a = a_{void}$ and $b = b_{void}$.

The second term of each chain rule in Eq. 4.31 is the gradient of the coordinates of the voids with respect to the coordinates of the connector, which are the following:

$$\frac{\delta x_{void_t}}{\delta x_{con_k}} = 1, \qquad \frac{\delta y_{con_k}}{\delta y_{con_k}} = 1, \qquad \frac{\delta \theta_{con_k}}{\delta \theta_{con_k}} = 1 \tag{4.33}$$

The third term of each chain rule is the gradient of the coordinates of the connectors with respect to their position on the cut line.

$$\frac{\delta x_{con_k}}{\delta x_{cut_i}} = 1 - s_{con_k} \quad (\text{for } i = k) \qquad \frac{\delta x_{con_k}}{\delta x_{cut_i}} = s_{con_k} \quad (\text{for } i = k+1) \tag{4.34}$$

And for the y values :

$$\frac{\delta y_{con_k}}{\delta x_{cut_i}} = 1 - s_{con_k} \quad (\text{for } i = k) \qquad \frac{\delta y_{con_k}}{\delta x_{cut_i}} = s_{con_k} \quad (\text{for } i = k+1) \tag{4.35}$$

The last term of the voids' contribution on Eq. 4.31 is the same as in the previous ones, found in Eq. B.46.

The sum of the sensitivities of both voids, one on each side of the connector, must be added.

4.2.4. Sensitivity analysis of the objective function with respect to the connector

The voids have a contribution to the cut line, and they also have a contribution to the connector movement over the cut line. The sensitivity analysis of the objective function with respect to the connector is shown below:

$$\frac{\delta J}{\delta s_{k_{con}}} = \sum_{e=1}^{N_e} \frac{\delta J}{\delta \eta_e} \frac{\delta \eta_e}{\delta \phi_{con_k}} \frac{\delta \phi_{con_k}}{\delta s_{k_{con}}} + \sum_{e=1}^{N_e} \frac{\delta J}{\delta \zeta_e} \frac{\delta \zeta_e}{\delta \phi_{void_t}} \frac{\delta \phi_{void_t}}{\delta s_{k_{con}}} \tag{4.36}$$

In the first chain rule, the first term is the gradient of the objective function over η_e. This has been calculated on Eq. B.8 and Eq. 4.14. The second term, the differentiation of η_e over ϕ_{con_k} is found on Eq. B.10, for $\phi = \phi_{con_k}$. The last term of the first sum is $\frac{\delta \phi_{con_k}}{\delta s_{k_{con}}}$. Which is the sum of the contributions of the different variables of s_{con_k}.

$$\frac{\delta \phi_{con_k}}{\delta s_{con_k}} = \sum_{e=1}^{N_e} \frac{\delta \phi_{con_k}}{\delta x_{con_k}} \frac{\delta x_{k_{con}}}{\delta s_{con_k}} + \frac{\delta \phi_{con_k}}{\delta y_{con_k}} \frac{\delta y_{k_{con}}}{\delta s_{con_k}} \tag{4.37}$$

Where the first term in both sums is previously calculated on Eq. 4.19 for $x = x_{con}$ and Eq. 4.32 for $y = y_{con}$. There is no contribution of the angle, as it's not optimized and is the same as in the cut line.

The derivative of x_{con_k} respect to s_{con_k} is equal to:

$$\frac{\delta x_{con_k}}{\delta s_{con_k}} = x_{cut_{i+1}} - x_{cut_i} \tag{4.38}$$

for i = k

and the derivative of y_{con_k} respect to s_{con_k} is equal to:

$$\frac{\delta y_{con_k}}{\delta s_{con_k}} = y_{cut_{i+1}} - y_{cut_i} \tag{4.39}$$

for i = k

The second sum is the contribution of the voids. As in the other case, the contribution of both voids must be added.

$$\frac{\delta \phi_{void_t}}{\delta s_{k_{con}}} = \sum_{e=1}^{N_e} \frac{\delta \phi_{void_t}}{\delta x_{void_t}} \frac{\delta x_{void_t}}{\delta x_{k_{con}}} \frac{\delta x_{k_{con}}}{\delta s_{k_{con}}} + \frac{\delta \phi_{void_t}}{\delta y_{void_t}} \frac{\delta y_{void_t}}{\delta y_{k_{con}}} \frac{\delta y_{k_{con}}}{\delta s_{k_{con}}} \tag{4.40}$$

The first two terms on both sums are the same as calculated on the contribution of the voids in the cut line on Eq. 4.31. However, in this case, there is no contribution of the angle. The last term in both sums is the differentiation of the x and y coordinate over s_{con_k}, which is the same as in Eq. 4.38 for the x coordinate and in Eq. 4.39 for the y coordinate.

4.2.5. Sensitivity analysis of volume constraint with respect to the element density variable

Here the volume constraint g_v is differentiated with respect to the density as follows:

$$\frac{\delta g v}{\delta \widetilde{\rho}_e} = \mathrm{V_{eo}}\, \widetilde{\rho}_e\, \zeta_e\, (\epsilon + \mathrm{V_{eo}}\, \widetilde{\rho}_e\, \gamma_e)^{q-1} \left((\epsilon + \mathrm{V_{eo}}\, \widetilde{\rho}_e\, \gamma_e)^q + (\mathrm{V_{ec}}\, \eta_e)^q \right)^{\frac{1}{q}-1} \tag{4.41}$$

4.2.6. The remaining sensitivity analysis

The previous sensitivity analysis shows the main idea of how the contributions are added and how the equations are obtained. There is a volume constraint as well as a non-overlap constraint. These sensitivities are also needed for the optimizations. However, they are calculated with the same approach as the ones explained above. These sensitivities are detailed in the Appendix. B.4.3.1. In the appendix, the sensitivity analysis of the volume constraint with respect to the cut line, the sensitivity analysis of the volume constraint with respect to the connector and the sensitivity analysis of the non-overlap constraint with respect to the connector are shown.

4.2.7. Simplified optimization problem and sensitivities

The optimization can be simplified into different separate optimizations. The optimization the only a connector is explained in Appendix. B.1, and the optimization with the voids is found in Appendix B.2. For the cut lines, the optimization of a simple cut line and for multiple cut lines in found in Appendix B.3. In Appendix B.4.1, the optimization problem with the cut line and ca connector in the middle is found and in Appendix. B.4.2 the one for the single cut line connector optimization. The optimization problem for these parts also includes the sensitivity analysis.

4.3. Stopping criteria

In some optimizations, the optimization process is terminated when the following convergence criteria are satisfied:

$$\frac{\|\rho_k - \rho_{k-1}\|}{\|\rho_k\|_2} \leq \omega \tag{4.42}$$

where ρ_k and ρ_{k-1} represent element relative density vectors for the k^{th} and $k-1^{th}$ iterations in the optimization process. ω is an allowable convergence error. This is set to $\omega = 0.1\%$.

With the addition of the connectors, voids and cut lines, the convergence on Eq. 4.42 is not met when ε is 0.05 as used in other cases. This is due to the density changing with a minimum oscillation movement of the connector and the cut line. If the convergence condition cannot be met, the maximum number of iterations allowed is set to 150 or 200. In literature, this problem is also found, for example, on Wang et al., 2020 and Pollini and Amir, 2020, which have a similar method, and they create a set of maximum number of iterations as the stopping method.

Other stopping criteria that can be used also involve the convergence criteria. However, this time not with the density field, but with the objective function. The change is calculated with the following equation:

$$\|J_k - J_{k-1}\| \leq \omega_J \tag{4.43}$$

where J_k and J_{k-1} represent element relative density vectors for the k^{th} and $k-1^{th}$ iterations in the optimization process. ω_J is an allowable convergence error. This is set to $\omega_J = 0.05$. The difference between stopping the optimization by the change of J and by the maximum number of iterations is shown in the stopping criteria section of the results, in Section. 5.6.

4.4. Overview of the optimization process

To have an overview of the optimization progress, a flowchart is shown in Fig. 4.2. The flow chart of the numerical implementation for solving the simultaneous optimization of multi-part structure topologies and connection points problem, subject to the volume constraint and non-overlap constraints.

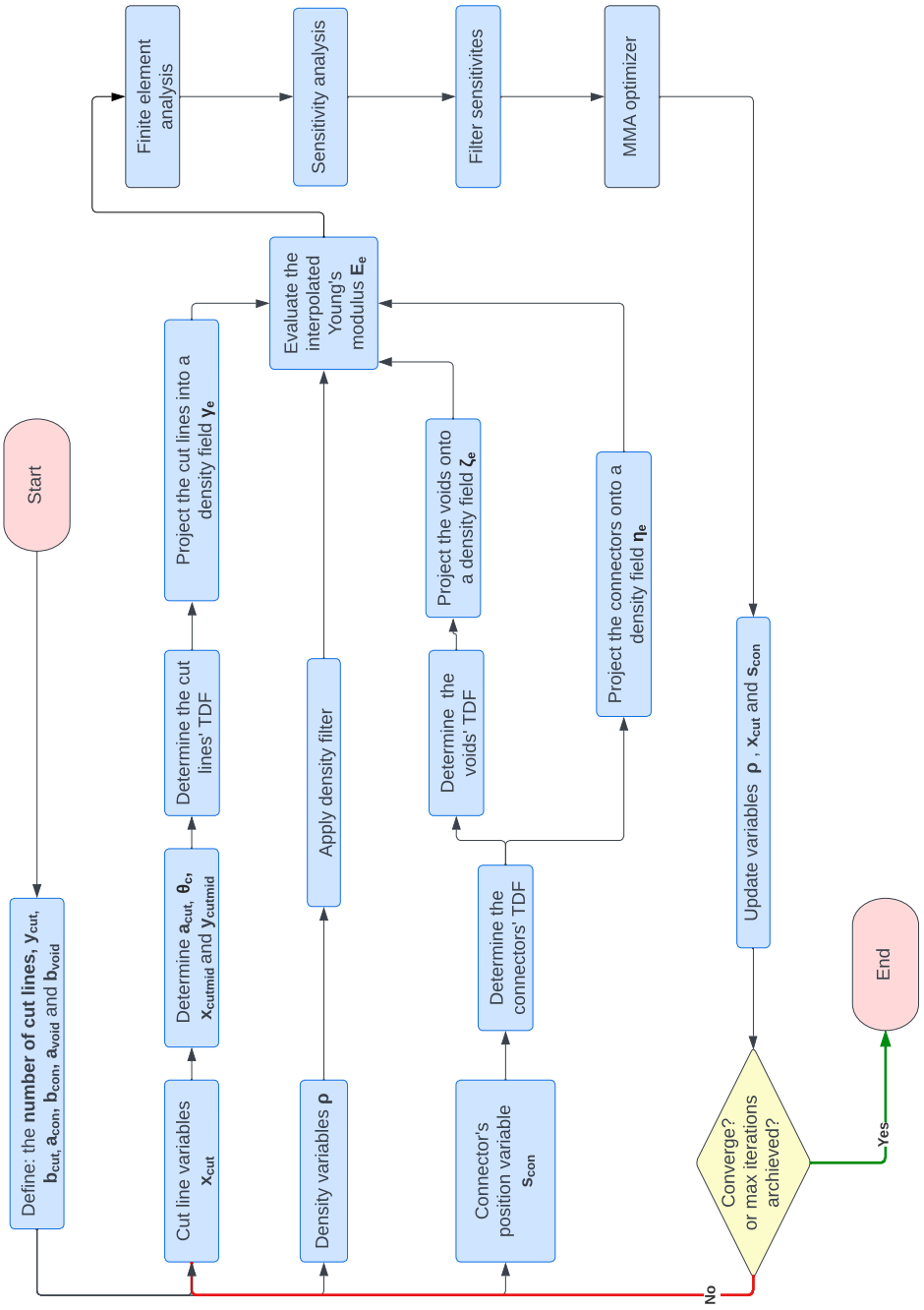

Figure 4.2: Flow chart of the optimization

5

Results

In this chapter, the results of the optimization explained above are shown. The first set of optimizations is made to check the influence of the connector with voids, where different voids sizes and starting positions are shown. Following the structure in Chapter 3, the next sets of results shown are the optimization of the structure with cut lines, followed by the complete optimization. The complete optimization consists of optimizing the structure, which is entirely cut, and the cut line positioning with its respective connectors and voids. The positioning of the connectors on the cut line is also optimized. Then, a parameter study is done, where the influence of the initial starting positions and parameters is observed. Regarding the stopping criteria of the simulations, the first two sets of results are due to the stopping criteria in Eq. 4.42. However, a set number of interactions is the stopping method for the complete optimization and parameter study. This will be discussed further later in this chapter.

In Appendix A.1, the initial challenge obtained when running the simulations can be appreciated, changing from the sensitivity filter to the density filter with the initial equation for the material interpolation scheme (E_e) created a blurry part around the connector in the structure, meaning there was no solid connection between them. Furthermore, with the change of the volume constraint and a new equation of E_e, the problem was solved.

In this chapter, only the final results are shown. However, more simplified problems were optimized for each section, and more tests of individual aspects can be found in Appendix C. All the numerical results are shown in tables in Appendix E. The initial and final layouts are provided for each optimisation, following the initial idea in Fig. 2.1. The connector will be shown in green, the voids in blue and the cut line in red. The final compliance of the optimization is stated in the caption of the figures.

All the optimizations are performed using the MBB beam.

5.1. MBB-beam

The MBB beam is the fundamental geometry used in this research. The MBB is one of the most used in topology optimization. Fig. 5.1a shows the full beam load cases. The beam is constrained on both sides in the bottom corners, and a vertical load is applied in the middle of the beam. The lower right constraint is only applied in the vertical axes.

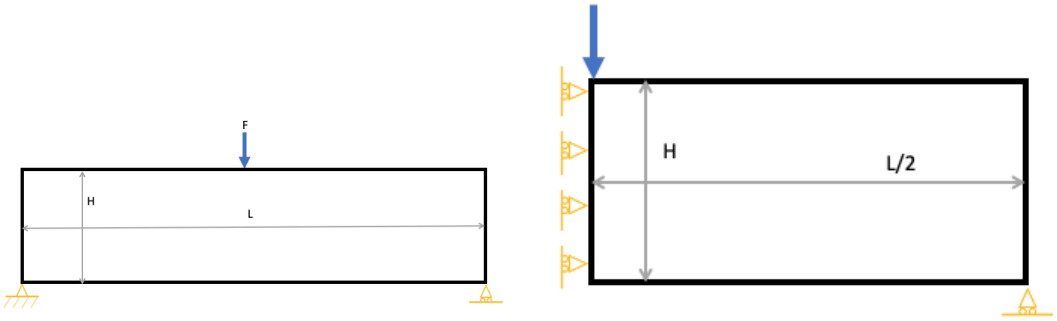

(a) The full MBB beam (b) Half MBB beam

Figure 5.1: The load cases for the MBB beam

As the beam is symmetric, it can be divided into two equal parts, as the second image in Fig. 5.1b. This reduces the computational costs. A new boundary is added when the beam is divided. A displacement constraint as a boundary condition is added on the left side. The default boundary condition of the beam is having a load vertically applied in the upper left corner with support in the lower right corner. This half beam is used in all the optimization cases in this report. The H is equal to Nely (number of elements in the y direction), and L/2 is equal to Nelx (number of elements in the x direction).

5.2. Initial topology optimization, only the structure optimized

Firstly, before starting the optimizations with the addition of a connector, cut line or voids, the MMB beam is optimized using the 99-line code from Sigmund, 2001, these optimizations are on Fig. 5.2. These cases are optimized to compare them to the optimization results when connectors, voids and cut lines are added.

The difference between the two optimizations in Fig. 5.2 is the number of elements. The first is 60x20 elements, 60 on the x and 20 on the y, and the second is 120x40 elements. The initial optimizations are solved with the 60x20 elements mesh, the 120x40 elements mesh is used in the complete optimization as it is a finer mesh, which improves the accuracy of the results by reducing the interpolation errors. The other parameter inputs are the same in both optimizations, $r_{min} = 1.5$, p = 3, and the f_1 is = 0.5. The compliance of the first case is 203.30, and the second is 193.12.

(a) 99 line code optimization with 60x20 elements - J=203.30 (b) 99 line code optimization with 120x40 elements - J=193.12

Figure 5.2: Examples obtained with the 99 line code optimization (Sigmund, 2001)

5.3. Optimization with a single connector with voids

Following the methodology explained in the previous section, the topology optimization of the MBB beam is performed by adding a connector. In this case, the connector does not behave as a connecting point as the structure is not divided yet, now, it is an additional connector that contributes to the structural stiffness. The position of the connector will be optimized with the structure simultaneously. Table 5.1 shows the different values for the constant parameters.

Constant	Value	Eq.
E_o	1	3.19
E_c	1	3.19
V_{ec}	1	4.4
V_{eo}	1	4.4
β	8	3.9, 3.12 and 3.18
p_1, p_2, p_3	3	3.19
E_{min}	1e-6	3.19
q	30	3.19
F	1	4.2

Table 5.1: Constant parameters in the optimization

In this section, examples of how the connector and the structure are optimized are given. The optimization is done only with a single connector and the voids, one on each side of the connector.

Different optimization cases are performed to check how the connector with the holes behaves and the influence on the final layout. In this section, three cases are shown. The optimizations' initial and final layouts are shown in the three cases. In each case, different void sizes are optimized, one with a small size, one with a medium size and one with the void having the same height as the connector. The small voids are 1x1 ($a_{void} \times b_{void}$) element, the medium voids have a size of 2x1 elements, and the large voids have a size of 2x2 elements.

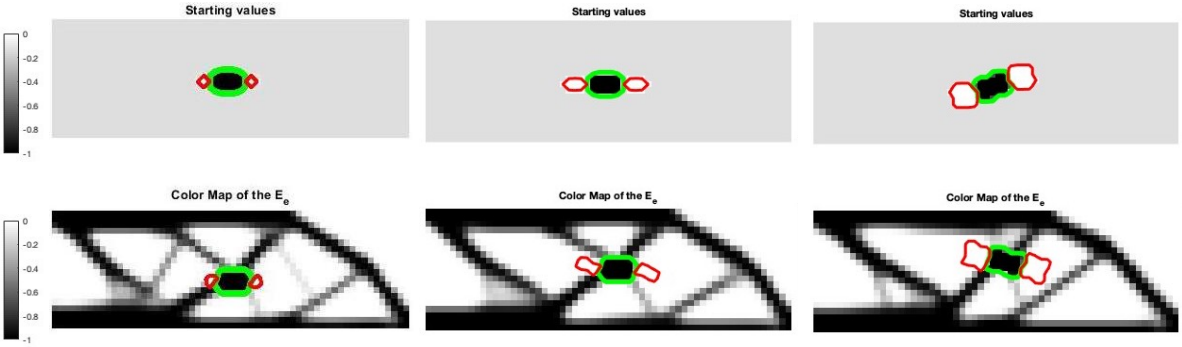

(a) Case 1 - J = 216.87 (b) Case 2 - J = 218.38 (c) Case 3 - J = 218.53

Figure 5.3: Optimization of the structure with the connectors with voids

When optimizing a connector with voids, the expected results are to have the connector on a member of the structure and the voids on a section where the density is zero to minimize compliance and not to add extra material as it contributes to the overall volume of the structure and the optimization problem has a volume fraction constraint.

The addition of the connector increases the structure's compliance if compared to Fig. 5.2a, which is the optimized structure without any connectors and has a compliance of 203.30. This is due to the addition of the connector and its positioning, which affect the stiffness of the structure.

In the first two cases, Case 1 in Fig. 5.3a and Case 2 in Fig. 5.3b, the starting position is the same, and in Case 3, the initial position on an angle. In these cases, the final positioning is similar in all the cases, however, it is not the same. This is due to the influence of the starting position and the void size. Another reason the results vary, and they are not optimized to the same position, is that there are many valid solutions due to the problem having several local optima.

The numerical results, the initial and final values, of these cases are found in Table. E.2 in Appendix E. The table shows the initial and final positions and the constant values as the voids and connectors sizes. Furthermore, intermediate results, where only the connector with no voids are optimized and more results with the connector with the voids, are shown in Appendix C.1.

5.4. Optimizing the division of the structure, the cut lines

This section is dedicated to the subdivision of the structure into several parts. The structure is divided using cut lines. The cut lines are optimized to find their most optimal positioning. This section shows examples of how the cut line is optimized. This section will not show the optimization of the part fully divided into two. This is because breaking the part without any connection point will lead to a separate part, which generates an error when optimizing due to not having a connection point between the two parts.

Multiple cut lines are optimized to observe their behaviour when they are optimized. The cut lines' positions are optimized by optimizing the x coordinates. As the coordinates to optimize are the cut line's top and bottom points, when there are several ones, each cut line shares an x variable with the adjacent line. The angle θ_{c_k} and vertical direction a_{cut_l} depend on the cut line's position, b_{cut}, and the y coordinates stay constant during the optimizations. Each cut line will have its own angle θ_{c_k} and vertical direction a_{cut_l}.

Fig. 5.4 shows the initial and optimized layout for two cases with multiple cut line optimizations. Case 1 is shown in Fig. 5.4a, and Case 2 is shown in Fig. 5.4b. The initial position of the cut lines is different in both cases.

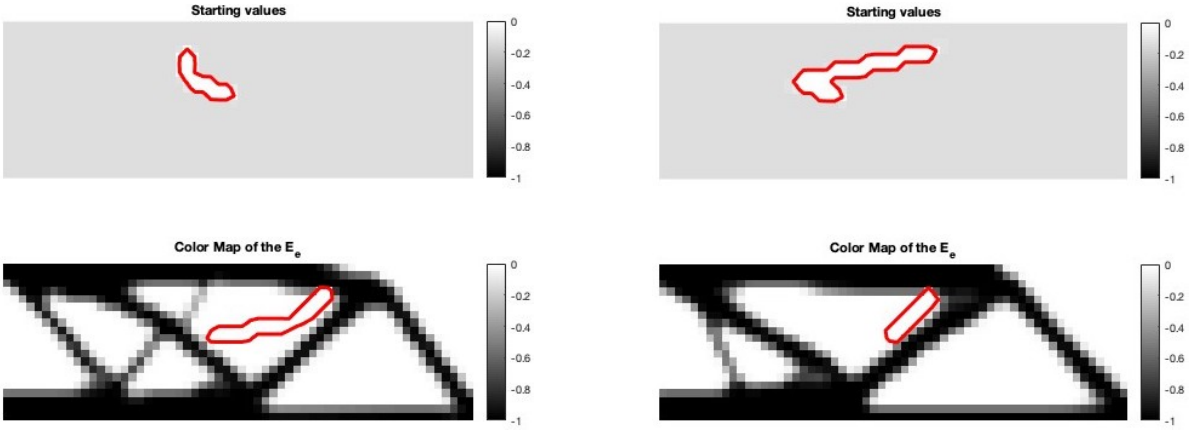

(a) Case 1 - J = 220.20

(b) Case 2 - J = 214.47

Figure 5.4: Optimization of the structure and multiple cut lines

It can be observed the cut line's initial position influences the final optimized layout. The starting position of the cut lines is the same on the y-axis, the only change is the initial values of x_{cut}. The influence was concluded by observing how the change of the x values leads to a different optimization of the cut line and the structure. The reason why there are two results on the same boundary conditions is that the structure has several local optima solutions. A local optimal is a solution which is optimal within a neighbouring set of candidate solutions, and the starting position of the cut lines influences it.

In both cases, the optimizer tries to optimize the structure and the position of the cut lines to not damage them. Therefore, places the cut lines in an area where the density field of the structure is zero. Moreover, the compliance does not differ much between the cases. However, it is higher than in the optimization with no cut lines and some of the cases with the connector and the voids. This is influenced by the position of the cut lines.

Table E.4 shows the starting and optimized values and corresponds to the cases shown in Fig.5.4. Furthermore, intermediate results, only the connector with no voids and more results with the connector with the voids are shown in Appendix. C.2.

5.5. Full optimization, optimizing the structure, cut lines and connectors with voids

This report aims to model a structure, divide it with cut lines, and join the two parts with a non-destructive connection method. Looking at the initial idea where the bolt is shown in Fig. 2.1, some requirements are needed to use a bolt. For example, the value of b_{void} needs to be larger than b_{con} to insert the bolt.

In terms of the vertical length, the connector needs to have a larger value for a_{con} than a_{void} to be able to connect the connector with the structure, and the bolt needs to be smaller than a_{void} to be able to tighten the bolt and the nut with a wrench. A bolt connection is not as strong as a non-divided structure. Therefore, the Young's modulus of the connectors needs to be lower than the structure, however, how weak the bolt connection is depends on the type of connection. There are more parameters and requirements for a bolt, however, in this report, these are the only ones considered.

The next two cases consist of three cut lines and three connectors, each with two voids, one on each side. The initial starting point of the connector on the cut line s_{con} is 0.5, therefore, it will start in the middle of the cut line. The thickness of the cut line, b_{cut}, is set to 1 element. The initial coordinates of the cut lines are $x_{cut} = 48, 72, 60, 60$ elements and $y_{cut} = 0, 12, 28, 40$ elements. These values were chosen randomly.

The value of E_c is lower than one, and the voids' sizes are chosen regarding the connector's size and the requirements mentioned above. Two cases with two sizes for the voids and the connector are tried. In the first case, the connectors' size is 6x2 ($a_{con} \times b_{con}$) elements and the voids size is 2x3 ($a_{void} \times b_{void}$) elements, this is Case 1 on Fig. 5.5a. The value of $E_c = 0.8$. In the second case, the connectors' size is 6x3 ($a_{con} \times b_{con}$) elements and the voids size is 3x4 ($a_{void} \times b_{void}$) elements, this is Case 2 on Fig. 5.5b. The value of $E_c = 0.8$, as in the previous case. These values are assumed to meet the bolt requirement, but this has not been proved. One observation made from these two cases is that both connectors on the bottom are joined together, creating a member of the structure to avoid having a cut line. Furthermore, compared to the previous cases, the full optimization has higher compliance than the other cases, where the cut line or the connector is optimized. This is due to the connection point being weaker and having the full optimization with the cut line, voids and connectors. Looking at the top connector, it can be seen that the optimizer tries to position on an angle so the left void is outside the design domain.

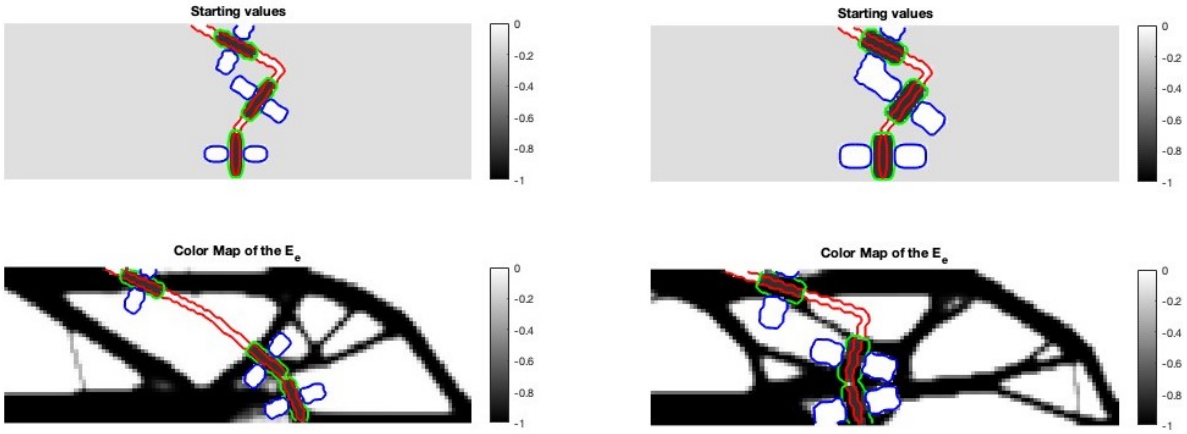

(a) Case 1 - J = 242.88

(b) Case 2 - J = 315.51

Figure 5.5: Optimization considering the bolts requirements

Until now, the structure has always been cut vertically, however, in the following case, the structure is cut horizontally. This case is to observe the difference in the optimized structure. The boundary conditions for the MBB Beam shown in Fig. 5.1b are changed to obtain a horizontal cut. The rotated boundary conditions are shown in Fig. 5.6a, which are the same as before, to obtain the same optimized structure, but rotated so the axis change. This change is because the x_{cut} values are the optimized design variables, and the y_{cut} values are constant for the cut line. The final optimized layout figure in Fig. 5.6b is rotated to have the same orientation as the other layouts. Fig. 5.6b is the optimization of three connectors and cut lines, the size of the connector is 8x3 ($a_{con} \times b_{con}$), and the size of the void is 2x3 ($a_{void} \times b_{void}$). As in the previous two cases, the Young's modulus of the connector is 0.8. The first cut line changes its positioning to have the connector on an angle where it's more beneficial to connect the structure. It can be seen that also, for a horizontal cut line, the method works as intended. In terms of performance, comparing the vertical and horizontal cuts, as most examples are done in the vertical cut, can not be determined which cut is more beneficial, this will need further investigation.

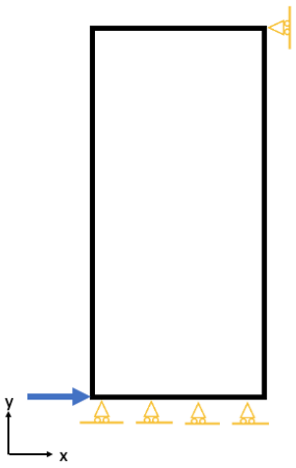

(a) The rotated boundary conditions of the beam

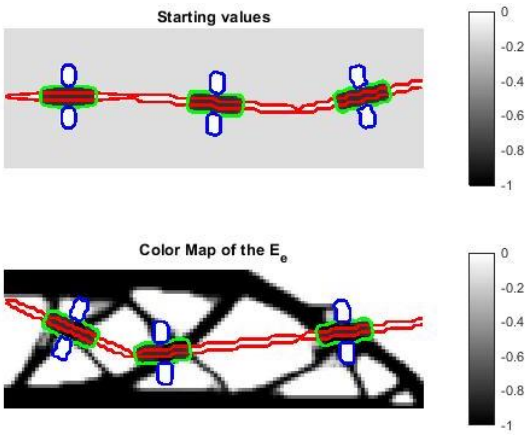

(b) Case 3 - J = 224.96

Figure 5.6: Optimization with a horizontal cut and boundary conditions

5.6. Stopping criteria

As mentioned before, when the full optimizations are performed, the stopping criteria in Eq. 4.42 is not satisfied due to the small oscillations of the cut line and connector. To see the number of iterations, a graph was made to check the changes of it. The case used in Case 1a from the parameter studies is found in Fig. 5.16a. Fig. 5.7 shows the optimization results in different iterations.

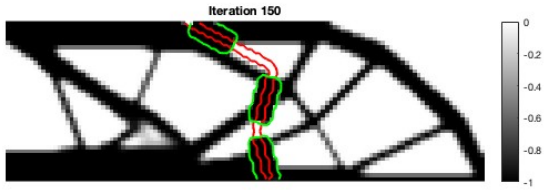

(a) Optimization at 150 iterations

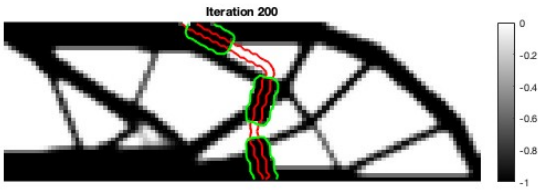

(b) Optimization at 200 iterations

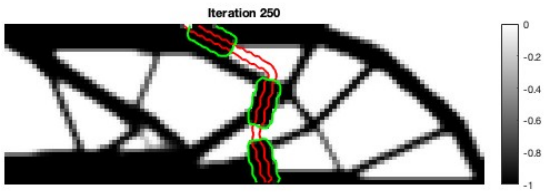

(c) Optimization at 250 iterations

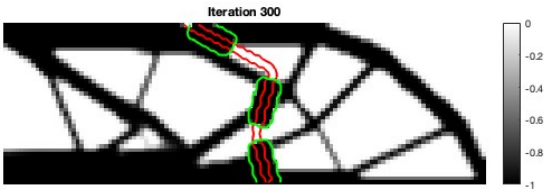

(d) Optimization at 300 iterations

Figure 5.7: Optimizations showing the different number of iterations.

In Fig. 5.7, it can be appreciated that in all the iterations plots, 150, 200, 250 and 300 iterations, the optimized position of the cut line, the connector and the structure is the same. As mentioned, this is due to small oscillations, which create small changes in the density values, preventing the density's convergence. Therefore, stopping the optimization with the number of iterations instead of using Eq. 4.42 will not affect the result. In the previous optimizations, 150 iterations were used to calculate the results. However, in more complex cases, as the full optimization, 200 iterations are used.

The values of the objective function on each iteration are shown in Fig. 5.8. It can be appreciated that the maximum compliance is achieved in the first iteration, then starts decreasing until there are only minor changes. This is around 120 iterations.

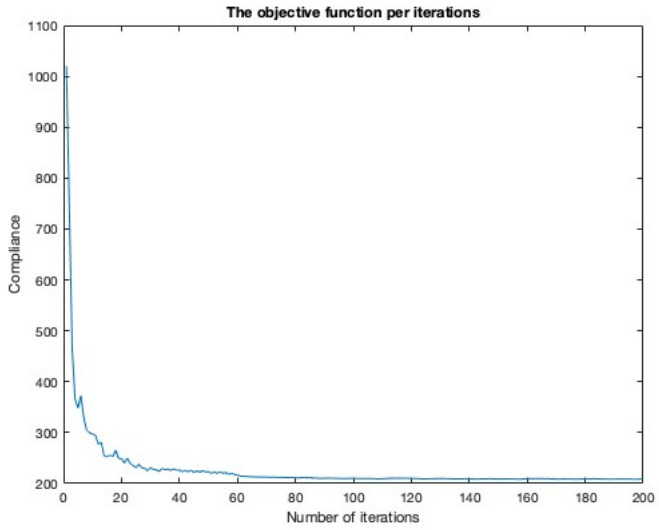

Figure 5.8: Objective function per iteration.

Another stopping criterion was proposed in Eq. 4.43 in the methodology chapter. As mentioned before, with the complete optimization, the convergence criteria using the densities are not satisfied, and a maximum number of loops are set to stop the optimization. Here, the difference between stopping the optimization with a set number of 200 iterations and with Eq. 4.43 is shown. Fig. 5.9 shows both of the cases, stopped by the maximum number of iterations of 200 in Fig. 5.9a, and by the converge equation with the objective function in Fig. 5.9b. The compliance obtained using the maximum number of loops is 210.74, and the compliance using the convergence function is 213.72. The number of iterations in the case with the converge equation is 132, which is a lower number than in the other case. Also, comparing both figures in Fig. 5.9, it can be appreciated that the positioning of the connectors and cut lines are different, which is why compliance is different. Looking at Fig. 5.8, from iteration 90 to iteration 110, the compliance is also constant, and then there is a drop and again constant after iteration 120. The optimization is different, therefore, the number of iterations is different than in Fig. 5.8, but this can be a reason why they are different.

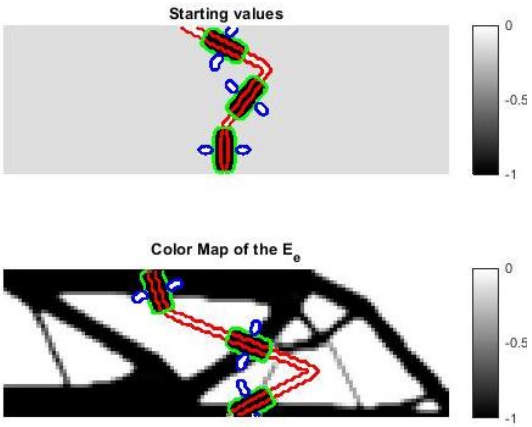

(a) Using a maximum number of loops as the stopping criteria. J = 210.74

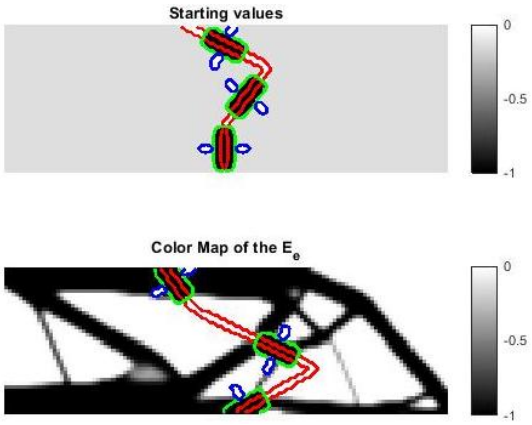

(b) Using the convergence equation for the objective function in Eq. 4.43. J= 213.72

Figure 5.9: Visual comparison on the stopping criteria for the most complete optimization

In all the cases of the full optimization, the maximum number of iterations is used as the stopping method.

5.7. Parameter studies

One observation from the previous optimizations is that the starting position and parameters influence the final optimization. This section aims to see how the parameters and starting values change the final results. The approach taken in this section is to have a reference case, Case 1a in Fig. 5.16a with no voids and Case 1b in Fig. 5.10b with voids. The variables are changed, one per case, to observe what consequences they have on the optimized structure and the influence of the voids.

More detailed parameter studies are done individually to Case 1a and then to Case 1b to observe how the parameters influence with and without voids. The detailed studies are found in Appendix. D.

5.7.1. Reference cases

The first cases in Fig. 5.10 is used as a reference to observe how one change influences the optimization. The initial values for Young's modulus in the first cases is $E_c = 1$. There are three cut lines which will cut the whole structure, the initial coordinates of the cut lines are $x_{cut} = 48, 72, 60, 60$ and $y_{cut} = 0, 12, 28, 40$. The starting point of the connector on the cut line s_{con} is 0.5, therefore, it will start in the middle of the cut line. The connector's size is $a_{con} = 6$ x $b_{con} = 3$ elements. The thickness of the cut line, b_{cut}, is set to 1 element.These values are the same in Case 1a in Fig 5.10a and Case 1b in Fig. 5.10b. In the second reference case, Case 1b, the difference is that the voids are added, the size of the voids is kept constant at $a_{void} = 1$ and $b_{void} = 2$.

The first cases, Case 1a and Case 1b, which are the reference cases, are the following:

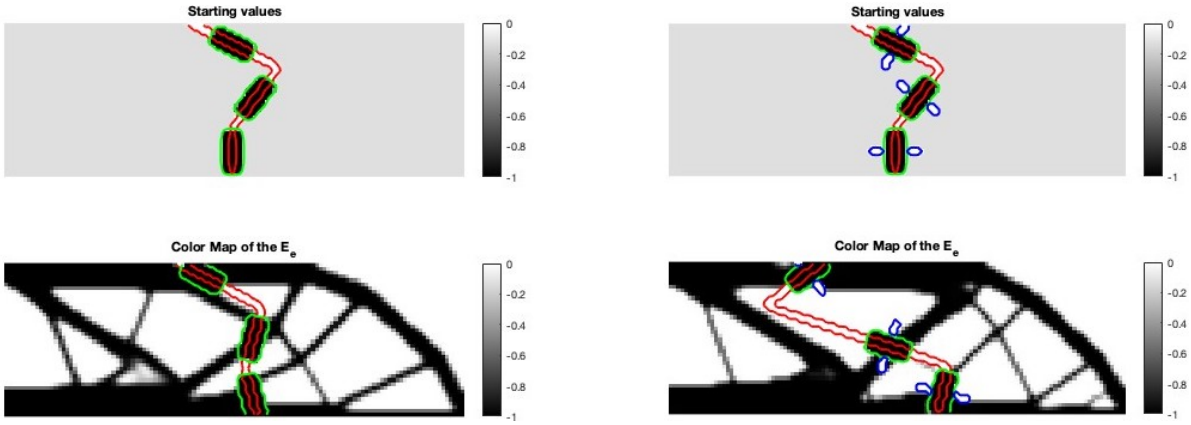

(a) Case 1a - J = 208.92

(b) Case 1b - J = 213.89

Figure 5.10: Reference cases for the parameter studies, one with and one without voids

Comparing both reference cases in Fig. 5.10, the influence of the voids can be observed. Case 1a, without the void, and Case 1b, with the voids, have already different results due to the addition of the voids. Case 1b has higher compliance due to the addition of the voids and the different positioning of the connectors and cut lines on the structure. The main reason for the change is to try to place the voids, not to weaken the structure. Comparing the compliance with the case where the only thing optimized in the structure, in Fig. 5.2b, the compliance is higher in these cases, which was expected from the observation done in the previous cases. In Case 1b, the optimizer chooses a place for the middle connector that is not the most beneficial when looking at the optimized structure, meaning that the expected result would have been at another angle or place. The reason for this positioning is due to the shape of the cut line, as it is a straight line, the optimizer prioritizes positioning the outer connectors in the most beneficial position, making the middle connector not have the most suitable position.

In the following sections, all the a cases will be compared to Case 1a, and the b cases will be compared to Case 1b. Therefore, all the a cases will be without voids, and the b cases will have the same voids size.

5.7.2. Influence of a lower connector's Young's modulus

The first parameter to change is the Young's modulus (E_c) of the connector. There are two main comparisons, one comparing Case 1a and one comparing Case 1b.

In Case 2a (Fig. 5.11b), the value of E_c is 0.5. This change means that now, the connector's Young's modulus is half of the structure one. As it can be appreciated, the different values of E_c affect the positioning of the connectors and the cut lines. The final compliance is also affected. The case with the lowest Young's modulus has higher compliance. This is due to the connector's lower strength. In Case 2a, it can be observed that the structure is under the connector. This is due to the equation of E_e (Eq. 3.19), where the q-norm is used. The optimiser places the connectors on the outer cut lines in the top and bottom members of the structure and the middle connector connecting the structure in the middle. This is what is expected to do as the outer part of the structure is the most important and affects the stiffness of the structure. Another observation is that the final compliance of Case 2a, which has a connector which is half as strong as the structure, still has low compliance. The compliance is only 0.5% higher than in Case 1a and 8.8 % higher than in the original MBB case in Fig.5.2b.

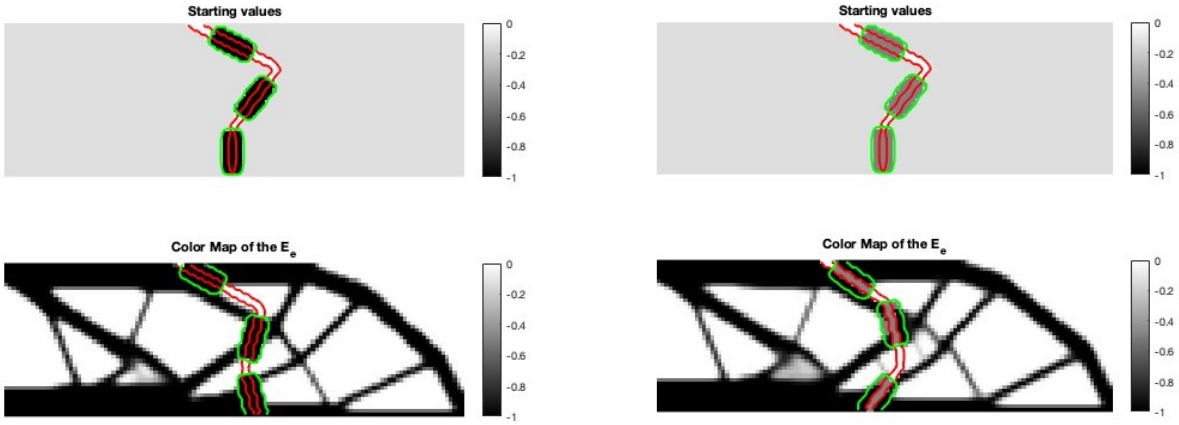

(a) Case 1a - J = 208.92 (b) Case 2a - J = 210.07

Figure 5.11: Comparison of Case 1a to a case with a lower connector's Young's modulus E_c

Case 2b, in Fig. 5.12b, is compared to the reference Case 1b. In this case, the E_c is modified to 0.8, making the connector weaker than the structure. Here, it can be observed that the optimizer tries to join both connectors together to create a beam. They are not overlapping due to the non-overlap constraint in Eq. 4.2. This could be due to the optimizer trying to create a structure member and avoid the cut of the structure while maximising the efficiency of the volume constraint.

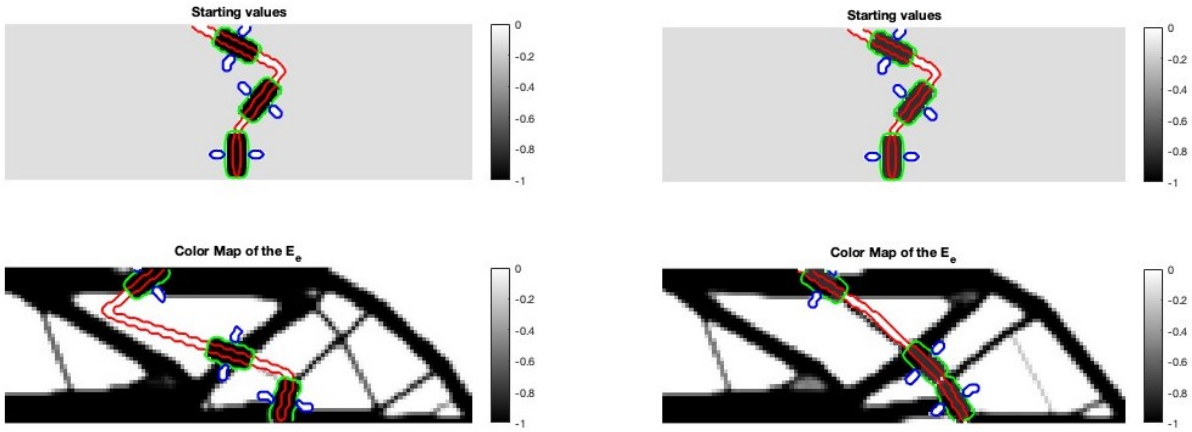

(a) Case 1b - J = 213.89 (b) Case 2b - J = 221.17

Figure 5.12: Comparison of Case 1b to a case with a lower connector's Young's modulus E_c

5.7.3. Influence of the different number of connectors and cut lines

One of the input parameters is the number of cut lines and connectors. In the reference cases, the number of cut lines and connectors is chosen to be three, however, this might not be the optimal number.

In Case 3a (Fig. 5.13a), the number of connectors and cut lines is lower; it only has two. With only two cut lines, the optimizer places the connectors on the top and bottom members of the structure, as they have a big influence on the stiffness of the structure. The number of cut lines and connectors is four in Case 4a in Fig. 5.13c. The connector size is also modified to fit the extra connector. With the addition of a cut line and connector, the compliance increases. An optimized structure with two cut lines and connectors has the lowest compliance.

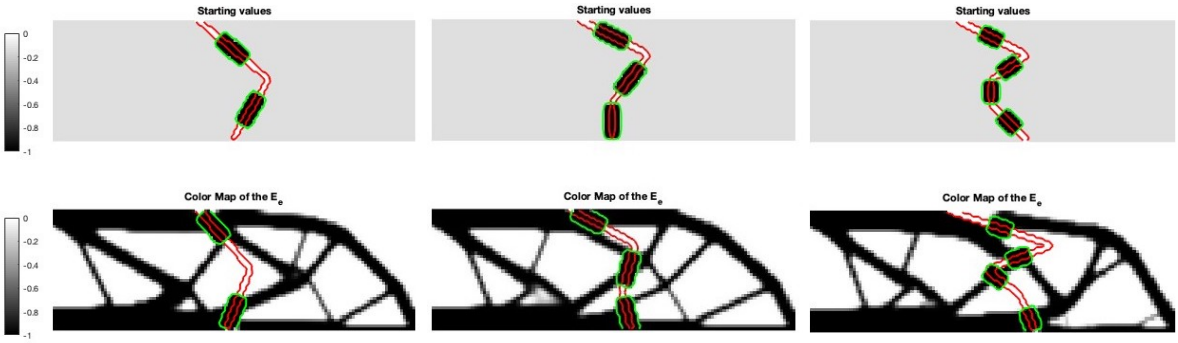

(a) Case 3a - J = 204.87 (b) Case 1a - J = 208.92 (c) Case 4a - J = 220.60

Figure 5.13: Comparison of Case 1a to a case with more connectors and cut lines and a case with only two

As in the previous cases, Fig. 5.14 shows Case 1b with two and four cut lines and connectors. In Case 3b in Fig. 5.14a, the number of cut lines has decreased to two, and the number of connectors and cut lines is four in Case 4b, in Fig. 5.14c. In Case 3b, as in the previous optimization with the two connectors, their position is on the structure's outer members. In Case 4b, as in Case 4a, the connector size is also changed to fit an extra connector and avoid the connector being the same length as the cut line. Due to the voids, the connector's size is not as small as in Case 4a to have an area where the connector can merge with the structure. This case also has the highest final compliance of all these cases. This can be due to the size of the connectors and the higher number of cut lines and connectors, making it more challenging to place them as it is forced to place the voids where it is not beneficial for the stiffness of the structure.

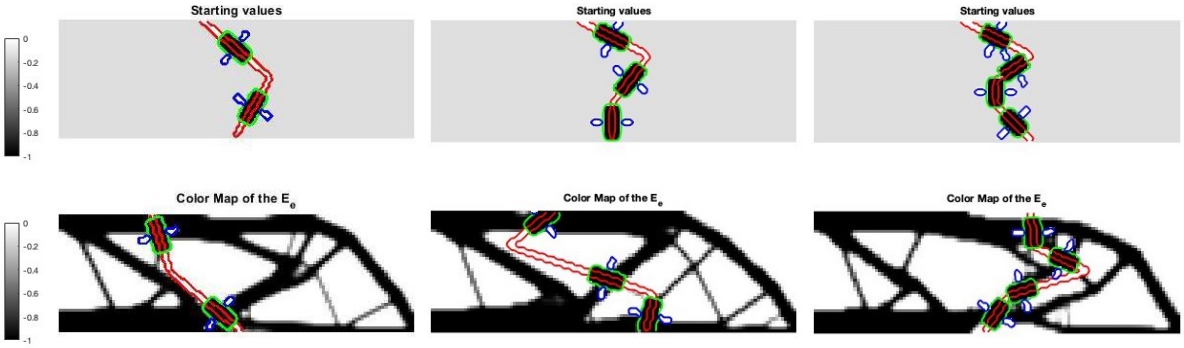

(a) Case 3b - J = 218.37 (b) Case 1b - J = 213.89 (c) Case 4b - J = 251.84

Figure 5.14: Comparison of Case 1b to a case with one more connector and cut lines

5.7.4. Influence of the connector and cut line dimensions

The a and b parameters are the width and length of the connector (a_{con} and b_{con}), and for the cut lines (a_{cut} and b_{cut}). In terms of the cut line, only b_{cut} is a parameter as a_{cut} is dependent on x_{cut}, as shown in Eq. 3.17. For this section, the cases compared are not with the reference case, the comparison is done between the cases with the same change with and without the voids.

Firstly, the thickness of the cut line has been modified. In these cases, the cut line has a thickness of 2 elements, whereas in all the previous cases had a thickness of 1 element. With a cut line with the same thickness as the connector, the top and bottom sides of the connector are no longer able to be used to connect to the structure as a void is forced due to the cut line. In Case 5a, shown in Fig. 5.15a, the other sides of the connector can fully connect to the structure, however, in Case 5b, shown in Fig. 5.15b,

there are two voids, one in each side of the connector, constraining the connection of the connector with the structure. Therefore, the optimizer has it more difficult to make those connections, leading to having voids inside the structural members forced by the position of the connectors in this case. One conclusion is that with thicker cut lines, it is possible to get well-performing designs. Nevertheless, the thickness of the connector must always be larger than the thickness of the cut line, $b_{cut} < b_{con}$ to have a better connection between the structure and the connector.

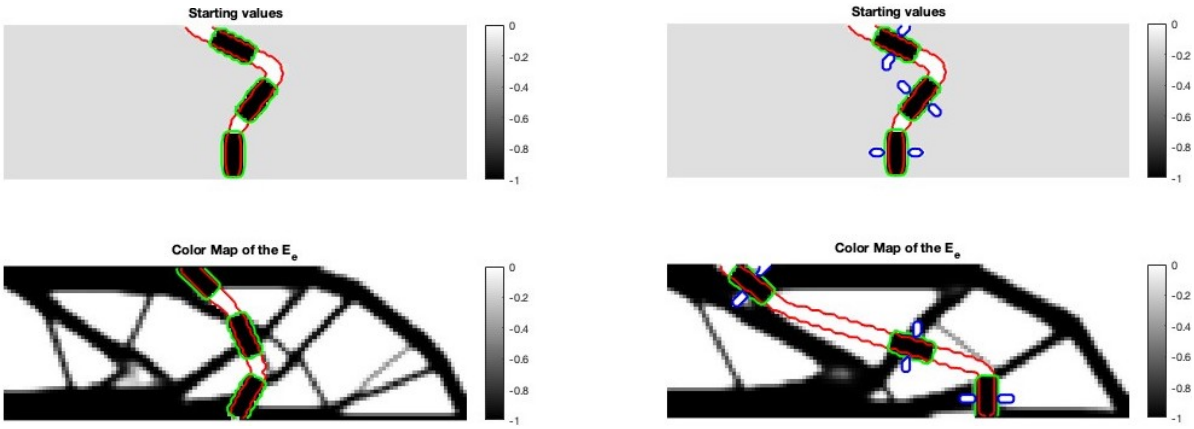

(a) Case 5a - J = 206.99 (b) Case 5b - J = 226.57

Figure 5.15: Observation of the influence of the b_{cut} parameter on Case 1a and Case 1b

Regarding the connectors' size, the parameters that can change are a_{con} and b_{con}. In the first comparison, Case 1a is compared to two different sizes of connectors. Case 6a has smaller connectors, and Case 7a has larger ones than Case 1a. Then, Case 7a is compared to Case 1b with the same connector size, which is Case 7b.

In the first comparison, Case 6a in Fig. 5.16b has smaller connectors in both horizontal and vertical values than Case 1a, and Case 7a in Fig. 5.16c has a larger connector on the horizontal length and the same element length on the vertical side as in Case 6a. The compliance on both increases respect to the first case. Moreover, the structure also changes to accommodate better the changes in the connector's size, which is an expected behaviour. The optimization with larger connectors has lower compliance; it is a 1% increase in Case 1a.

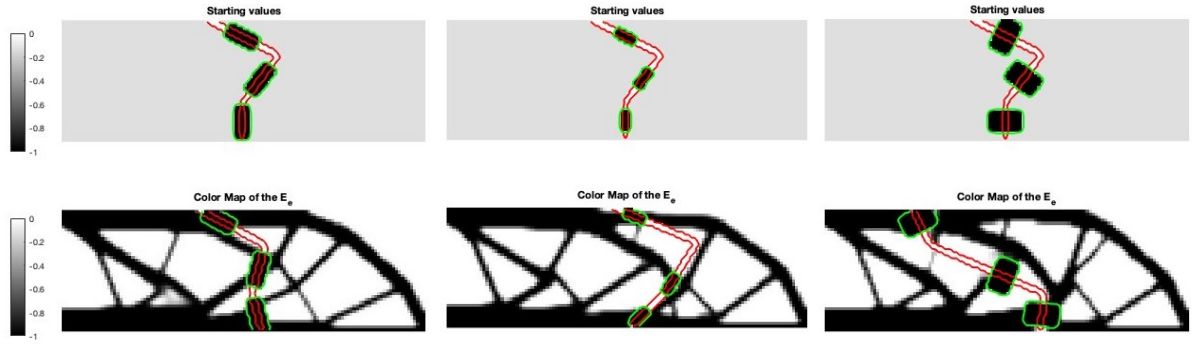

(a) Case 1a - J = 208.92 (b) Case 6a - J = 219.24 (c) Case 7a - J = 213.45

Figure 5.16: Different cases based on Case 1a with different connector's sizes, one bigger, one smaller

As mentioned, the size of the connector of Case 7a (Fig. 5.17a) and in Case 7b (Fig. 5.17b) is the same. The main difference is the voids. Comparing Case 7a and Case 7 b, it can be observed that the position of the cut and connector is similar in both cases. However, it is not the same due to the voids. As mentioned before, the voids in Case 7b constrain the connector's position to prevent one of the voids from damaging the structure with a gap in it.

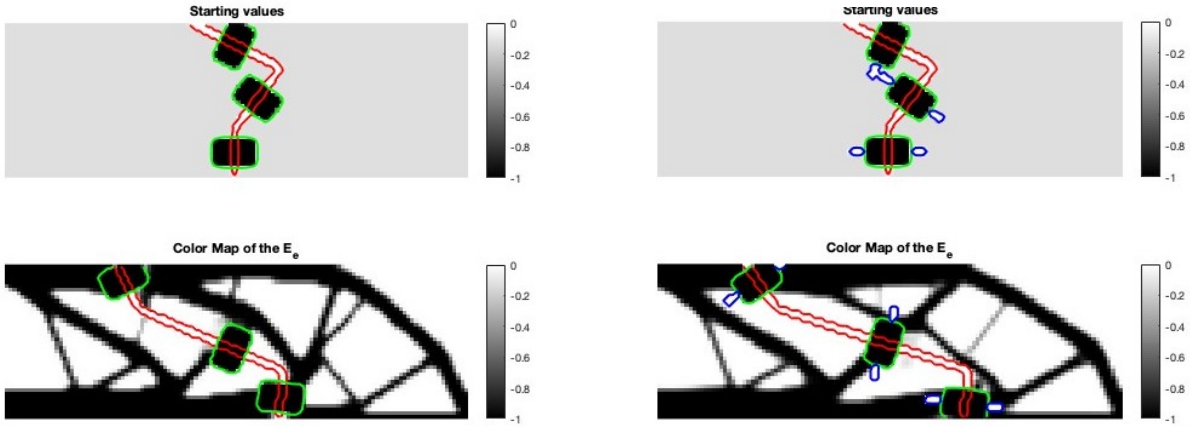

(a) Case 7a - J = 213.45

(b) Case 7b - J = 217.35

Figure 5.17: Change of a_{con} and b_{con}, a case with and a case without voids from the previous comparison.

5.7.5. Influence of the starting position

The position of the cut lines and the connector's position on the cut line are the optimized values. Previously, it was observed that the starting positions do influence the final optimized layout due to having different local optima. In this section, the influence of the starting position is observed.

In Case 8a in Fig. 5.18a and in Case 8b in Fig. 5.18b, the starting position of the cut line is changed to a straight line. In these cases, only the starting position of the cut lines is changed, the starting position of the connector has changed in terms of the coordinates, but it has not changed in terms of s_{con}, the starting point on the cut line.

As expected, the different starting position does affect the final optimized position. It can be observed that compliance is higher in Case 8b, this is due to the voids. A straight starting position gives a lower optimized compliance on Case 8a than the reference case, Case 1a, by a 1.5% and for Case 8b a 1.02% higher than Case 1b.

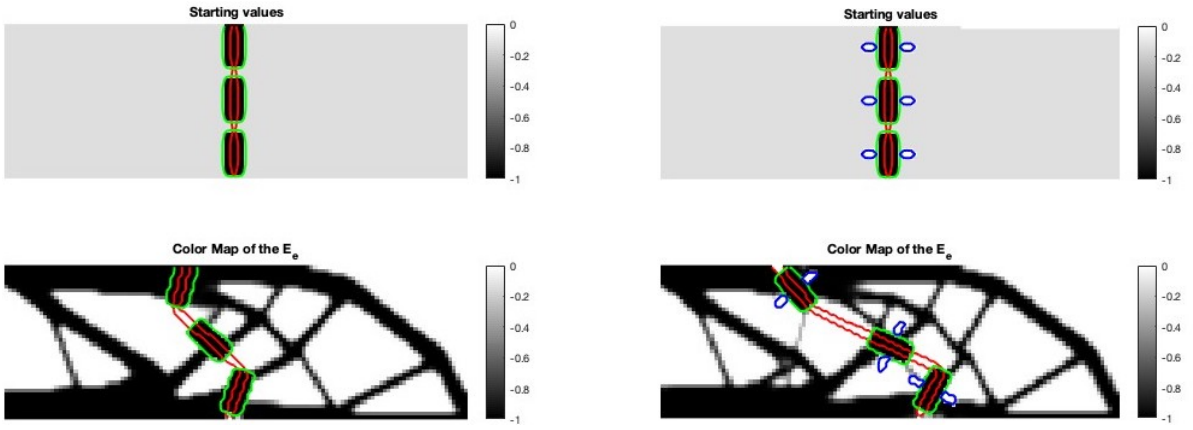

(a) Case 8a - J = 205.85

(b) Case 8b - J = 217.33

Figure 5.18: Optimization of the cut lines with the connectors, with a starting position of a straight line.

In terms of the starting position of the connector in the cut lines, which until now was $s_{con} = 0.5$, which is in the middle of the cut lines, it is now shifted to $s_{con} = 0.7$. This change is observed in Case 9a in Fig. 5.19a and Case 9b in Fig. 5.19b. Where the connector starts at a lower position on the cut line. In Case 9a, the trend observed previously is shown again, the optimizer tries to connect two connectors to form a member of the structure to avoid the cut of the structure. Looking at Fig. 5.19b and focusing on the lower connector, it seems like the optimizer is trying to position it outside the design domain to avoid having the voids affect the structure. This is allowed as the connector is optimized on the middle point, therefore, when $s_{con} = 0$ for the bottom connector and 1 for the top connector, half of the connector is outside the domain.

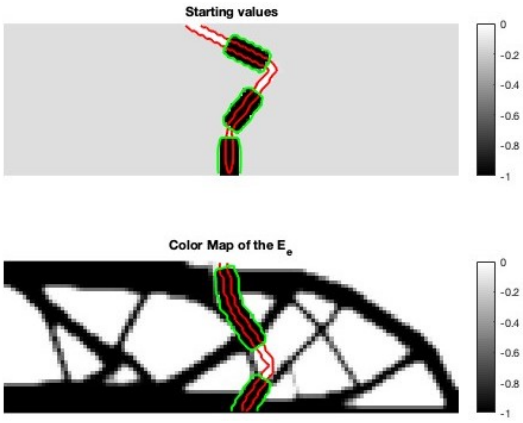

(a) Case 9a- J = 207.53

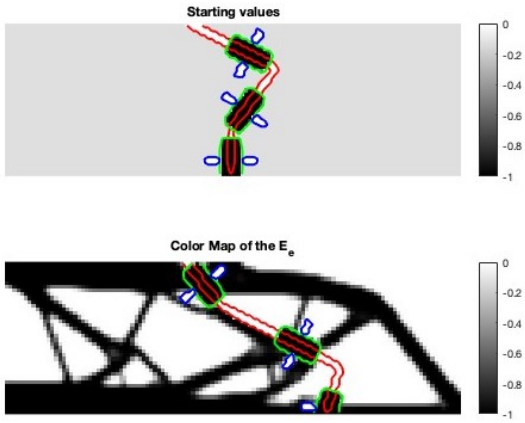

(b) Case 9b - J = 210.89

Figure 5.19: Optimization of the cut lines with the connectors, with a change of s_{con}.

5.7.6. Influence of the void's dimensions

One of the influences observed in the previous cases is that the addition of the voids does influence the final layout and compliance of the optimization. This influence was observed when comparing Case 1a and Case 1b, shown in Fig. 5.10 and in other cases of the parameter study. In this section, the influence and behaviour of the size of the voids are observed by how it influences the optimized layout.

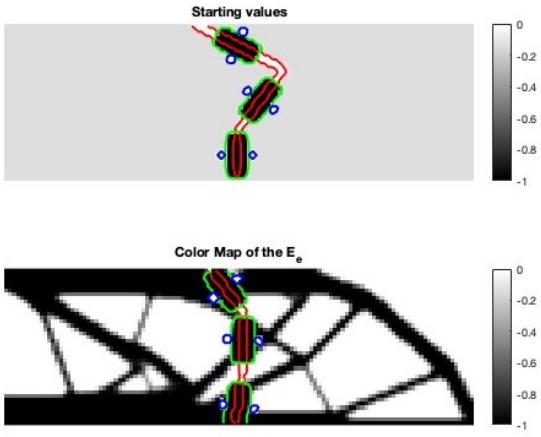

(a) Case 10b - J = 213.14, void size = 1x1 element

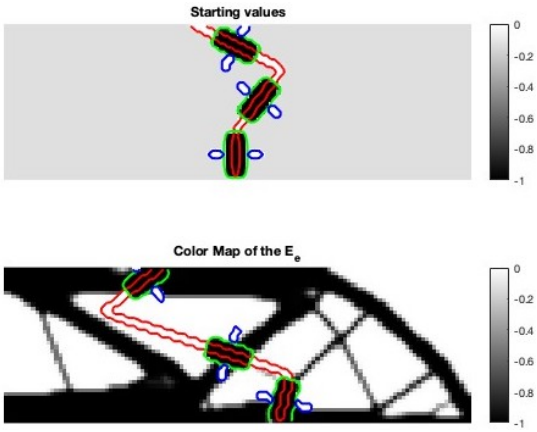

(b) Case 1b - J = 213.89, void size = 1x2 element

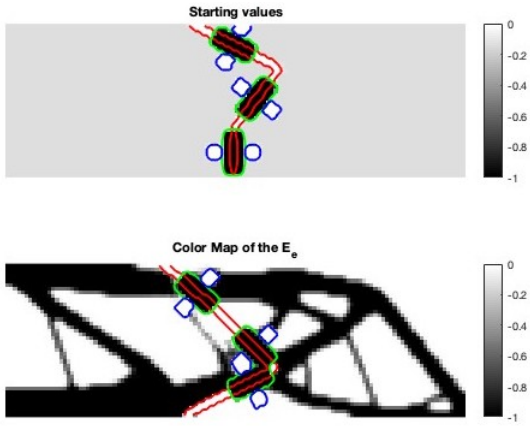

(c) Case 11b - J = 260.80, void size = 2x2 element

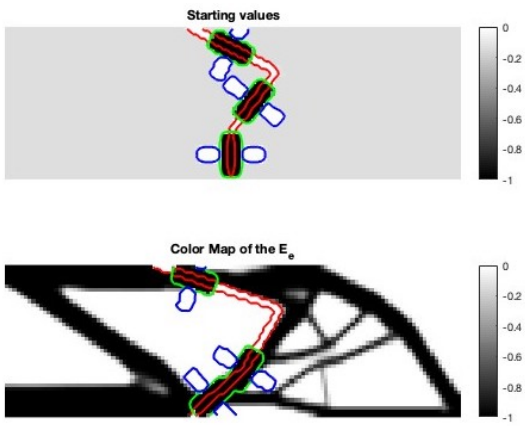

(d) Case 12b - J = 236.76, void size = 2x3 element

Figure 5.20: Effect of varying the dimensions of the voids on the initial reference case, Case 1b

Case 1b and three other cases are shown here. They all have the same starting parameters as in

the reference case, Case 1b. The only parameters modified in each case are a_{void} and b_{void}, the width and length of the voids. In this first case, Case 10b in Fig. 5.20a, the voids have a 1x1 (a_{void} x b_{void}) element size, which creates a small void. The second figure in Fig. 5.20 is Case 1b, which has a void size of 1x2 elements. In the third case, Case 11b in Fig. 5.20c, the void size is double (2x2 element size) than in Case 10b, and in the last case, Case 12b in Fig. 5.20d, the b_{void} is increased by one element, therefore, the voids have a size of 2x3 element. The size of the voids creates a constraint on the optimization, meaning that when the void has larger dimensions, the area where the connector can connect to the structure is limited.

In Case 11b and Case 12b, the optimizer tries to connect the structure and create a structural member with the connectors. This optimizer's behaviour was also observed in previous cases on the parameter study. As mentioned before, this could be due to the optimizer trying to create a structure member and avoid the cut of the structure while maximizing the efficiency of the volume constraint. Furthermore, in Case 11b, it can be observed that two voids of the bottom two connectors are aligned to avoid the voids weakening the structure. The overlapping of the voids is allowed as the voids do not have a no-overlap constraint. If the voids overlap, the bolts could still be taken out.

In Appendix D, there are more cases where the influence of the size of the voids is observed by changing their sizes and other parameters.

5.7.7. Avoiding spurious connections between connectors

The optimizer tends to connect the connectors to create a structure member, as was observed in previous cases. One solution to avoid this can be to restrain the limits of the position of the connector along the cut line. The new limits of s_{con} will change from one to zero to a larger number than a_{con}, which is the length of the connector from the midpoint to the top or bottom side. These limits will avoid the connection.

The solution proposed is tested in Fig. 5.21. Case 1 in Fig. 5.21a is the same as Case 12b in Fig. 5.20d. This case was chosen due to the connection between the connectors. Then, a new optimization was performed with the s_{con} limits as 0.1 and 0.9. The result is shown in Fig. 5.21b. By implementing the limits, the connectors are optimized to a different position, which was expected. The compliance of the case with the limits is higher than in the case without the limits. These new limits also constrain the connectors on the top and bottom cut lines, which does not allow the connectors to be placed on the structure's lower and upper members, which is one of the reasons why the compliance is higher as these members have a significant influence on the structural stiffness.

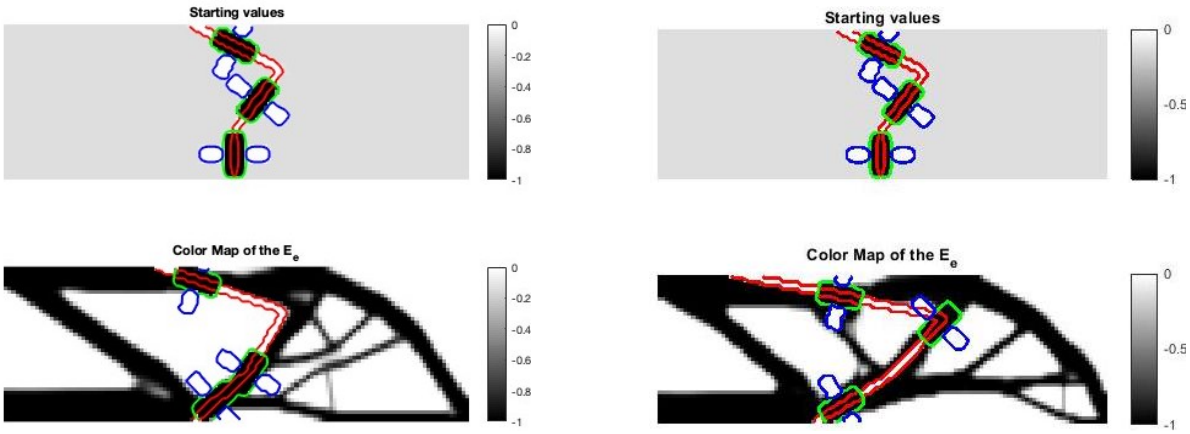

(a) Case 1 - 236.7600 (b) Case 2 - 265.4862

Figure 5.21: Optimization with the constraint s_{con} cannot be 0 or 1, new limits 0.9 and 0.1

Stacking the connectors has yet to be tested to determine whether it is beneficial. More research will need to be done to observe the influence of this. The idea of the connection point is to divide the connector in two and bolt it together. Another approach to the problem, when the connectors create the member on the structure, is to weld the bottom and top of the connectors creating the structural member. These parts must be welded in each part of the structure separately. It will not affect the structure's sustainability as the division line remains.

6

Discussion

In Chapter 5, a few aspects were observed while solving different optimization problems. What the optimizer tends to do and some limitations of the model were observed. Furthermore, some improvements were identified.

Discussion of the different sets of results

In the first set of results, the structure was optimized simultaneously with a connector with two voids. The main observation obtained is that the void's size influences the structure's shape, compliance and the optimized position of the connector. In all the cases, the expected solution was obtained. The expected result is for the optimizer to optimize the position of the connector and the structure to have the connector on a member of the structure and the voids on a section where the density is zero to minimize compliance and not to add extra material as it has the volume fraction constraint.

The second set of results optimized the structure and cut lines simultaneously. From these cases, it was observed that the cut lines' starting position influences the optimized position. Furthermore, as in the previous set of results, the optimized position of the cut lines was expected to be on an area of the optimized structure where the density is zero to avoid weakening the structure. The starting point influences the final optimization due to the optimization having several local optima.

Long et al., 2018 state that local optimum in multi-material topology optimization easily occurs in the SIMP method updated by the MMA algorithm. A local optimum solution is where the objective function is minimized among feasible points. However, it is not guaranteed a lower objective value than all other feasible points (Boyd and Vandenberghe, 2004). Having multiple local optima means that the initial configurations may lead to different optimized designs, which is the case in these optimizations. Having multiple local optima is a limitation of the problem due to not obtaining the global optima in every optimization. In a global optimization, the global optimum solution, which is the true solution of the optimization problem, is found. However, finding the global optimum compromises efficiency. In the optimizations done in this research, as the aim is to develop the initial idea for the optimizations, the global optima solution is not required.

The third set of results is the complete optimization, where the structure is optimized with the cut lines and the connector, with the voids included. In these optimizations, some important requirements for the bolts are considered, such as the space to insert, tighten and remove them. Three cases are presented, two with a vertical cut and one with a horizontal cut. For the vertical cut, an observation is that optimizer tries to place the connector as a structural member. This positioning could be due to the optimizer trying to create a structure member and avoid the cut of the structure while maximizing the efficiency of the volume constraint. These results also have the highest compliance from all the previous cases due to the complete optimization. In the complete optimization, the cut lines and the voids impose a zero density area on the four sides of the connector, the cut line on the top and bottom sides, and the voids on the other sides. The voids on all sides make it more challenging to position the connector.

Discussion of the stopping criteria and parameter studies

Regarding the stopping criteria, with the first two sets of optimizations, one where a connector with its voids is optimized and one where the cut lines are optimized, the stopping method used is the converging equation using the density. However, for the most complex optimizations, the full optimizations and the cases for the parameter studies, a set number of iterations is used as the stopping method. This stopping criterion is not the most accurate as each case might need a different iteration number, some examples might need a higher and some lower. And in this case, the number of iterations was set according to how complex the optimization was. With the starting number basing it on the optimization of several connectors and cut lines without the voids. Another stopping criterion for the complete optimization was tried and compared to the one with the set number of iterations. It was concluded that the maximum number of iterations was more suitable for optimizations due to the results observed in the graph for the compliance over the iteration number. The compliance can be equal in a few numbers of iterations, but then it drops to a lower value. With this criterion, the optimization will stop at not the lowest compliance.

In the parameter study, there are two reference cases, one with voids and one without and the starting position is changed to observe the optimizer's trends and behaviour. Several observations were made, and some are already mentioned as they were already observed in the previous optimization cases.

One of the main observations in the previous cases is that the initial position and parameters are critical and affect the value of the local solution obtained. That is why there are no cases where the final optimization is identical. Predicting how far from the global optima the local solution is challenging.

When optimizing, an observation made is that the outer connectors are optimized to be positioned on the top and bottom members of the structure, these members contribute to the stiffness of the structure. In all the results, the optimizer does what is expected, trying to optimize the structure and place the connector on a solid part of the structure, the cut lines in a structural hole and the voids, when possible, on a structural hole where the density is zero.

Another main observation is that in some cases, the optimizer chooses to position a connector where is not the most beneficial position when looking at the optimized structure. This means the expected result would have been at another angle or place. The reason for this positioning is due to the shape of the cut line. As it is a straight line, in some cases, only some connectors and cut lines can obtain the desired angles or positions due to the connectivity and the influence of the adjacent lines. Changing the cut line definition to allow for more flexibility might reduce this problem.

The parameter study changed the void size to observe its influence on the final optimized result. It was observed that the larger the area the void covers of the connector, the more difficult for the optimizer to position. This difficulty can be due to reducing the area where the connector can connect to the structure, weakening the connection point between the structure and the connector.

In some cases, the optimizer tries to combine connectors to create a limb on the structure and minimize the cut line by maximizing the connection area between the connectors and the cut line. This positioning is because the connector is on the cut line; therefore, if connectors are joined, the cut is minimized. The connector's positioning is always respecting the non-overlap constraint. The non-overlap constraint avoids having the connectors overlap each other. Therefore, in these cases, the connectors are aligned with each other, not over. The cut line also constrains the final positioning of the connectors.

Limitations and improvements

As mentioned, one of the clear solutions the optimizer looks for is to create a limb or a member by stacking two connectors together. One solution can be to limit the position of the connector on the cut line, avoiding it being 0 or 1, so there is always a gap between the connectors. A case with new limits on the s_{con} was tried, and it was observed that by constraining the position of the connector on the cut line, they were also influenced by being unable to position the connector on a limit. For example, the connectors on the outer sides usually tend to be positioned on the outer members of the structure, which usually is done by placing the connectors on the ends of the cut lines, which with the new limits, is not possible. Another approach similar to this method to avoid the connectors stacking together is limiting only the middle components. Another approach that can be taken, which allows the connectors to stack together to create a structure member, is to weld those parts together. The idea is that the

connector is divided into two separate parts and joined with a bolt. Therefore, if two connectors on the same side are together, they can be welded on each separate part to be later connected by bolts. The welding will not affect the product's sustainability, as the part's disassembly will not be affected. Further investigation can be done to determine if the stacking of the connectors needs to be avoided or if they can be welded.

This research aims to answer the research question of how a structure can be divided into different parts by optimizing the position of the cut lines and the connection points simultaneously while optimizing the structure using topology optimization. The approach presented has some limitations, there are some assumptions and design decisions which may need to be more suitable for the optimizations. For example, the void sizes on each side of the connectors are set to be the same size, this may not be needed as the bolt can be inserted on one side, and that void should be larger than the bolt. However, the other side might be adequate without such a large void. Another design decision made is to have a single connector with a single bolt on each cut line. Different numbers of connectors on a cut line might be more beneficial in some cases, or in others, a connector might not be needed on a cut line. Also, it is set for each connector to have a single bolt, but multiple bolts can be used on a single connector. This will also need to include multiple voids on them, two per bolt.

On the full optimization results, it was mentioned that a bolt connection is weaker than having an entire structure. However, the connection's strength depends on many factors, such as the connector size, the bolts used and the type of connection points. For example, the bolt's material, size, diameter, and installation influence the connection point. The stiffness of a connection point is not only determined by the stiffness of the bolt used. It is also determined by the stiffness of the connected parts and the design of the connection points. These and more requirements are needed to model the correct connection stiffness. To achieve the appropriate performance and stiffness of the connection point, proper analysis, design, and selection of the bolted connection type are essential, as well as consideration of the application and desired stiffness requirements.

7

Conclusion

7.1. Conclusion

A new approach was presented in this research to answer the question of how a structure can be divided into different parts by simultaneously optimizing the position of the cut lines and the connection points while optimizing the structure using topology optimization. In the approach presented, the idea is to divide the structure in two and have a connection point where both parts are joined by a bolt, which is a non-destructive disassembly method. The approach taken uses level set functions to model the cut of the structure, as well as the connectors and the voids. Then, they are converted into a density field. A SIMP-motivated method is used to join all the different density fields into an equation for the interpolated elasticity modulus and later optimized using the MMA (Method of Moving Asymptotes) method.

Three final cases with the requirements of the bolts were presented, two with a vertical cut and one with a horizontal cut. In these cases, the optimizer's behaviour could be predicted by the observations made on the parameter studies, where the influence of the initial conditions was observed. The optimization cases and parameter studies identified trends, limitations, and improvements.

This is a new approach where topology optimization and sustainability can be joined by designing for disassembly using bolts as a non-destructive method. The research question is answered on a simple approach, meaning that the main idea of optimizing a structure using topology optimization and simultaneously dividing it and optimizing the connector's position is done. However, there are some limitations on the optimization, as some assumptions and design considerations are not accurate. For example, the stiffness of the connector, which also affects the size of the components and voids, the side of the voids being the same on each side of the connector, or having a single connector on each cut line, which is not proven to be the most optimal solution.

In conclusion, this research introduces a solution to answer the research question presented in the introduction. This approach gives the initial method for developing this idea, which needs further research to obtain accurate results.

7.2. Future work

Recommendations for future work include the following:

- Use a different cut line shape for the optimization. Sometimes, the optimizations were constrained and could not use the more optimal angle due to the cut line being a straight line. As they are connected, they influence each other. Instead of using a straight line, a curved line could be used. This can be achieved by changing the topology description function. This change can also reduce the number of cut lines to one and have more connectors in each cut line.

- Optimize the number of cut lines and the y_{cut}. In this research, the number of cut lines is a user input, optimizing the number of cut lines and their positioning. This can be approached by optimizing the y_{cut} of middle lines, as the outer ones need to be fixed at the edges of the design domain to divide the structure entirely. A new variable must be introduced to optimize

the number of cut lines, and the cut line's position will depend on it. The number of variables is discrete, making this suggestion challenging.

- Optimize the number of connectors. Now, there is a single connector in each cut line; however, it needs to be checked that the optimal number of connectors is over each cut line. This can be done by optimizing the number of components in each cut line, which may lead to having different numbers of components in each cut line. Moreover, in some cases having no component might be the optimal solution. The number of connectors is a discrete number, which creates difficulty.
- Optimize the size of the connector and the voids, respectively. This can be done by optimizing the size of the connector a_{con} and b_{con}. With this change, the minimum requirements for the size of the voids can be stated and be changed as the connectors change. This can be done by changing the values of a_{void} and b_{void} to be dependent on the values of a_{con} and b_{con}. This can be beneficial as, depending on the connector's size and the bolt used, the stiffness of the connection point is different. It might be the case where different connectors' sizes in a structure can be the optimal solution.
- Cut the structure into more than two parts and not only on a vertical line. This recommendation is similar to optimizing the x and y coordinates of the structure, focusing more on vertical and horizontal cuts. The number of parts the structure is divided into could be a user input or an optimized value.
- Changing the stopping criteria. The stopping criterion on the complete optimization is now set to be a fixed iteration number. However, this might not be the most accurate stop criterion in some cases.
- Model the problem in 3D. This paper only uses 2D modelling and a new axis must be added. Therefore, the constraints and the design variables must be adapted to the new dimension. Modelling the problem in 3D will be more challenging. For example, there will be more design requirements in the connection point, such as the bolt size and the type of connection. The cut lines need to become a cut plane, and its position will require two coordinates. The cut plane will also have an angle of rotation of the connector in the cut plane will be another variable introduced.
- The correct stiffness of the connection. As mentioned in the discussion chapter, the stiffness of a connection point depends on many factors. To achieve the appropriate performance and stiffness of the connection point, proper analysis, design, and selection of the bolted connection type are essential, as well as consideration of the application and desired stiffness requirements.
- A different connection method. For this approach, bolts are chosen to be the connection method. However, there are different non-destructive connection methods which can also be used. The requirements for the different types of connections need to be considered to model them.

Bibliography

Andreassen, E., Clausen, A., Schevenels, M., Lazarov, B. S., & Sigmund, O. (2011). Efficient topology optimization in matlab using 88 lines of code. *Structural and Multidisciplinary Optimization*, *43*(1), 1–16. https://doi.org/10.1007/s00158-010-0594-7

Battaia, O., Dolgui, A., Heragu, S. S., Meerkov, S. M., & Tiwari, M. K. (2018). Design for manufacturing and assembly/disassembly: Joint design of products and production systems. https://doi.org/10.1080/00207543.2018.1549795

Bendsøe, M. P. (1989). Optimal shape design as a material distribution problem. *Structural optimization*, *1*(4), 193–202. https://doi.org/10.1007/BF01650949

Bendsøe, M. P., & Sigmund, O. (1999). Material interpolation schemes in topology optimization. *Archive of applied mechanics*, *69*(9), 635–654. https://doi.org/10.1007/s004190050248

Bendsøe, M. P., & Kikuchi, N. (1988). Generating optimal topologies in structural design using a homogenization method. *Computer methods in applied mechanics and engineering*, *71*(2), 197–224. https://doi.org/10.1016/0045-7825(88)90086-2

Boyd, S. P., & Vandenberghe, L. (2004). *Convex optimization*. Cambridge university press. https://doi.org/10.1017/CBO9780511804441

Brennan, L., Gupta, S. M., & Taleb, K. N. (1994). Operations planning issues in an assembly/disassembly environment. *International Journal of Operations & Production Management*. https://doi.org/10.1108/01443579410066767

Bruns, T. E., & Tortorelli, D. A. (2001). Topology optimization of non-linear elastic structures and compliant mechanisms. *Computer methods in applied mechanics and engineering*, *190*(26-27), 3443–3459. https://doi.org/10.1016/S0045-7825(00)00278-4

Castillo, E., Mínguez, R., & Castillo, C. (2008). Sensitivity analysis in optimization and reliability problems. *Reliability Engineering & System Safety*, *93*(12), 1788–1800. https://doi.org/10.1016/j.ress.2008.03.010

Chang, M., Ong, S., & Nee, A. (2017). Approaches and challenges in product disassembly planning for sustainability. *Procedia Cirp*, *60*, 506–511. https://doi.org/10.1016/j.procir.2017.01.013

Chickermance, H., Gea, H. C., Yang, R., & Chuang, C. (1999). Optimal fastener pattern design considering bearing loads. *Structural optimization*, *17*(2), 140–146. https://doi.org/10.1007/BF01195938

Chickermane, H., & Gea, H. C. (1996). Design of multi-component structural systems for optimal layout topology and joint locations. *International Design Engineering Technical Conferences and Computers and Information in Engineering Conference*, *97591*, V003T03A073. https://doi.org/10.1007/BF01200050

Deaton, J. D., & Grandhi, R. V. (2014). A survey of structural and multidisciplinary continuum topology optimization: Post 2000. *Structural and Multidisciplinary Optimization*, *49*(1), 1–38. https://doi.org/10.1007/s00158-013-0956-z

Diaz, A., & Sigmund, O. (1995). Checkerboard patterns in layout optimization. *Structural optimization*, *10*, 40–45. https://doi.org/10.1007/BF01743693

Gielis, J., Shi, P., Beirinckx, B., Caratelli, D., & Ricci, P. (2021). Lamé-gielis curves in biology and geometry. *Proceedings of the Conference Riemannian Geometry and Applications RIGA 2021*.

Guo, X., Zhang, W., & Zhong, W. (2014). Doing topology optimization explicitly and geometrically—a new moving morphable components based framework. *Journal of Applied Mechanics*, *81*(8). https://doi.org/10.1115/1.4027609

Hoang, V.-N., & Jang, G.-W. (2017). Topology optimization using moving morphable bars for versatile thickness control. *Computer Methods in Applied Mechanics and Engineering*, *317*, 153–173. https://doi.org/j.cma.2016.12.004

Imperatives, S. (1987). Report of the world commission on environment and development: Our common future. *Accessed Feb*, *10*, 1–300.

Kang, Z., & Wang, Y. (2013). Integrated topology optimization with embedded movable holes based on combined description by material density and level sets. *Computer methods in applied mechanics and engineering*, *255*, 1–13. https://doi.org/10.1016/j.cma.2012.11.006

Kumar, P., & Saxena, A. (2015). On topology optimization with embedded boundary resolution and smoothing. *Structural and Multidisciplinary Optimization*, *52*, 1135–1159. https://doi.org/10.1007/s00158-015-1272-6

LeVeque, R. (1998). Finite difference methods for differential equations.

Li, Y., Saitou, K., & Kikuchi, N. (2004). Topology optimization of thermally actuated compliant mechanisms considering time-transient effect. *Finite elements in analysis and design*, *40*(11), 1317–1331. https://doi.org/10.1016/j.finel.2003.05.002

Long, K., Wang, X., & Gu, X. (2018). Local optimum in multi-material topology optimization and solution by reciprocal variables. *Structural and Multidisciplinary Optimization*, *57*, 1283–1295. https://doi.org/10.1007/s00158-017-1811-4

Mayyas, A., Qattawi, A., Omar, M., & Shan, D. (2012). Design for sustainability in automotive industry: A comprehensive review. *Renewable and Sustainable Energy Reviews*, *16*(4), 1845–1862. https://doi.org/10.1016/j.rser.2012.01.012

Mlejnek, H. (1992). Some aspects of the genesis of structures. *Structural optimization*, *5*(1), 64–69. https://doi.org/10.1007/BF01744697

Oinonen, A., Tanskanen, P., Björk, T., & Marquis, G. (2010). Pattern optimization of eccentrically loaded multi-fastener joints. *Structural and Multidisciplinary Optimization*, *40*(1), 597–609. https://doi.org/10.1007/s00158-009-0392-2

Osher, S., & Sethian, J. A. (1988). Fronts propagating with curvature-dependent speed: Algorithms based on hamilton-jacobi formulations. *Journal of computational physics*, *79*(1), 12–49. https://doi.org/10.1016/0021-9991(88)90002-2

Pollini, N., & Amir, O. (2020). Mixed projection-and density-based topology optimization with applications to structural assemblies. *Structural and Multidisciplinary Optimization*, *61*(2), 687–710. https://doi.org/10.1007/s00158-019-02390-9

Querol, M. (2021). Sustainable product policy. https://ec.europa.eu/jrc/en/research-topic/sustainable-product-policy

Saeed, N., Long, K., Ansari, J. A., Jaffri, N. R., & Abrar, U. (2021). Implementation of structural assemblies by simultaneous projection and density-based topology optimization. *Journal of Mathematics*, *2021*. https://doi.org/10.1155/2021/8603046

Saxena, A. (2011). Topology design with negative masks using gradient search. *Structural and Multidisciplinary Optimization*, *44*, 629–649. https://doi.org/10.1007/s00158-011-0649-4

Sethian, J. A., & Wiegmann, A. (2000). Structural boundary design via level set and immersed interface methods. *Journal of computational physics*, *163*(2), 489–528. https://doi.org/10.1006/jcph.2000.6581

Shalaby, M., & Saitou, K. (2008). Design for disassembly with high-stiffness heat-reversible locator-snap systems. https://doi.org/10.1115/1.2991134

Sigmund, O. (2001). A 99 line topology optimization code written in matlab. *Structural and multidisciplinary optimization*, *21*(2), 120–127. https://doi.org/10.1007/s001580050176

Sigmund, O., & Petersson, J. (1998). Numerical instabilities in topology optimization: A survey on procedures dealing with checkerboards, mesh-dependencies and local minima. *Structural optimization*, *16*(1), 68–75. https://doi.org/10.1007/BF01214002

Stegmann, J., & Lund, E. (2005). Discrete material optimization of general composite shell structures. *International Journal for Numerical Methods in Engineering*, *62*(14), 2009–2027. https://doi.org/10.1002/nme.1259

Svanberg, K. (1987). The method of moving asymptotes—a new method for structural optimization. *International journal for numerical methods in engineering*, *24*(2), 359–373. https://doi.org/10.1002/nme.1620240207

Usmani, F. (2021). Design for x or dfx: Definition, examples, and uses. https://pmstudycircle.com/design-for-x-dfx/

Wang, X., Hu, P., & Kang, Z. (2020). Layout optimization of continuum structures embedded with movable components and holes simultaneously. *Structural and Multidisciplinary Optimization*, *61*(2), 555–573. https://doi.org/10.1007/s00158-019-02378-5

Wang, X., Long, K., Hoang, V.-N., & Hu, P. (2018). An explicit optimization model for integrated layout design of planar multi-component systems using moving morphable bars. *Computer Methods in Applied Mechanics and Engineering*, *342*, 46–70. https://doi.org/10.1016/j.cma.2018.07.032

Wein, F., Dunning, P. D., & Norato, J. A. (2020). A review on feature-mapping methods for structural optimization. *Structural and multidisciplinary optimization*, *62*, 1597–1638. https://doi.org/10.1007/s00158-020-02649-6

Willems, B., Dewulf, W., & Duflou, J. R. (2006). Concepts and verification model for pressure triggered one-to-many disassembly fasteners. *Proceedings of 13th CIRP International Conference on Life Cycle Engineering*, *2*, 405–410.

Willems, B., Dewulf, W., & Duflou, J. (2007). Active snap-fit development using topology optimization. *International Journal of Production Research*, *45*(18-19), 4163–4187. https://doi.org/10.1080/00207540701440311

Yi, B., & Saitou, K. (2021). Multicomponent topology optimization of functionally graded lattice structures with bulk solid interfaces. *International Journal for Numerical Methods in Engineering*. https://doi.org/10.1002/nme.6700

Zhang, J., Zhang, W., Zhu, J., & Xia, L. (2012). Integrated layout design of multi-component systems using xfem and analytical sensitivity analysis. *Computer methods in applied mechanics and engineering*, *245*, 75–89. https://doi.org/10.1016/j.cma.2012.06.022

Zhang, W., Zhong, W., & Guo, X. (2015). Explicit layout control in optimal design of structural systems with multiple embedding components. *Computer Methods in Applied Mechanics and Engineering*, *290*, 290–313. https://doi.org/10.1016/j.cma.2015.03.007

Zhou, M., & Rozvany, G. (1991). The coc algorithm, part ii: Topological, geometrical and generalized shape optimization. *Computer methods in applied mechanics and engineering*, *89*(1-3), 309–336. https://doi.org/10.1016/0045-7825(91)90046-9

Zhu, J.-H., Zhang, W.-H., & Xia, L. (2016). Topology optimization in aircraft and aerospace structures design. *Archives of Computational Methods in Engineering*, *23*, 595–622. https://doi.org/10.1007/s11831-015-9151-2

A

Appendix

This appendix shows the initial challenge with the filtering, the method used to check the sensitivities and examples with a bar to see how the optimizer works.

A.1. Filtering the optimization

The original code where the material interpolation scheme equation (E_e) was obtained in Wang et al., 2020 uses a sensitivity filter. Furthermore, when changing it to a density filter, the connector and the structure do not connect. Furthermore, there was not a solid connection in the sensitivity filter either. This can be appreciated in Fig. A.1b for the result with a sensitivity filter and Fig. A.1a for a result with a density filter.

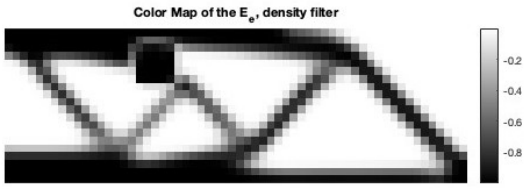

(a) Initial Eq. of E_e with density filter

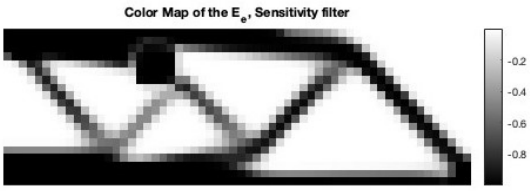

(b) Initial Eq. of E_e with sensitivity filter

Figure A.1: Difference between the filters

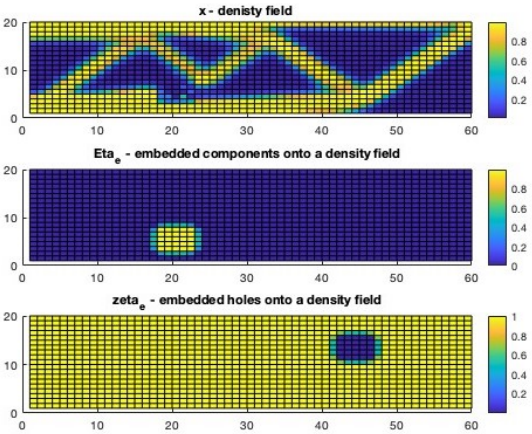

(a) Different fields for density, connector and void. Not connected

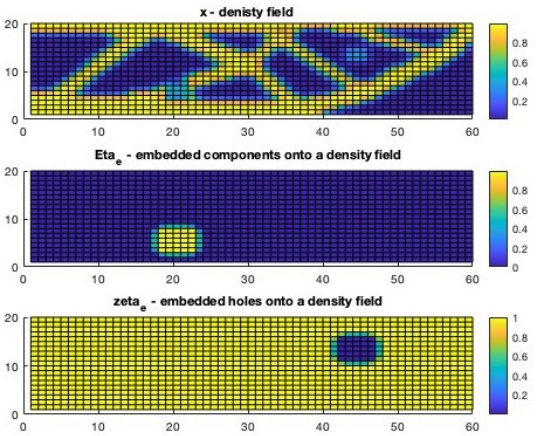

(b) Different fields for density, connector and void. With a connection

Figure A.2: Different fields comparison, with and without the connection

In Fig. A.2a the different fields for the density (ρ), connector (η_e) and void (ζ_e) can be seen. This case is for the density filter. In the density field, it can be seen that there is no material in the area where the connector is; therefore, when both fields are joined, there is a gap between the structure and the connector. This needed to be fixed.

The approach taken to fix this error is to change the equation of E_e. The original equation also creates an error in the finite element analysis due to the low values of E_e. A p-norm was added, which takes the maximum value between the density and the connector field to avoid not having the connection. A E_{min} is also added with a low value, which avoids an error on the finite element analysis by adding a minimum value to the field. In addition, the volume constraint is changed to the new equation, which is similar to the E_e equation.

Once this is changed, a new optimization is performed. Fig. A.3a shows the optimizations, and Fig. A.2b shows the fields. The structure's connection with the connector is visible comparing Fig. A.1a and Fig. A.3a. As well as, if both figures of the fields, Fig. A.2a and Fig. A.2b, are compared, on the density field, there is some density underneath the connector, and this creates a connection between them.

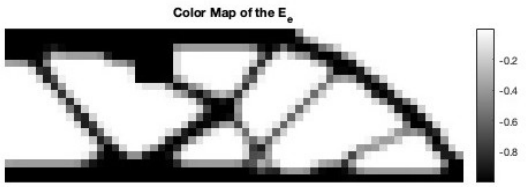

(a) Changed Eq. of E_e with density filter

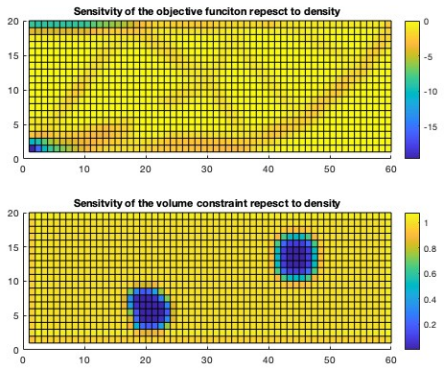

(b) Sensitivities of dV and dJ

Figure A.3: Optimized beam with the changed equation of E_e and its sensitivity graph

Fig. A.3b shows the sensitivities on each element for the sensitivities of the objective function with respect to density (dJ) and the sensitivities of the volume constraint with respect to density.

A.2. Checking the sensitivities

The sensitivities were checked by checking the derivatives using the forward finite difference method. The forward finite difference is one type of finite difference method. The Finite Difference Method (FDM) is one of the methods used to solve differential equations that are difficult or impossible to solve analytically (LeVeque, 1998).

The equation for the forward finite difference method is:

$$f'(x) = \frac{f(x+h) - f(x)}{h} \tag{A.1}$$

where $f'(x)$ is the derivative of a function f at a point x, and h is the perturbation for each variable. After the equations are checked, optimization is done to check that it works visually.

A.2.1. Bar sensitivity checks

The MBB structure can have multiple solutions; therefore, some optimisations on the bar example were checked to check that the optimizations and the sensitivities were working. The bar example uses the MMB Beam structure with a different force, it is like a tensile beam. Comparing the boundary condition of the beam in Fig. A.4a to the MBB beam in Fig. 5.1b, the force is changed. In the bar example, the force is on the right side and in the x direction.

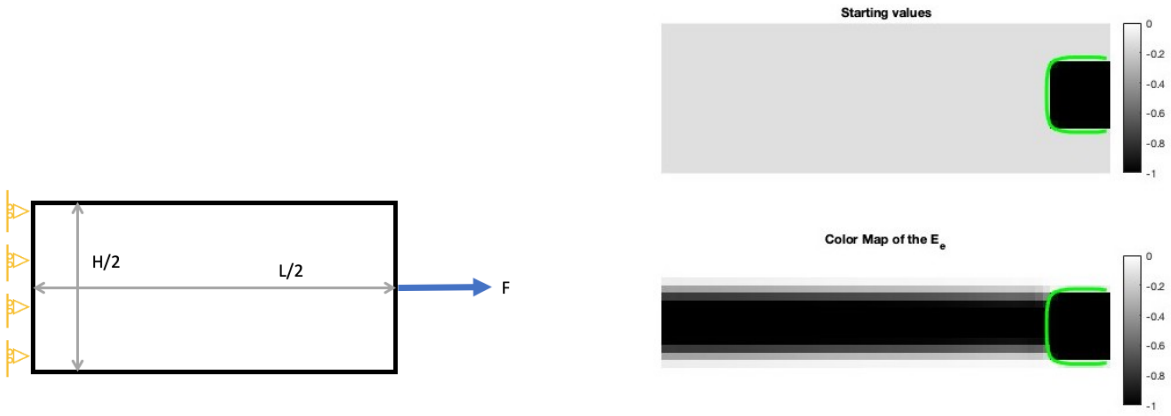

(a) Boundary conditions of the bar example

(b) Optimization where only the density is optimized

Figure A.4: The new boundary conditions and an optimized beam with the changed equation of E_e

The first case optimized in the bar example is the connection between the structure and the component. This case is explained in Section. A.1. In this case, the position of the connector is not optimized.

The following cases show the optimization with the connector. As the aim is to check if the optimizer does what it is meant to do, two different cases are tried. In the first case, a square connector is placed in the upper half of the structure. The connector should move to the optimized bar to check that the optimization works. A similar case as in the previous optimization with the fixed connector. In the following case, to make it more challenging for the optimizer, a long connector is placed with a reduction of the volume constraint to 0.3. This will lead to a thinner optimized bar. The expected position of the connector is to be inside the thin bar. The starting position and optimised layout for both cases are shown in Fig. A.7. The optimized position is what is expected in both cases.

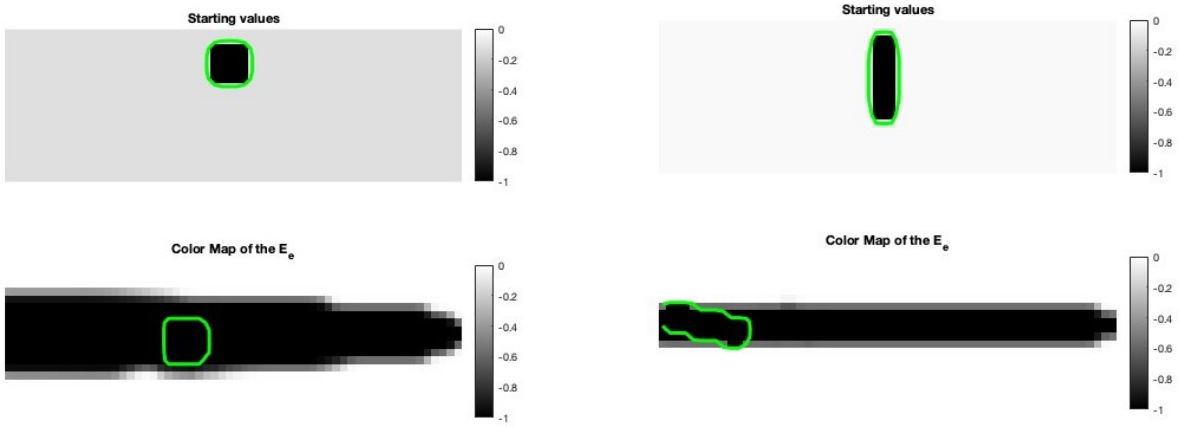

(a) Case 1, optimization of a bar with a connector with a volume constraint of 0.5

(b) Case 3, optimization with a connector with a lower volume constraint

Figure A.5: Bar example with the optimization of the connector

The next step in the optimizations, once the connector is optimized, is the addition of the voids. Again, two different cases were done. In the first case, there is a single void inside the connector. This void is a thin line which influences the component's orientation. The initial and final positions can be appreciated in Fig. A.6a. The expected positioning, the same as the one obtained, is to have the void in the same direction as the bar. The second case is a connector with two voids. The connector size is similar to the bar's thickness. The final result in Fig. A.6b with the connector on the bar and the voids on the sides is expected.

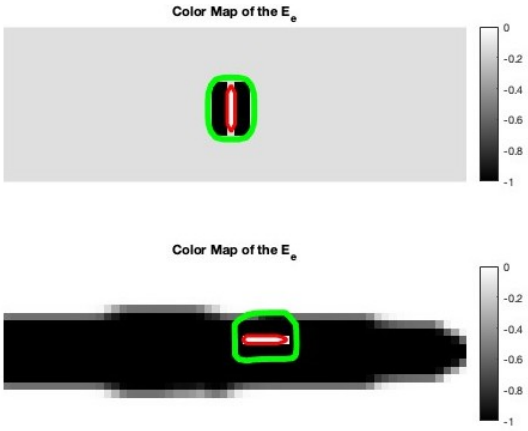

(a) Case 4, optimization with the component and a void in the middle

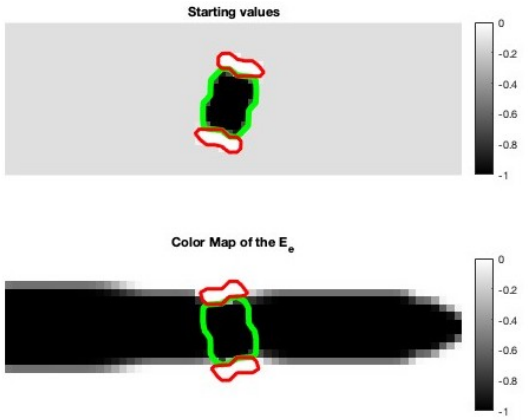

(b) Case 5, optimization with the component two voids on each side

Figure A.6: Bar example with the optimization of the connector and voids

The final trial is to optimize the structure with the cut lines. This is modelled the same as the voids, a zero-density field. Two cases are also tried again. In these optimizations, one primary consideration is that the only optimized values are the x position, and the y coordinate stays constant. This constrains the optimization. Fig. A.7a, Case 6, shows the optimization with two cut lines, and Fig. A.7b, Case 7, shows the optimization with three cut lines. In both optimizations, the bar is separated on the opposite side of where the force is acting, and the cut lines position themselves on the division. This is also an expected behaviour.

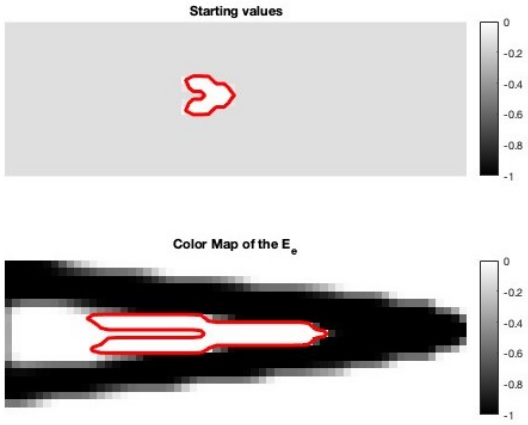

(a) Case 6, optimization with two cut lines

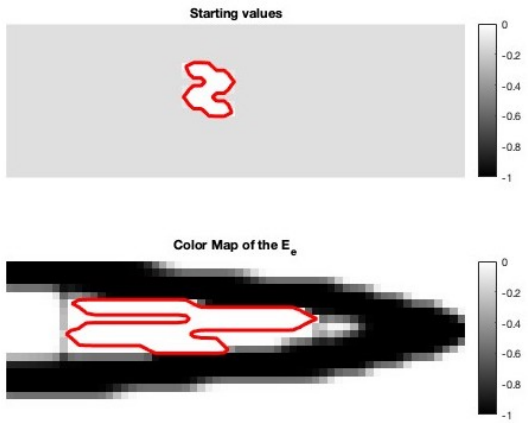

(b) Case 7, optimization with three cut lines

Figure A.7: Bar example with the optimization of cut lines

B

Methodology, optimization problem and sensitivities

The full optimisation is explained in Chapters 3 and 4. However, this chapter shows the optimization problems and the sensitivity analysis of the intermediate optimizations.

B.1. Modelling, optimization problem and sensitivities of the connectors

B.1.1. Material interpolation scheme

The initial elastic interpolation scheme from the paper Wang et al., 2020 is the following:

$$E_e = E(\rho_e, \eta_e) = \rho_e^{p_1}(1-\eta_e^{p_2})E_0 + \eta_e^{p_2}(1-\rho_e^{p_1})E_c \tag{B.1}$$

However, equation B.1 was modified. One of the reasons for this modification is the change of the density $\widetilde{\rho_e}$, due to the filter used, and a q-norm is used to obtain the smooth maximum between the density and the solid connector. E_{min} and ϵ are also added to avoid undercut and errors on the finite element analysis. This is shown in the Eq. 3.10

B.1.2. Optimization problem

To start the optimization problem, it is necessary to optimize the position of the connectors and the topology of the structure, aiming to maximise the stiffness of the overall system. For this purpose, the overall structure's compliance is minimized.

$$Find: \begin{cases} \rho = (\rho_1, \rho_2, ..., \rho_{N_e}) \\ \mathbf{c}_{con_k} = (\mathbf{c}_{con_1}, \mathbf{c}_{con_2}, ..., \mathbf{c}_{con_N c}) \end{cases} \qquad min: J = \mathbf{F}^T\mathbf{U} \tag{B.2}$$

$$S.t. \begin{cases} \mathbf{KU} = \mathbf{F} \\ g_v = \sum_{e=1}^{N_e} E_e V_e - f_1 V_o \leqslant 0 \\ g_c = \sum_{e=1}^{N_e}(1-\zeta_e)V_e - (V_o - \sum_{N_c}^{c=1} V_c) \leqslant 0 \\ 0 \leqslant \rho_e \leqslant 1 \\ c_{min} \leqslant \mathbf{c} \leqslant c_{max} \end{cases} \tag{B.3}$$

where the objective function J can be further expressed as follows:

$$J = \mathbf{U}^T\mathbf{KU} = \sum_{e=1}^{N_e} E_e \mathbf{u}_e^T \mathbf{k}_0 \mathbf{u}_e \tag{B.4}$$

This is explained in the section 4.1. However, as the optimization variables of the connector are different, the changes are explained here. The term **c** introduced in B.2 is the geometric variables vector

which consists of the horizontal and vertical coordinates and the rotation angle against the horizontal of the connectors, **c** is: $c_k = \{x_{con_k}, y_{con_k}, \theta_{con_k}\}$, where $k = (1, 2, ..., N_c)$. Nc is the number of connectors. c_{con_k} also has has a lower (c_{min}) and upper (c_{max}) bounds on the geometry design variable. All the connectors are set to the same values.

B.1.3. Sensitivity analysis

This section introduces the sensitivity analysis for the different design variables and the constraints.

Sensitivity analysis of the objective function with respect to the element relative density variable

The design sensitivities of the objective function with respect to the element relative density variable $\widetilde{\rho}_e$ can be written using the adjoint method as follows:

$$\frac{\delta J}{\delta \widetilde{\rho}_e} = -\frac{\delta E_e}{\delta \widetilde{\rho}_e} * \mathbf{u}_e^T \mathbf{K}_o \mathbf{u}_e \tag{B.5}$$

The result of differentiating the equation E_e (equation B.1) with respect to $\widetilde{\rho}_e$ is equal to:

$$\frac{\delta E_e}{\delta \widetilde{\rho}_e} = \mathrm{E_o}\, p_1\, \widetilde{\rho}_e^{p_1-1} \left((\mathrm{E_c}\, {\eta_e}^{p_2})^q + \left(\epsilon + \mathrm{E_o}\, \widetilde{\rho}_e^{p_1} \right)^q \right)^{\frac{1}{q}-1} \left(\epsilon + \mathrm{E_o}\, \widetilde{\rho}_e^{p_1} \right)^{q-1} \tag{B.6}$$

Sensitivity analysis of the objective function with respect to the geometric variable of connectors

Assuming z_{con_k} represents the design variable $c_{con_k} = \{x_{con_k}, y_{con_k}, \theta_{c_k}\}$ for the k^{th} connector, and each z_{con_k} is a function of $z_{con_{k_{in}}}$. The design sensitivity analysis respect to $z_{con_{k_{in}}}$ is calculated as :

$$\frac{\delta J}{\delta z_{con_{k_{in}}}} = \sum_{e=1}^{N_e} \frac{\delta J}{\delta \eta_e} \frac{\delta \eta_e}{\delta \phi_{con_k}} \frac{\delta \phi_{con_k}}{\delta z_{con_k}} \frac{\delta z_{con_k}}{\delta z_{con_{k_{in}}}} \tag{B.7}$$

where:

$$\frac{\delta J}{\delta \eta_e} = -\frac{\delta E_e}{\delta \eta_e} * \mathbf{u}_e^T \mathbf{k}_0 \mathbf{u}_e \tag{B.8}$$

The result of differentiating the equation E_e (equation B.1) with respect to η_e is equal to:

$$\frac{\delta E_e}{\delta \eta_e} = \mathrm{E_c}\, {\eta_e}^{p_2-1}\, p_2 \left((\mathrm{E_c}\, {\eta_e}^{p_2})^p + \left(\epsilon + \mathrm{E_o}\, \widetilde{\rho}_e^{p_1} \right)^p \right)^{\frac{1}{p}-1} (\mathrm{E_c}\, {\eta_e}^{p_2})^{p-1} \tag{B.9}$$

The derivative of η_e respect to ϕ_{con_k} is obtained by differentiating in Eq. 3.9:

$$\frac{\delta \eta_e}{\delta \phi_{con_k}} = -(1 - \eta_e) \frac{\beta exp(-\beta \phi_{con_k})}{(1 + exp(-\beta \phi_{con_k}))} \tag{B.10}$$

The equation $\frac{\delta \phi_{con_k}}{\delta z_{con_k}}$ is derived from the equation for the topology description function in equation 3.8. They are calculated for each variable $(x, y$ and $\theta_{c_k})$ as follows:

$$\frac{\phi_{con_k}}{\delta z_{con_k}} = 6\left(\frac{\bar{x}}{a}\right)^5 \frac{-cos\theta_{c_k}}{a} + 6\left(\frac{\bar{y}}{b}\right)^5 \frac{sin\theta_{c_k}}{b} \qquad (z_{con_k} = x_{con_k})$$

$$\frac{\phi_{con_k}}{\delta z_{con_k}} = 6\left(\frac{\bar{x}}{a}\right)^5 \frac{-sin\theta_{c_k}}{a} + 6\left(\frac{\bar{y}}{b}\right)^5 \frac{cos\theta_{c_k}}{b} \qquad (z_{con_k} = y_{con_k}) \tag{B.11}$$

$$\frac{\phi_{con_k}}{\delta z_{con_k}} = 6\left(\frac{\bar{x}}{a}\right)^5 \frac{-sin\theta_{c_k}(x - x_o) + cos\theta_{c_k}(y - y_o)}{a}$$
$$+6\left(\frac{\bar{y}}{b}\right)^5 \frac{-cos\theta_{c_k}(x - x_o) + sin\theta_{c_k}(y - y_o)}{b} \qquad (z_{con_k} = \theta_{c_k})$$

The last term of equation is the gradient of z_{con_k} with respect to $z_{con_{k_{in}}}$:

$$\frac{\delta z_{con_k}}{\delta z_{con_{k_{in}}}} = \frac{\delta x_{con}}{\delta x_{con_{in}}} = c_x, \quad \frac{\delta z_{con_k}}{\delta z_{con_{k_{in}}}} = \frac{\delta y_{con}}{\delta y_{con_{in}}} = c_y, \quad \frac{\delta z_{con_k}}{\delta z_{con_{k_{in}}}} = \frac{\delta \theta_c}{\delta \theta_{c_{in}}} = 2\pi \tag{B.12}$$

Sensitivity analysis of the volume constraint with respect to the element relative density variable

This sensitivity analysis involves the constraints g_v stated in equation B.3.
As well as previous ones, they need the derivative with respect to the design variables.
The constraint g_v can be calculated by using the following formula:

$$g_v = \left(\mathrm{E}_{\min} + \left((\epsilon + \mathrm{V}_{\mathrm{eo}}\,\widetilde{\rho}_e)^p + (\mathrm{V}_{\mathrm{ec}}\,\eta_e)^p\right)^{1/p}\right) \tag{B.13}$$

Where V_{eo} is the element volume of the structure and V_{ec} is the element volume of the connectors. The volume for g_v is the entire structure. However, there is no penalisation as in the equation B.1.

$$\frac{\delta g_v}{\delta \widetilde{\rho}_e} = \mathrm{V}_{\mathrm{eo}}\left((\epsilon + \mathrm{V}_{\mathrm{eo}}\,\widetilde{\rho}_e)^p + (\mathrm{V}_{\mathrm{ec}}\,\eta_e)^p\right)^{\frac{1}{p}-1}(\widetilde{\rho}_e + \mathrm{V}_{\mathrm{eo}}\,\widetilde{\rho}_e)^{p-1} \tag{B.14}$$

Sensitivity analysis of the volume constraint with respect to the geometric variable of the connectors

As g_v is also a function of $x_{con_{k_{in}}}, y_{con_{k_{in}}}, \theta_{con_{k_{in}}}$. The gradient of g_v due to the variables must also be calculated. $z_{con_{k_{in}}}$ can be $x_{in}, y_{in}, \theta_{c_k}$

$$\frac{\delta g_v}{\delta z_{con_{k_{in}}}} = \sum_{e=1}^{N_e} \frac{\delta g_v}{\delta \eta_e}\frac{\delta \eta_e}{\delta \phi_{con_k}}\frac{\delta \phi_{con_k}}{\delta z_{con_k}}\frac{\delta z_{con_k}}{\delta z_{con_{k_{in}}}} \tag{B.15}$$

where:

$$\frac{\delta g_v}{\delta \eta_e} = \mathrm{V}_{\mathrm{ec}}\left((\epsilon + \mathrm{V}_{\mathrm{eo}}\,\widetilde{\rho}_e)^p + (\mathrm{V}_{\mathrm{ec}}\,\eta_e)^p\right)^{\frac{1}{p}-1}(\mathrm{V}_{\mathrm{ec}}\,\eta_e)^{p-1} \tag{B.16}$$

and $\frac{\delta \eta_e}{\delta \phi_{con_k}}$, $\frac{\delta \phi_{con_k}}{\delta z_{con_k}}$ and $\frac{\delta z_{con_k}}{\delta z_{con_{k_{in}}}}$ are calculated as mentioned previously in Eq. B.10, Eq. B.11 and eq. B.12 simultaneously.

Sensitivity analysis of the non-overlap constraint respect to the design variables

This sensitivity analysis involves the constraints g_c stated in equation B.3. In terms of the non-overlapping of connector constraint g_c, the sensitivity of the constraints with respect to $z_{con_{k_{in}}}$ can be calculated by the chain rule as follows:

The constraint g_c is;

$$g_c = \sum_{e=1}^{N_e}(1-\eta_e)V_e - (V_o - \sum_{N_c}^{c=1} V_c) \tag{B.17}$$

and its sensitivity is:

$$\frac{\delta g_c}{\delta z_{con_{k_{in}}}} = \sum_{e=1}^{N_e} \frac{\delta g_c}{\delta \eta_e}\frac{\delta \eta_e}{\delta \phi_{con_k}}\frac{\delta \phi_{con_k}}{\delta z_{con_k}}\frac{\delta z_{con_k}}{\delta z_{con_{k_{in}}}} \tag{B.18}$$

where,

$$\frac{\delta g_c}{\delta \eta_e} = -1 \tag{B.19}$$

and where $\frac{\delta \eta_e}{\delta \phi_{con_k}}$, $\frac{\delta \phi_{con_k}}{\delta z_{con_k}}$ and $\frac{\delta z_{con_k}}{\delta z_{con_{k_{in}}}}$ are the same as calculated previously on equations B.10, B.11 and B.12 respectively.

B.2. Modelling, optimization problem and sensitivities of the connectors with the voids

In this section, the changes to the optimization problem as well as the sensitivities due to the addition of the two voids to the connector are shown.

B.2.1. Optimization problem

The position of the voids is not optimized, therefore, the optimization problem stays the same as in the optimization of the connector found in section B.1.2.

B.2.2. Sensitivity analysis

They differ from the previous analysis due to the contribution of the voids, as when the connector is optimised and moves, the voids also move.

Sensitivity analysis of the objective function respect to the element relative density variable

The design sensitivities of the objective function with respect to the element relative density variable $\widetilde{\rho}_e$ can be written using Eq. B.5. Where the result of differentiating the equation E_e (Eq. 3.13) with respect to $\widetilde{\rho}_e$ is equal to:

$$\frac{\delta E_e}{\delta \widetilde{\rho}_e} = \mathrm{E_o}\, p_1\, \widetilde{\rho}_e^{\,p_1-1}\, {\zeta_e}^{p_3} \left((\mathrm{E_c}\, {\eta_e}^{p_2})^q + \left(\epsilon + \mathrm{E_o}\, \widetilde{\rho}_e^{\,p_1}\right)^q \right)^{\frac{1}{q}-1} \left(\epsilon + \mathrm{E_o}\, \widetilde{\rho}_e^{\,p_1}\right)^{q-1} \tag{B.20}$$

Sensitivity analysis of the objective function with respect to the geometric variable of connectors

The two voids at each side of the solid also contribute to the optimization in sensitivities. Equation B.7 has to be modified to add the contribution of the voids. The following equation shows how the contribution is added.

$$\frac{\delta J}{\delta z_{con_{k_{in}}}} = \sum_{e=1}^{N_e} \left(\frac{\delta J}{\delta \eta_e} \frac{\delta \eta_e}{\delta \phi_{con_k}} \frac{\delta \phi_{con_k}}{\delta z_{con_k}} \frac{\delta z_{con_k}}{\delta z_{con_{k_{in}}}} + \sum_{t=2k-1}^{2k} \frac{\delta J}{\delta \zeta_e} \frac{\delta \zeta_e}{\delta \phi_{void_t}} \frac{\delta \phi_{void_t}}{\delta z_{void_t}} \frac{\delta z_{void_t}}{\delta z_{con_k}} \frac{\delta z_{con_k}}{\delta z_{con_{k_{in}}}} \right) \quad \text{(B.21)}$$

The first part is the same as previously calculated in Eq. B.7. The new part is the second part, the summation of the contribution of the voids.

The first equation is the gradient of the objective function with respect to the voids field. This is calculated as shown below.

$$\frac{\delta J}{\delta \zeta_e} = -\frac{\delta E_e}{\delta \zeta_e} * \mathbf{u}_e^T \mathbf{k}_0 \mathbf{u}_e \quad \text{(B.22)}$$

where:

$$\frac{\delta E_e}{\delta \zeta_e} = p_3 \, {\zeta_e}^{p_3 - 1} \left(\mathrm{E_{min}} + \left(\left(\epsilon + \mathrm{E_o} \, \tilde{\rho}_e^{p_1} \right)^q + \left(\mathrm{E_c} \, {\eta_e}^{p_2} \right)^q \right)^{1/q} \right) \quad \text{(B.23)}$$

The second term on the contribution of the voids is the gradient of ζ_e with respect to ϕ_{void_t}.

$$\frac{\delta \zeta_e}{\delta \phi_{void_t}} = \zeta_e \frac{\beta exp(-\beta \phi_{void_t})}{(1 + exp(-\beta \phi_{void_t}))} \quad \text{(B.24)}$$

The derivative of ϕ_{con_k} respect to z_{void_t} is obtained by differentiating Eq. 3.8. The result of this differentiation is the same as in equation B.11.

$$\frac{\delta \phi_{void_t}}{\delta z_{void_t}} = \frac{\delta \phi_{con_k}}{\delta z_{con_k}} \quad \text{(B.25)}$$

The equation of the differentiation of z_{void_t} respect to z_{con_k}. The equations for z_{void_t} are shown in Eq. 3.11.

$$\frac{\delta z_{void_t}}{\delta z_{con_k}} = \frac{\delta x_{void_t}}{\delta x_{con_k}} = 1, \qquad \frac{\delta z_{void_t}}{\delta z_{con_k}} = \frac{\delta y_{void_t}}{\delta y_{con_k}} = 1, \qquad \frac{\delta z_{void_t}}{\delta z_{con_k}} = \frac{\delta \theta_{void_t}}{\delta \theta_{c_k}} = 1 \quad \text{(B.26)}$$

The last term is the differentiation, which is shown in Eq. B.12.

Sensitivity analysis of the volume constraint with respect to the relative density variables

The constraint g_v can be calculated by using the following formula:

$$g_v = \zeta_e \left(\mathrm{E_{min}} + \left((\epsilon + \mathrm{V_{eo}} \, \tilde{\rho}_e)^q + (\mathrm{V_{ec}} \, \eta_e)^q \right)^{1/q} \right) \quad \text{(B.27)}$$

The gradient with respect to the density is the following:

$$\frac{\delta g_v}{\delta \rho_e} = \mathrm{V_{eo}} \, \zeta_e \left((\epsilon + \mathrm{V_{eo}} \, \tilde{\rho}_e)^q + (\mathrm{V_{ec}} \, \eta_e)^q \right)^{\frac{1}{q} - 1} (\tilde{\rho}_e + \mathrm{V_{eo}} \, \tilde{\rho}_e)^{q-1} \quad \text{(B.28)}$$

Sensitivity analysis of the volume constraint with respect to the geometric variable of connectors

This sensitivity analysis involves the constraints g_v stated in B.3. As well as previous ones, they need the derivative with respect to the design variables. As g_v is also a function of $x_{con_{k_{in}}}, y_{con_{k_{in}}}, \theta_{c_{k_{in}}}$. The new equation with the voids contribution is needed for the gradient of g_v due to the addition of the voids. The new equation obtained is:

$$\frac{\delta g_v}{\delta z_{con_{k_{in}}}} = \sum_{e=1}^{N_e} \left(\frac{\delta g_v}{\delta \eta_e} \frac{\delta \eta_e}{\delta \phi_{con_k}} \frac{\delta \phi_{con_k}}{\delta z_{con_k}} \frac{\delta z_{con_k}}{\delta z_{con_{k_{in}}}} + \sum_{t=2k-1}^{2k} \frac{\delta g_v}{\delta \zeta_e} \frac{\delta \zeta_e}{\delta \phi_{void_t}} \frac{\delta \phi_{void_t}}{\delta z_{void_t}} \frac{\delta z_{void_t}}{\delta z_{con_k}} \frac{\delta z_{con_k}}{\delta z_{con_{k_{in}}}} \right) \quad \text{(B.29)}$$

where:

$$\frac{\delta g_v}{\delta \eta_e} = \mathrm{V_{ec}}\,\zeta_e \left((\epsilon + \mathrm{V_{eo}}\,\widetilde{\rho}_e)^q + (\mathrm{V_{ec}}\,\eta_e)^q\right)^{\frac{1}{q}-1} (\mathrm{V_{ec}}\,\eta_e)^{q-1} \tag{B.30}$$

and $\frac{\delta \eta_e}{\delta \phi_{con_k}}$, $\frac{\delta \phi_{con_k}}{\delta z_{con_k}}$ and $\frac{\delta z_{con_k}}{\delta z_{con_{k_{in}}}}$ are calculated as mentioned previously in Eq. B.10, Eq. B.11 and Eq.B.12

where the first term of the contribution of the void is calculated as:

$$\frac{\delta g_v}{\delta \zeta_e} = \mathrm{E_{min}} + \left((\epsilon + \mathrm{V_{eo}}\,\widetilde{\rho}_e)^q + (\mathrm{V_{ec}}\,\eta_e)^q\right)^{1/q} \tag{B.31}$$

The next terms have been calculated previously on equation B.24, B.25, B.26 and B.12.

Sensitivity analysis of the non-overlap constraint respect to the geometric variable of connectors

This sensitivity analysis involves the constraints g_c stated in equation B.3. As the addition of the voids does not change the non-overlapping of connector constraint g_c, the sensitivity of the constraints with respect to $z_{con_{k_{in}}}$ stays the same as in Eq. B.18.

B.3. Modelling, optimization problem and sensitivities of the cut lines

This step shows how the cut lines are modelled and optimized. Here, there is no connector or voids.

B.3.1. Material interpolation scheme

In this part, the equation for E_e is the same as in Eq. 3.19.

B.3.2. Optimization problem

Now, the x position of the cut line is optimized. This changes the optimization from the previous one shown in Eq. B.3.

$$Find: \begin{cases} \rho = (\rho_1, \rho_2, \ldots, \rho_{N_e}) \\ x_{cut} = (x_{cut_1}, x_{cut_2}, \ldots, x_{cut_{nc+1}}) \end{cases} \qquad min: J = F^T U \tag{B.32}$$

where nc is the number of cut lines.

$$S.t. \begin{cases} KU = F \\ g_v = \sum_{e=1}^{N_e} E_e V_e - f_1 V_o \leqslant 0 \\ 0 < \rho_{min} \leqslant \rho_e \leqslant 1 \\ x_{cut_{min}} \leqslant x_{cut} \leqslant x_{cut_{max}} \end{cases} \tag{B.33}$$

where the objective function J can be further expressed as in Eq. B.4:

B.3.3. Sensitivity analysis

In this part, the sensitivity analysis of the cut lines is done.

Sensitivity analysis of objective function respect to the element relative density variable

The design sensitivities of the objective function with respect to the element relative density variable ρ_e is the same as in Eq. B.5. The result of differentiating the equation E_e (Eq. 3.19) with respect to ρ_e is equal the same as in Eq. 4.10.

Sensitivity analysis of volume constraint respect to the element relative density variable

The result of differentiating the equation g_v with respect to $\widetilde{\rho}_e$ is equal to the one calculated on Eq. 4.41.

Sensitivity analysis of objective function respect to the cut line's position
The equation of the derivative of δJ over $x_{cut_{i_{in}}}$ is:

$$\frac{\delta J}{\delta x_{cut_{i_{in}}}} = \sum_{l=i-1}^{i} \sum_{e=1}^{N_e} \frac{\delta J}{\delta \gamma_e} \frac{\delta \gamma_e}{\delta \phi_{cut_l}} \frac{\delta \phi_{cut_l}}{\delta x_{cut_i}} \frac{\delta x_{cut_i}}{\delta x_{cut_{i_{in}}}} \tag{B.34}$$

.

The sensitivity on x_{cut_i}, where two lines have a common point, both cut lines' contribution needs to be added. For example, in Fig. 3.5, for x_{cut_2}, the sensitivities of line one and line two need to be added at point x2. This is added into Eq. B.34 with the summation $\sum_{l=i-1}^{i}$. This means for the i^{th} x_{cut_i}, the contribution of the $l = i - 1$ and $l = i$ are added, where l is the number of the cut line. For the initial point, x_{cut_1} and the last point, $x_{cut_{nc}}$, the contribution is only a single line. The sensitivities of the common x coordinate are not double; they are added as the sensitivities from a single line's top or bottom x coordinate are different. Both lines can have different values for a and θ_{c_k}. The derivatives of $\frac{\delta \theta_{c_k}}{\delta x_{cut_i}}$ and $\frac{\delta a_{con}}{\delta x_{cut_i}}$ are different when l = 1 and 2, as one will be derived as a top cut value and the other as a bottom cut value.

In Eq. B.34, the derivative of the objective function over the cut line field is:

$$\frac{\delta J}{\delta \gamma_e} = -\frac{\delta E_e}{\delta \gamma_e} * \mathbf{u}_e^T \mathbf{k}_0 \mathbf{u}_e \tag{B.35}$$

where:

$$\frac{\delta E_e}{\delta \gamma_e} = \mathrm{E_o}\, p_4\, \widetilde{\rho}_e^{\,p_1}\, \zeta_e{}^{p_3}\, \gamma_e{}^{p_4-1} \left((\mathrm{E_c}\, \eta_e{}^{p_2})^q + \left(\epsilon + \mathrm{E_o}\, \widetilde{\rho}_e^{\,p_1}\, \gamma_e{}^{p_4}\right)^q \right)^{\frac{1}{q}-1} \left(\epsilon + \mathrm{E_o}\, \widetilde{\rho}_e^{\,p_1}\, \gamma_e{}^{p_4}\right)^{q-1} \tag{B.36}$$

Sensitivity analysis of volume constraint respect to the cut line

As with the objective function, the sensitivities of both lines in the common point need to be added.

$$\frac{\delta g_v}{\delta x_{cut_{i_{in}}}} = \sum_{e=1}^{N_e} \frac{\delta g_v}{\delta \gamma_e} \frac{\delta \gamma_e}{\delta \phi_{cut_l}} \frac{\delta \phi_{cut_l}}{\delta x_{cut_i}} \frac{\delta x_{cut_i}}{\delta x_{cut_{i_{in}}}} \tag{B.37}$$

where:

$$\frac{\delta g_v}{\delta \gamma_e} = \zeta_e \left(\gamma_e \left(\epsilon + \mathrm{V_{eo}}\, \widetilde{\rho}_e\right)\right)^{q-1} \left(\left(\gamma_e \left(\epsilon + \mathrm{V_{eo}}\, \widetilde{\rho}_e\right)\right)^q + \left(\mathrm{V_{ec}}\, \eta_e\right)^q \right)^{\frac{1}{q}-1} \left(\epsilon + \mathrm{V_{eo}}\, \widetilde{\rho}_e\right) \tag{B.38}$$

where in both cases, $\frac{\delta \phi_{cut_l}}{\delta x_{cut_i}}$ is equal to:

$$\frac{\delta \phi_{cut_l}}{\delta x_{cut_i}} = \sum_{l=i-1}^{i} \frac{\delta \phi_{cut_l}}{\delta x_{cut_{mid_i}}} \frac{\delta x_{cut_{mid_i}}}{\delta x_{cut_i}} + \frac{\delta \phi_{cut_l}}{\delta \theta_{c_k}} \frac{\delta \theta_{c_k}}{\delta x_{cut_i}} + \frac{\delta \phi_{cut_l}}{\delta a_{cut_l}} \frac{\delta a_{cut_l}}{\delta x_{cut_i}} \tag{B.39}$$

where:

$$\frac{\delta \phi_{cut_l}}{\delta x_{cut_{mid_1}}} = 6 \left(\frac{\bar{x}}{a_{cut_l}}\right)^5 \frac{-cos\theta_{c_k}}{a_{cut_l}} + 6 \left(\frac{\bar{y}}{b_{cut}}\right)^5 \frac{sin\theta_{c_k}}{b_{cut}} \tag{B.40}$$

and

$$\frac{\delta x_{cut_{l_{mid}}}}{\delta x_{cut_i}} = 0.5 \qquad (i = l) \tag{B.41}$$

This derivative of the mid-point is the same for the cut's top and bottom x coordinates.
The topology description function with respect to the angle is:

$$\begin{aligned}\frac{\delta \phi_{cut_l}}{\delta \theta_{ck}} = 6\left(\frac{\bar{x}}{a}\right)^5 \frac{-sin\theta_{c_k}(x - x_o) + cos\theta_{c_k}(y - y_o)}{a} \\ +6\left(\frac{\bar{y}}{b}\right)^5 \frac{-cos\theta_{c_k}(x - x_o) + sin\theta_{c_k}(y - y_o)}{b}\end{aligned} \tag{B.42}$$

for $a = a_{cut_l}$ and $b = b_{cut}$
The angle in Eq.3.16 with respect to the top and bottom x coordinates of a single cut is:

$$\begin{aligned}\frac{\delta \theta_{c_k}}{\delta x_{cut_i}} &= \frac{y_{cut_{i+1}} - y_{cut_i}}{(y_{cut_{i+1}} - y_{cut_i})^2 + (x_{cut_{i+1}} - x_{cut_i})^2} \qquad (\text{for} \quad i = k) \\ \frac{\delta \theta_{c_k}}{\delta x_{cut_i}} &= -\frac{y_{cut_i} - y_{cut_{i-1}}}{(y_{cut_i} - y_{cut_{i-1}})^2 + (x_{cut_i} - x_{cut_{i-1}})^2} \qquad (\text{for} \quad i = k + 1)\end{aligned} \tag{B.43}$$

where k = l.
The first term of the last sum in Eq. B.39, is the length from the mid-point to the cut coordinates a_{cut_l}:

$$\frac{\delta \phi_{cut_l}}{\delta a_{cut_l}} = -\frac{6\,\bar{x}^6}{a_{cut_l}^7} \tag{B.44}$$

The derivative of a_{cut_l} is different with respect to the top ($i = l$) and bottom ($i = l + 1$) x cut line.

$$\begin{aligned}\frac{\delta a_{cut_l}}{\delta x_{cut_i}} &= \frac{2\,x_{cut_i} - 2\,x_{cut_{i+1}}}{4\sqrt{\left(x_{cut_i} - x_{cut_{i+1}}\right)^2 + \left(y_{cut_i} - y_{cut_{i+1}}\right)^2}} \qquad (\text{for} \quad i = l) \\ \frac{\delta a_{cut_l}}{\delta x_{cut_i}} &= -\frac{2\,x_{cut_{i-1}} - 2\,x_{cut_i}}{4\sqrt{\left(x_{cut_{i-1}} - x_{cut_i}\right)^2 + \left(y_{cut_{i-1}} - y_{cut_i}\right)^2}} \qquad (\text{for} \quad i = l + 1)\end{aligned} \tag{B.45}$$

The last term is the derivative of the actual value with respect to the input one. The scaling factor:

$$\frac{\delta x_{cut_i}}{\delta x_{cut_{i_{in}}}} = c_x \tag{B.46}$$

B.4. Modelling and sensitivities of the complete optimization, with the cut lines, connectors and voids

The first optimization shown is the optimization of a cut line with a fixed connector. This means that the connector will always be at the $x_{cut_{l_{mid}}}$ and $y_{cut_{l_{mid}}}$. The angle of the connector will be the same as the angle of the cut.

B.4.1. Optimization of the cut line with fixed connector

As mentioned, the coordinates of the connector are:

$$\begin{aligned}x_{con_k} = x_{cut_{l_{mid}}} = \frac{x_{cut_i} + x_{cut_{i+1}}}{2}, \qquad y_{con_k} = y_{cut_{l_{mid}}} = \frac{y_{cut_i} + y_{cut_{i+1}}}{2} \\ \theta_{con_k} = \theta_{c_k} = tan^{-1}\left(\frac{y_{cut_{i+1}} - y_{cut_i}}{x_{cut_{i+1}} - x_{cut_i}}\right)\end{aligned} \tag{B.47}$$

for i = k.

B.4.1.1 Optimization problem

As the connector in the cut line, the optimization problems do not change from Part 2 in section B.3.2.

B.4.1.2 Sensitivity Analysis

Here the sensitivity analysis is shown. It is not the same as in the previous one, as the contribution of the fixed component needs to be added.

Sensitivity analysis of the objective function respect to the cut line

The new sensitivity of the cut line with respect to the objective function is the following:

$$\frac{\delta J}{\delta x_{cut_{i_{in}}}} = \sum_{e=1}^{N_e} \sum_{l=i-1}^{i} \frac{\delta J}{\delta \gamma_e} \frac{\delta \gamma_e}{\delta \phi_{cut_l}} \frac{\delta \phi_{cut_l}}{\delta x_{cut_i}} \frac{\delta x_{cut_i}}{\delta x_{cut_{i_{in}}}} + \sum_{e=1}^{N_e} \frac{\delta J}{\delta \eta_e} \frac{\delta \eta_e}{\delta \phi_{con_k}} \frac{\delta \phi_{con_k}}{\delta x_{cut_i}} \frac{\delta x_{cut_i}}{\delta x_{cut_{i_{in}}}} \tag{B.48}$$

The previous equation, Eq. B.48, shows the connector's contribution. This contribution is also shown in Eq. B.49.

$$\frac{\delta J}{\delta x_{cut_{i_{in}}}} = \sum_{e=1}^{N_e} \frac{\delta J}{\delta \eta_e} \frac{\delta \eta_e}{\delta \phi_{con_k}} \frac{\delta \phi_{con_k}}{\delta x_{cut_i}} \frac{\delta x_{cut_i}}{\delta x_{cut_{i_{in}}}} \tag{B.49}$$

In Eq. B.49, the terms $\frac{\delta J}{\delta \eta_e}$, $\frac{\delta \eta_e}{\delta \phi_{con_k}}$ and $\frac{\delta x_{cut_i}}{\delta x_{cut_{i_{in}}}}$ are the same as calculated in Eq.B.8 Eq.B.10 and Eq. B.46 respectively.

However, in Eq. B.8, the term $\frac{\delta Ee}{\delta \eta_e}$is changed. This is because the material interpolation scheme is changed to incorporate the cut line (γ_e) term. Therefore, the new differentiation is:

$$\frac{\delta Ee}{\delta \eta_e} = \mathrm{E_c}\, {\eta_e}^{p_2-1}\, p_2\, {\zeta_e}^{p_3} \left(({\mathrm{E_c}\, \eta_e}^{p_2})^q + \left(\epsilon + \mathrm{E_o}\, \tilde{\rho}_e^{p_1}\, {\gamma_e}^{p_4} \right)^q \right)^{\frac{1}{q}-1} ({\mathrm{E_c}\, \eta_e}^{p_2})^{q-1} \tag{B.50}$$

In Eq. B.49, the derivative of ϕ_{con_k} with respect to x_{cut} is the following function.

$$\frac{\delta \phi_{con_k}}{\delta x_{cut_i}} = \sum_{e=1}^{N_e} \frac{\delta \phi_{con_k}}{\delta x_{con_k}} \frac{\delta x_{con_k}}{\delta x_{cut_i}} + \frac{\delta \phi_{con_k}}{\delta \theta_{c_k}} \frac{\delta \theta_{c_k}}{\delta x_{cut_i}} \tag{B.51}$$

ϕ_{con_k} is a function of $\phi_{con_k}(x_{con_k}, y_{con_k}, \theta_{c_k}, a_{con_k}, b_{con_k})$. Where a_{con_k} and b_{con_k} are constant, and $y_{con_k} = y_{cut_{mid}}$, which is also constant in every iteration of the optimization.

In Eq. B.51, the term $\frac{\delta \phi_{con_k}}{\delta x_{con}}$ is equal as in Eq. B.11 for $z_{con_k} = x_o$. The term $\frac{\delta x_{con}}{\delta x_{cut_i}}$ is equal to Eq. B.41 as $x_{con_k} = x_{cut_{mid}}$. The term $\frac{\delta \phi_{con_k}}{\delta \theta_{c_k}}$ is equal as in Eq. B.11 for $z_{con_k} = \theta_{c_k}$. The last term, $\frac{\delta \theta_{c_k}}{\delta x_{cut_i}}$, is the same as B.43, as $\theta_{con_k} = \theta_{cut} = \theta_{c_k}$.

Sensitivity analysis of the volume constraint with respect to the cut line

For the volume constraint, the contribution should also be added. The way it is added is the same as with the objective function. The new equation for the sensitivities concerning the volume is:

$$\frac{\delta g_v}{\delta x_{cut_{i_{in}}}} = \sum_{e=1}^{N_e} \frac{\delta g_v}{\delta \gamma_e} \frac{\delta \gamma_e}{\delta \phi_{cut_l}} \frac{\delta \phi_{cut_l}}{\delta x_{icut}} \frac{\delta x_{icut}}{\delta x_{cut_{i_{in}}}} + \sum_{e=1}^{N_e} \frac{\delta g_v}{\delta \eta_e} \frac{\delta \eta_e}{\delta \phi_{con_k}} \frac{\delta \phi_{con_k}}{\delta z_{con_k}} \frac{\delta z_{con_k}}{\delta x_{i_{cut}}} \frac{\delta_{icut}}{\delta x_{cut_{i_{in}}}} \tag{B.52}$$

The first terms are the same as calculated in Eq B.37. And the contribution is:

$$\frac{\delta g_v}{\delta x_{cut_{i_{in}}}} = \sum_{e=1}^{N_e} \frac{\delta g_v}{\delta \eta_e} \frac{\delta \eta_e}{\delta \phi_{con_k}} \frac{\delta \phi_{con_k}}{\delta x_{cut_i}} \frac{\delta x_{cut_i}}{\delta x_{cut_{i_{in}}}} \tag{B.53}$$

In Eq. B.53, the derivatives of $\frac{\delta \eta_e}{\delta \phi_{con_k}}$, $\frac{\delta \phi_{con_k}}{\delta x_{cut_i}}$ and $\frac{\delta x_{cut_i}}{\delta x_{cut_{i_{in}}}}$ are the same as in the Eq. B.48. The derivative of the volume constraint with respect to term $\frac{\delta gv}{\delta \eta_e}$ is:

$$\frac{\delta g_v}{\delta \eta_e} = \mathrm{V_{ec}}\, \zeta_e\, (\mathrm{V_{ec}}\, \eta_e)^{q-1} \left((\epsilon + \mathrm{V_{eo}}\, \widetilde{\rho}_e\, \gamma_e)^q + (\mathrm{V_{ec}}\, \eta_e)^q \right)^{\frac{1}{q}-1} \tag{B.54}$$

B.4.2. Optimization of a cut line with movable a connector

Here, a cut line is optimized at the same time as the position of the connector on the cut line.

B.4.2.1 Sensitivity analysis

Sensitivity analysis of objective function respect to the cut line

The main equation of the $\frac{\delta J}{\delta x_{cut_{i_{in}}}}$ stays the same as in Eq. B.48. However, now the x_{con_k} is not equal to the mid-point of the cut line, and now the y_{con_k} is also optimized, therefore, has a contribution. This makes the term $\frac{\delta \phi_{con_k}}{\delta x_{cut_i}}$ change. The new equation is:

$$\frac{\delta \phi_{con_k}}{\delta x_{cut_i}} = \sum_{e=1}^{N_e} \frac{\delta \phi_{con_k}}{\delta x_{con_k}} \frac{\delta x_{con_k}}{\delta x_{cut_i}} + \frac{\delta \phi_{con_k}}{\delta y_{con_k}} \frac{\delta y_{con_k}}{\delta x_{cut_i}} + \frac{\delta \phi_{con_k}}{\delta \theta_{c_k}} \frac{\delta \theta_{c_k}}{\delta x_{cut_i}} \tag{B.55}$$

In Eq. B.55, the first two terms $\frac{\delta \phi_{con_k}}{\delta x_{con_k}}$, $\frac{\delta \phi_{con_k}}{\delta y_{con_k}}$ and $\frac{\delta \phi_{con_k}}{\delta \theta_{c_k}}$ are equal as in Eq. B.11 for $z_{con_k} = x_o$, $z_{con_k} = y_o$ and $\theta_{c_k} = y_o$ simultaneously. The other terms are the same as previously calculated in Eq. B.51. The new terms in Eq. B.55 are:

$$\frac{\delta x_{con_k}}{\delta x_{cut_i}} = 1 - s_{con_k} \quad (\text{for } i = k) \qquad \frac{\delta x_{con_k}}{\delta x_{cut_i}} = s_{con_k} \quad (\text{for } i = k+1) \tag{B.56}$$

And for the y values :

$$\frac{\delta y_{con_k}}{\delta x_{cut_i}} = 1 - s_{con_k} \quad (\text{for } i = k) \qquad \frac{\delta y_{con_k}}{\delta x_{cut_i}} = s_{con_k} \quad (\text{for } i = k+1) \tag{B.57}$$

Sensitivity analysis of volume constraint respect to the cut line

The main equation of the $\frac{\delta gv}{\delta x_{cut_{i_{in}}}}$ stays the same as in Eq. B.52. Due to the same reasoning as in the previous section with the objective function, the term $\frac{\delta \phi_{con_k}}{\delta x_{cut_i}}$ change to the same term as in Eq. B.55.

Sensitivity analysis of objective function respect to the connector

As the position of the connector on the cut line is optimized. A new sensitivity analysis for the s_{con_k} is needed.

$$\frac{\delta J}{\delta s_{con_k}} = \sum_{e=1}^{N_e} \frac{\delta J}{\delta \eta_e} \frac{\delta \eta_e}{\delta \phi_{con_k}} \frac{\delta \phi_{con_k}}{\delta s_{con_k}} \tag{B.58}$$

Where each term can be found in Eq. B.50 Eq. B.10. The term $\frac{\delta \phi_{con_k}}{\delta s_{con_k}}$ is calculated:

$$\frac{\delta \phi_{con_k}}{\delta s_{con_k}} = \sum_{e=1}^{N_e} \frac{\delta \phi_{con_k}}{\delta x_{con_k}} \frac{\delta y_{con_k}}{\delta s_{con_k}} + \frac{\delta \phi_{con_k}}{\delta y_{con_k}} \frac{\delta y_{con_k}}{\delta s_{con_k}} \tag{B.59}$$

and the derivative of x_{con_k} respect to s_{con_k} is equal to:

$$\frac{\delta x_{con_k}}{\delta s_{con_k}} = x_{cut_{i+1}} - x_{cut_i} \tag{B.60}$$

for i = k

and the derivative of y_{con_k} respect to s_{con_k} is equal to:

$$\frac{\delta y_{con_k}}{\delta s_{con_k}} = y_{cut_{i+1}} - y_{cut_i} \tag{B.61}$$

for i = k

Sensitivity analysis of volume constraint respect to the connector
here how the sensitivities of the position of volume constraint respect to the position of the connector

$$\frac{\delta gv}{\delta s_{con_k}} = \sum_{e=1}^{N_e} \frac{\delta gv}{\delta \eta_e} \frac{\delta \eta_e}{\delta \phi_{con_k}} \frac{\delta \phi_{con_k}}{\delta s_{con_k}} \tag{B.62}$$

Where each term can be found in Eq. B.54 Eq. B.10 and Eq. B.55

B.4.3. Addition of the voids

The optimization problem and the equation of E_e stay as in the previous optimization.

B.4.3.1 Continuation of the sensitivity analysis from main report

Here shows the continuity of the sensitivity analysis mentioned on 4.2.6. The previous sensitivity analysis is shown at 4.2.

Sensitivity analysis of the volume constraint with respect to the cut line

As well as with the objective function, the holes have contributed to the volume constraint.

$$\frac{\delta g_v}{\delta x_{cut_{i_{in}}}} = \sum_{e=1}^{N_e} \frac{\delta J}{\delta \gamma_e} \frac{\delta \gamma_e}{\delta x_{cut_{i_{in}}}} + \sum_{e=1}^{N_e} \frac{\delta J}{\delta \eta_e} \frac{\delta \eta_e}{\delta x_{cut_{i_{in}}}} + \sum_{e=1}^{N_e} \frac{\delta J}{\delta \zeta_e} \frac{\delta \zeta_e}{\delta x_{cut_{i_{in}}}} \tag{B.63}$$

Where $\frac{\delta \gamma_e}{\delta x_{cut_{i_{in}}}}$ is the same as in Eq. 4.16, $\frac{\delta \eta_e}{\delta x_{cut_{i_{in}}}}$ is the same as in Eq. 4.26 and $\frac{\delta \zeta_e}{\delta x_{cut_{i_{in}}}}$ is the same as in Eq. 4.30.

In Eq. B.63 all the sums, the terms $\frac{\delta g_v}{\delta \gamma_e}$ and $\frac{\delta g_v}{\delta \eta_{con}}$ have already been calculated, $\frac{\delta g_v}{\delta \eta_e}$ is shown on Eq. B.54. $\frac{\delta g_v}{\delta \gamma_e}$ is shown on B.38. And $\frac{\delta g_v}{\delta \zeta_e}$ is the following:

$$\frac{\delta g_v}{\delta \zeta_e} = \left((\epsilon + \mathrm{V_{eo}}\, \tilde{\rho}_e, \gamma_e)^q + (\mathrm{V_{ec}}\, \eta_e)^q \right)^{1/q} \tag{B.64}$$

Sensitivity analysis of the volume constraint with respect to the connector
The gradient of the volume constraint with respect to the connector's position on the cut line is shown here.

$$\frac{\delta g_v}{\delta s_{con_k}} = \sum_{e=1}^{N_e} \frac{\delta g_v}{\delta \eta_e} \frac{\delta \eta_e}{\delta \phi_{con_k}} \frac{\delta \phi_{con_k}}{\delta s_{con_k}} + \sum_{e=1}^{N_e} \frac{\delta J}{\delta \zeta_e} \frac{\delta \zeta_e}{\delta \phi_{void_t}} \frac{\delta \phi_{void_t}}{\delta s_{con_k}} \tag{B.65}$$

The terms $\frac{\delta \eta_e}{\delta \phi_{con_k}}$, $\frac{\delta \phi_{con_k}}{\delta s_{con_k}}$, $\frac{\delta \zeta_e}{\delta \phi_{void_t}}$ and $\frac{\delta \phi_{void_t}}{\delta s_{con_k}}$ are the same as in Eq. 4.36. The derivative of the volume constraint over η_e is shown in Eq. B.54, and the derivative over ζ_e is shown in Eq. B.64.

Sensitivity analysis of the non-overlap constraint with respect to the connector

The non-overlap constraint does not affect the cut line, the density or the voids. Therefore, the sensitivity analysis is only with the connector.

$$\frac{\delta g_c}{\delta s_{con}} = \sum_{e=1}^{N_e} \frac{\delta g_c}{\delta \eta_e} \frac{\delta \eta_e}{\delta \phi_{con_k}} \frac{\delta \phi_{con_k}}{\delta s_{con}} \tag{B.66}$$

The gradient of the non-overlap constraint with respect to η_e is -1. The second term is found on Eq. B.10, for $\phi = \phi_{con}$. And the last term of the differentiation is equal to the one calculated in Eq. B.59.

C

Extra results

In this chapter, more examples of optimizations are shown for the two first steps. In the main part, the final solutions are shown, here, the intermediate solutions and more other final solutions are shown.

C.1. Results for the optimization of the structure and the connector, with and without voids

First, the optimization is done only with a connector, followed by a connector with two voids.

C.1.1. Optimization of the structure with a single connector with no void

Different optimizations were performed in different conditions to prove that the optimization problems gave a reasonable solution. Due to the optimization problem and the conditions, several final positions could seem to give reasonable solutions for each initial condition. This is due to the optimization having several local optima.

In the first case (Fig.C.1a), the connector is placed in the middle of the part. The initial position is changed in the second case (Fig.C.1b). If both images are compared, one conclusion is that the connector's initial positioning influences the connector's final positioning and the initial and final compliance.

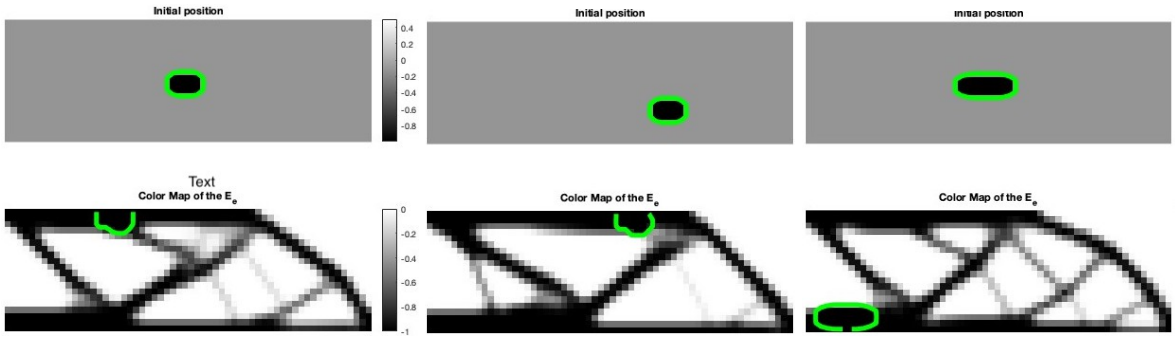

(a) Case 1- J = 223.14 (b) Case 2- J = 218.98 (c) Case 3- 223.31

Figure C.1: Optimization of the structure with a single connector

In Case 3 (Fig.C.1c) and Case 5 (Fig.C.2b), the size of the connector is changed. This also gives different positioning of the connectors and different structures. Case 4 (Fig.C.2a) has a finer mesh, 100x60 elements. Finally, in Case 6 (Fig.C.2c) and Case 7 (Fig.C.2d), try the different initial connector angles. One observation is that the optimizer optimizes the structure and looks to position the connector in a place with a member of the structure to minimize compliance and not to add extra material as it has the volume fraction constraint.

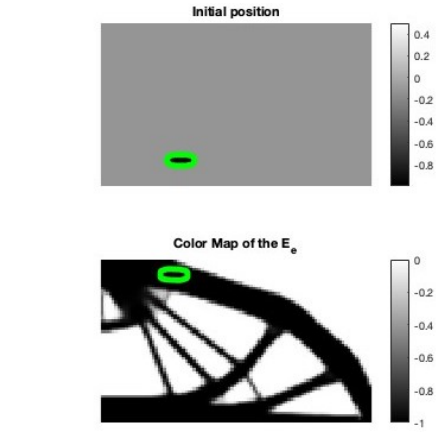

(a) Case 4 - 58.7475

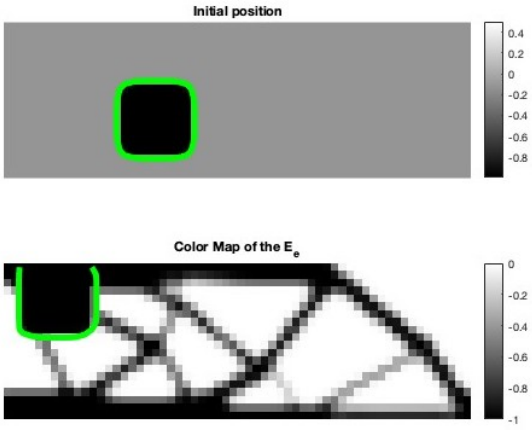

(b) Case 5- 231.3491

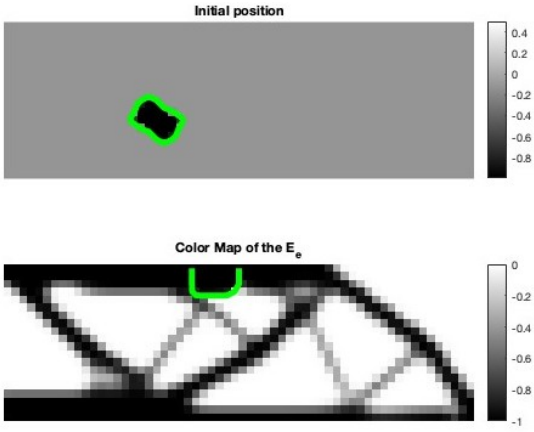

(c) Case 6 - 222.2608

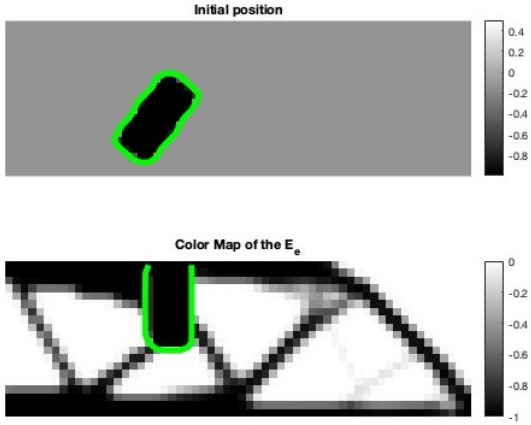

(d) Case 7 - 224.4761

Figure C.2: Optimization with only the connector

Table E.1 shows the values that remain constant in optimization and the initial and final values for the optimization. The number of cases matches those in Fig. C.1 and in Fig. C.2.

C.1.2. Optimization of the connector and two voids

Three cases are shown in the main report, two more cases were tried.

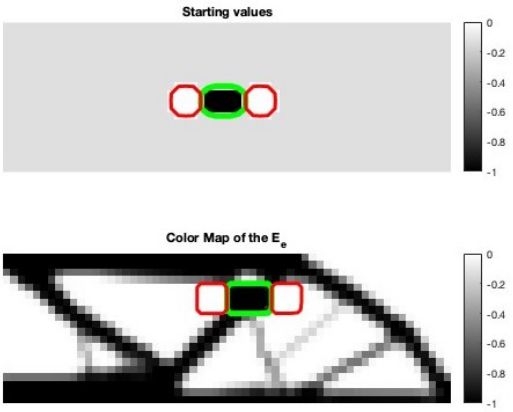

(a) Case 4 - 225.2292

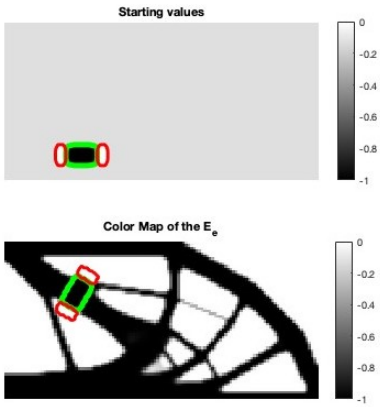

(b) Case 5 - 85.6168

Figure C.3: Extra optimization of the connectors with voids

One with a different starting position (Case 4 in Fig. C.3a) and one with a finer mesh (Case 5 in Fig.

C.3b). As mentioned in the main text, the results obtained are expected, and it was observed that the starting position does influence the final layout.

C.2. Results for the optimization of the structure and the cut lines

These cases are more examples where the cut line is optimized.

C.2.1. A single cut line

The first step is to simultaneously optimize the position of a single-cut line and the structure. Optimizing the cut line involves the optimization of the x coordinates of the top and bottom points, not the midpoints, as in the connector optimization.

Table E.3 shows the starting and optimized values. This table corresponds to the cases shown in Fig.C.4 and Fig. C.5. Most cut lines have a small thickness of one element (b_{cut}) due to the idea that when something is cut, it is a thin line. However, this is an user input and can be changed as desired. The vertical length a_{cut} is calculated with Eq. 3.17, using both points of the optimization. θ_{cut} is calculated using Eq. 3.16.

Fig. C.4 shows two different cases for optimising the cut line. New starting values are tried to observe how they influence the optimization results and if they influence the optimization process. In these optimizations, the initial conditions are the number of elements in the y and x direction, the cut line's initial positioning and the cut line's thickness. As mentioned, the angle θ_{cut} and vertical direction a_{cut} depend on other values. The thickness of the cut line and the y coordinates are optimized.

The cut line is optimised in the first case (Fig. C.4a), and the starting point is at an angle. In the second case (Fig. C.4b), the initial values for the y coordinates are the same, leading to a horizontal cut.

In both cases, the optimizer looks to place the cut line into a position where the density is 0. Moreover, the compliance does not differ much between the cases. This is an expected result so as not to influence the compliance of the structure, the cut line positions itself on an already existing area where the density is zero.

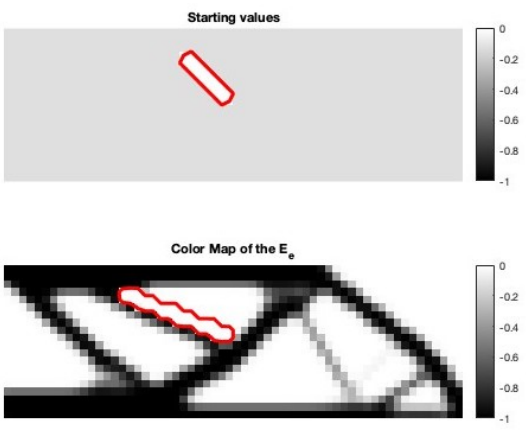

(a) Case 1 - J = 222.56

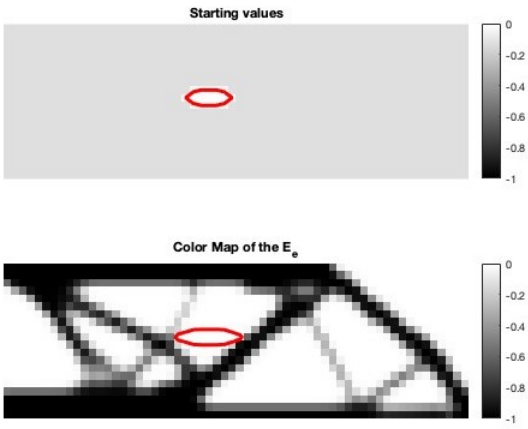

(b) Case 2 - J = 222.46

Figure C.4: Optimization with a single cut line

The third case's starting point is a vertical line (Fig. C.5a). In the optimized graph, the line doesn't look like a straight line, but this is due to the mesh. In the fourth case (Fig. C.5b), the starting position is forced at the top, whereas in the previous optimizations, there is a limb. This affects the structure. In the fifth case (Fig. C.5c), the thickness of the cut line is changed to half of the other values. Finally, the number of elements increases in the sixth case (Fig. C.5d).

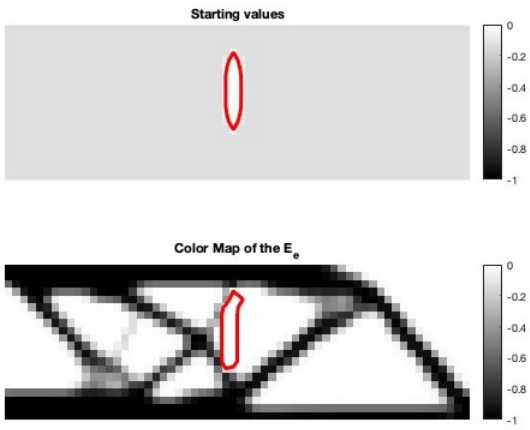

(a) Case 3 - 221.0927

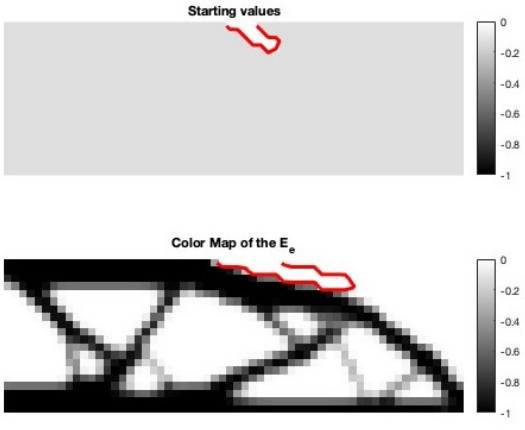

(b) Case 4 - 222.2679

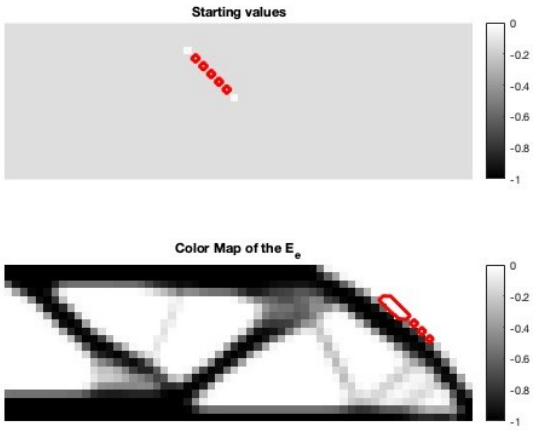

(c) Case 5 - 224.2951

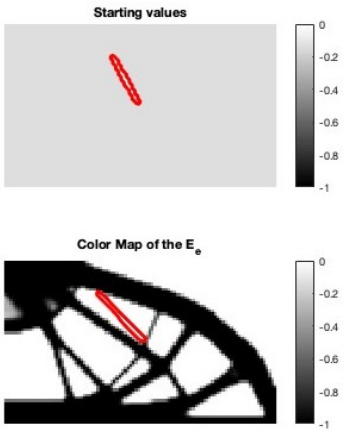

(d) Case 6 - 59.3146

Figure C.5: Optimization with a single cut line

In all the cases, the optimizer looks to place the cut line into a position where the density is 0. Moreover, the compliance does not differ much between the cases, the most significant difference is in Case 6, but this is due to the different number of elements.

C.2.2. Multiple cut lines

Here extra cases of how multiple cut lines are optimized are shown.

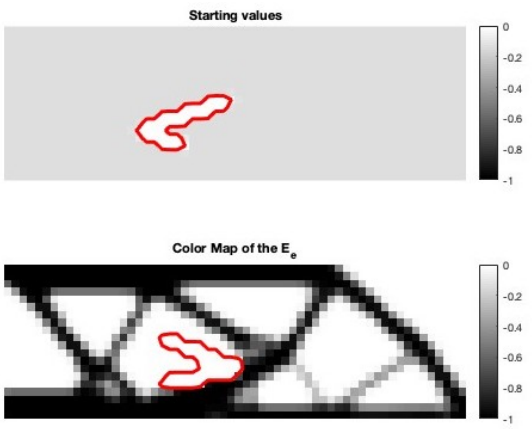

(a) Case 3 - 223.2710

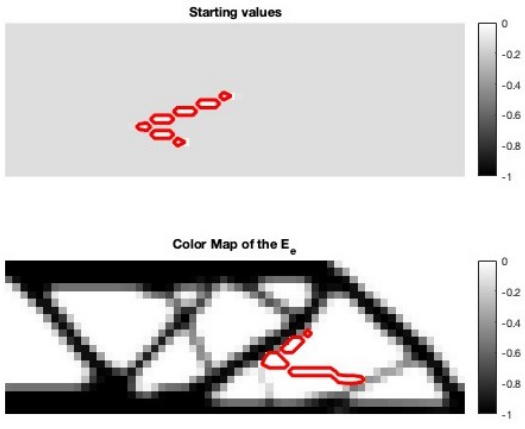

(b) Case 4 - 220.9120

Figure C.6: Optimization with multiple cut lines, Cases 3 and Case 4

From Case 3 (Fig. C.6a) to Case 4 in Fig. C.6b, the thickness of the cuts is altered. The thickness has changed to half in Case 4 (Fig. C.6b). The cut line, however, does not look straight or continuous due to the coarse mesh.

The number of cut lines can be changed from 1 to multiple ones. This is user input. Case 5 (Fig. C.7a) has three cuts, while in the previous cases, there were only two. The number of elements is changed in the last case, number 6 (Fig. C.7b).

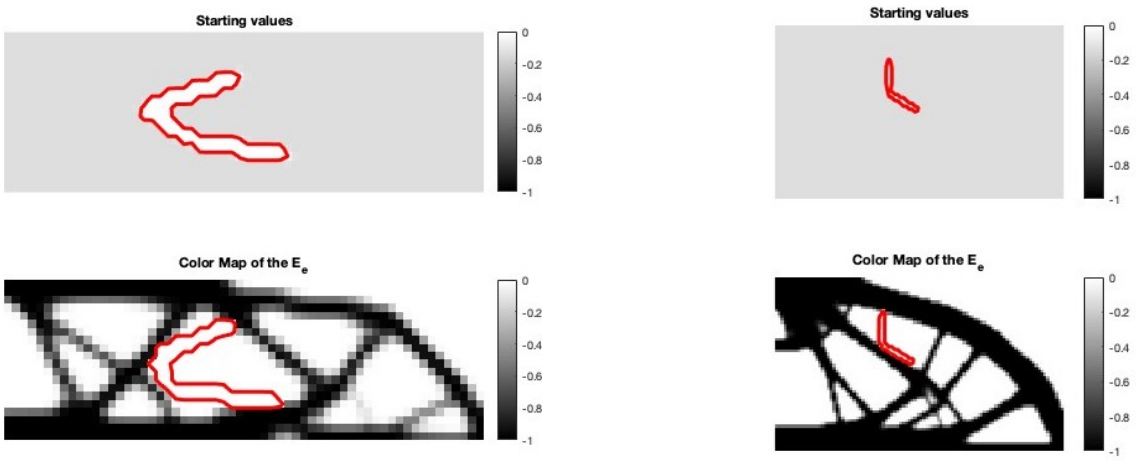

(a) Case 5 - 233.3603 (b) Case 6 - 59.3214

Figure C.7: Optimization with multiple cut lines, Case 5 and Case 6

C.3. Optimizing the structure with the cut lines, connectors and voids

In this section, the optimizations with the connector, the voids and the cut lines are done. In the following optimizations, the structure starts to be fully divided. As in the previous optimizations, several parameters are kept constant. These are shown in Table. 5.1.

C.3.1. Optimization of the cut line with a fixed connector

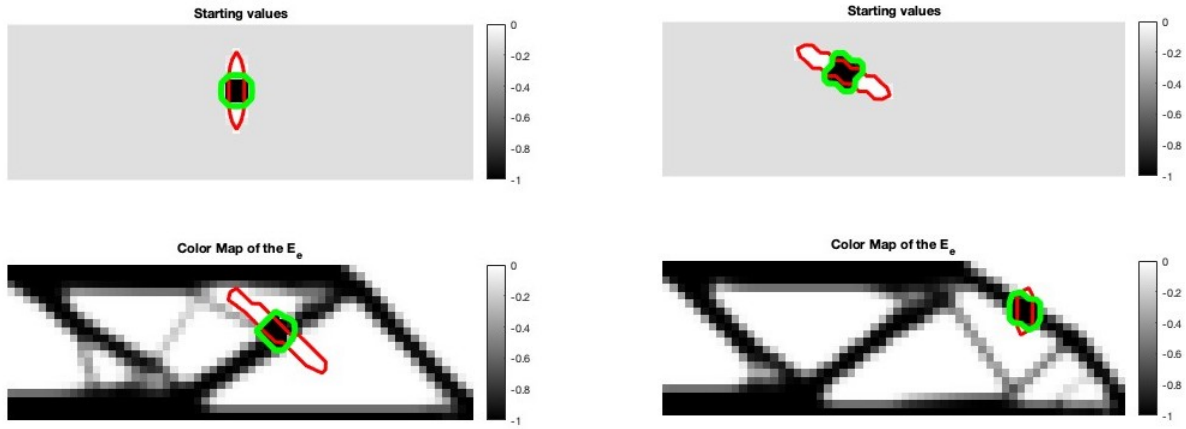

(a) Case 1 - J = 220.51 (b) Case 2 - J = 218.60

Figure C.8: Optimization with a fixed connector at the midpoint, Case 1 and 2

The methodology in Appendix B.4.1 explains how a cut line with a fixed component in the middle is optimized. In this section, different cases are optimized. The numerical results of this section are found in Table. E.5.

There are four cases optimized here. The first case, in Fig.C.8a, shows the optimization with an initial position of the component of a straight line. In Case 2 (Fig. C.8b), the initial position of the x_{cut} is changed. In Case 3 in Fig. C.9a, the value of a_{con} is changed to a higher one, making the connector larger. In the last case in Fig. C.9b, Case 4, the values of x_{cut} and y_{cut} are changed.

These cases were tried to observe how the cut line moves with the influence of the connector.

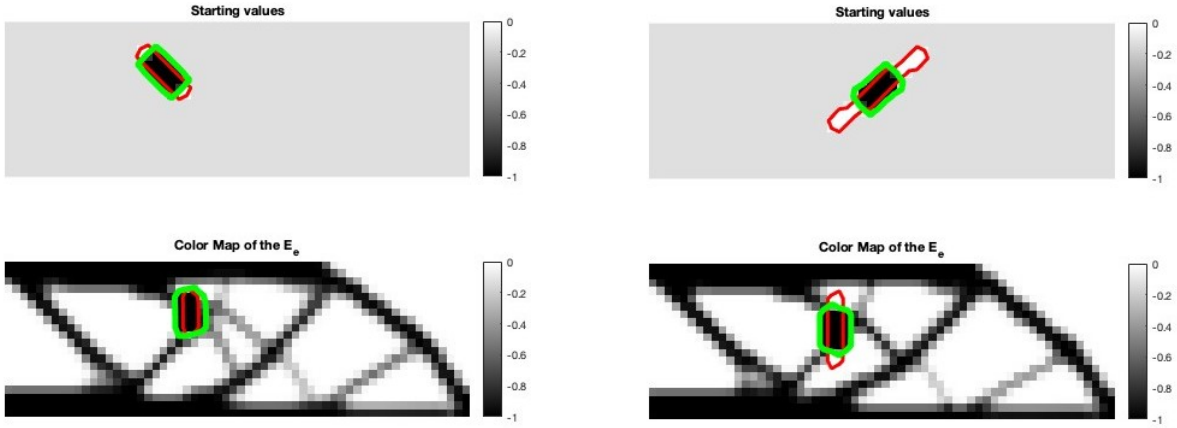

(a) Case 3 - J = 223.79

(b) Case 4 - J = 222.02

Figure C.9: Optimization with a fixed connector at the midpoint, Case 3 and 4

C.3.2. Optimization with movable connector

This section contains the results of optimising the connector and the cut line. The position of a single cut line is optimized at the same time as a single connector's position is optimized on the top of the cut line. One requirement in this section is that the thickness of the connector (b_{comp}) must be larger than the thickness of the cut line (b_{cut}). This is due to the component needing to connect both parts of the structure. Twelve cases were performed to observe how the initial values affect the final results. Different values are changed in each optimization to observe the impact of the user input values.

The component's initial size is kept constant in the first three cases, and the cut line's initial position is changed. In the first case (Fig. C.10a), it can be observed that the connector has an equal vertical length as the cut line in the starting position. However, when optimized, as the size of the cut line has increased due to the final positioning of x_{cut}, the value of a_{cut} has increased, and a_{con} remains two as this value is not optimized. In the second case (Fig. C.10b), the starting position of the cut is kept the same as in the previous case. However, the y values have moved. In Case 3 (Fig. C.10c), the starting x_{cut} values of the cut are changed. This leads to a change in the starting value of the connector's angle. In these cases, the optimized position of the structure is expected, the cut line moves to position the connector on a member of the optimized structure and looks to position the cut line on a hole to not affect the structural stiffness and compliance by breaking the structure.

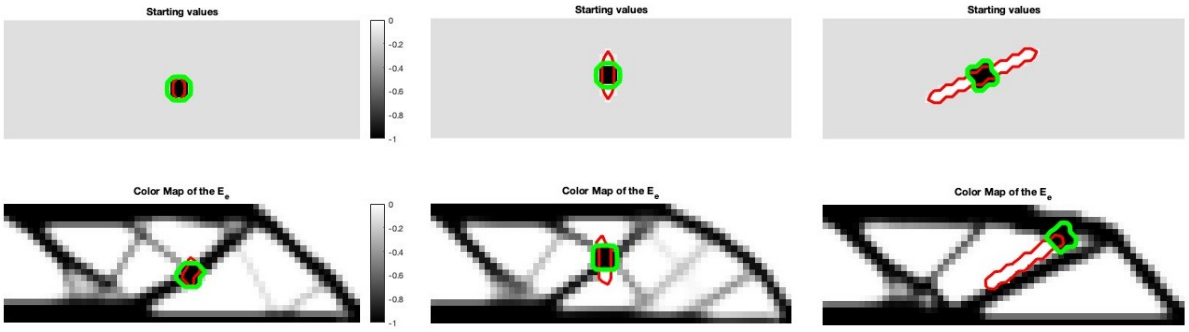

(a) Case 1 - J = 220.06

(b) Case 2 - J = 230.20

(c) Case 3 - J = 218.46

Figure C.10: Optimization of the cut line with the connector changing the cut line y coordinates.

In the next three cases, Case 4 (Fig. C.11a), Case 5 (Fig. C.11b) and Case 6 (Fig. C.11c), the

size of the connector is changed, in Case 6, the connector's thickness (b_{con}) is three times higher than the cut line, and in cases 5 and 6, the connector has the same thickness as the cut line. Comparing cases 4 and 5, the connector has increased on the b_{con} in Case 4 and a_{con} in Case 5. As well as the connector's size, both have different y_{cut} coordinates. This leads to different positioning. Case 6 starting point is similar to the second case, the main difference is the y positioning of the cut, which leads to different optimized results. In these three cases, the optimizer does what is expected, to place the connector on the structure, where there is material and the cut line in the holes.

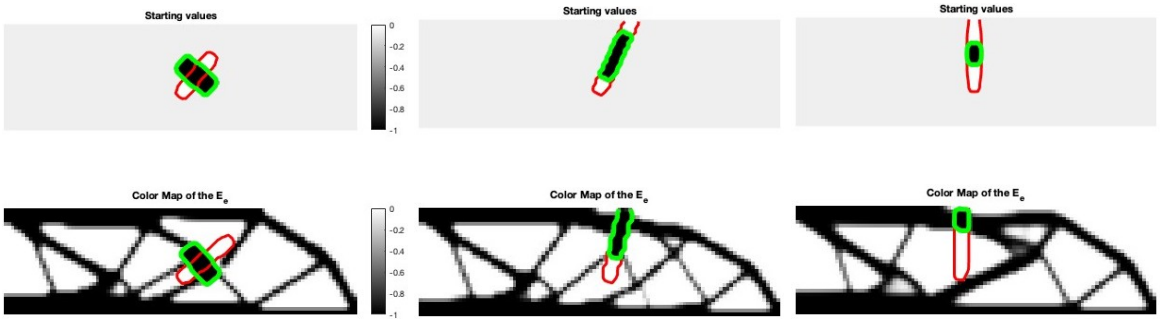

(a) Case 4 - J = 279.88 (b) Case 5 - J = 310.04 (c) Case 6 - J = 281.36

Figure C.11: Optimization of the cut line with the connector, the connector's thickness is the same as the cut line

Case 7, in Fig. C.12a, shows the optimization with a different number of elements. In this case, there are 180x60 elements. This change also changes the size of the component with respect to the structure, as the component length is determined by the number of elements and the cut line is scaled to the number of elements. Case 8 (Fig. C.12b) is the first image with a full structural cut. The component is larger than in other cases to allow the structure to optimize around it. This case has the highest compliance, this is due to the shape of the structure.

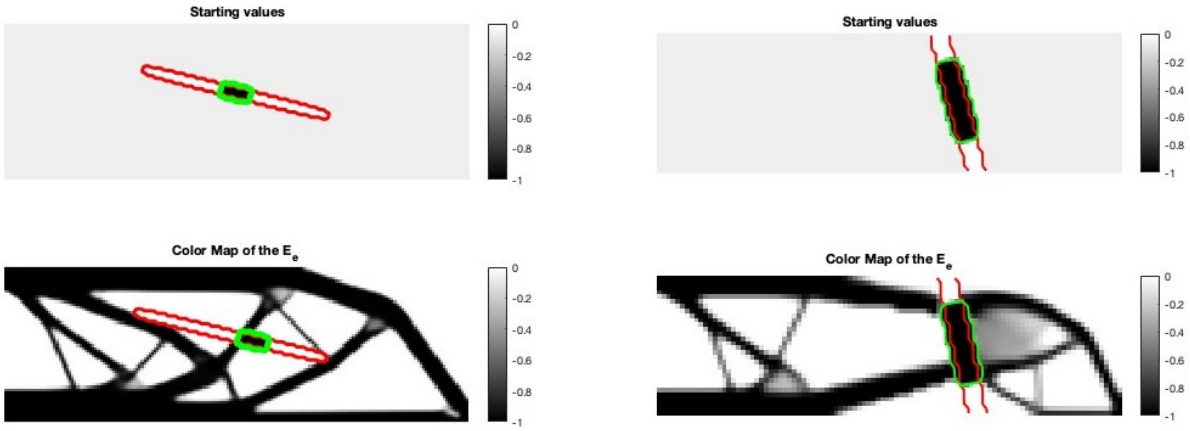

(a) Case 7 - J = 204.6239 (b) Case 8 - J = 346.89

Figure C.12: Optimization of the cut line with the connector, one case with a higher number of elements and another case with a full division of the structure.

The last four cases, Case 9 (Fig. C.13a), Case 10 (Fig. C.13b), Case 11 (Fig. C.13c) and Case 12 (Fig. C.13d), the E_c changes. In Case 9, the E_c is changed to 0.7. This means that the component now is 30% weaker than the structure. This time the component is supported by a higher number of beams than in the other cases. In cases 10 and 11, the initial position is the same, however, they have different Young's modulus. The connector's position is different in both cases, as well as the position of the cut line, although they are similar. The main visual difference is on the top structural member.

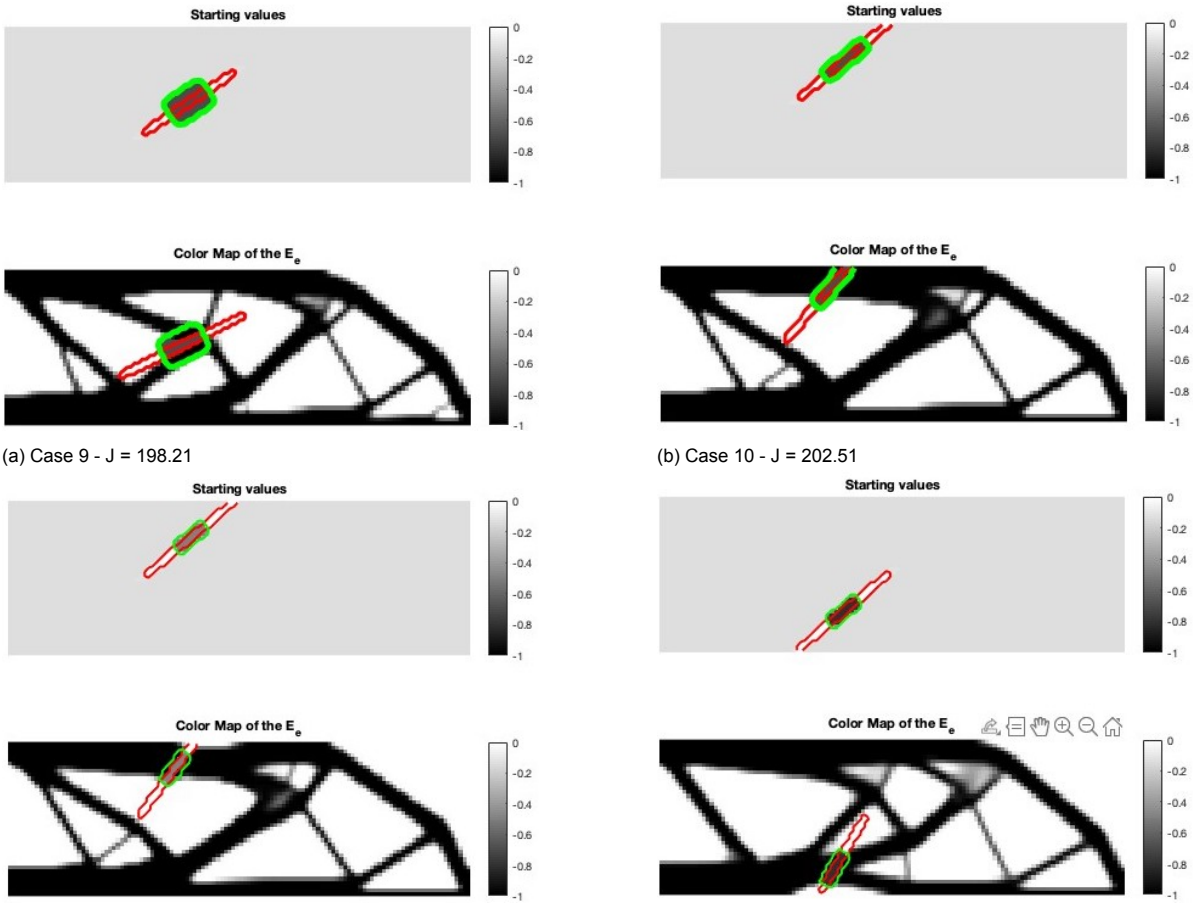

(a) Case 9 - J = 198.21

(b) Case 10 - J = 202.51

(c) Case 11 - J = 208.71

(d) Case 12 - J = 207.16

Figure C.13: Optimization of the cut line with the connector, cases with a lower E_c

Regarding optimized compliance, Case 10 has 202.51, and Case 11 has 208.71. Case 12 has the same E_c as in Case 1. However, the starting position is different; now, it tries to cut the bottom part of the structure. In this case, the compliance is 207.16. Moreover, comparing both figures, they create a small deviation of their closer structural member, meaning they are no longer straight. In these cases, the optimizer places the connector and the cut line where it is expected.

The numerical solutions, as well as the starting design variables, are plotted in Table. E.6 and Table. E.7. The results are divided into two tables to be easier to read.

C.3.3. Optimization with movable connector and voids

This section adds two voids on the connector's side, one on each side. As in previous sections, a few optimisations are performed to analyse the influence of the voids. In this section, nine different cases were optimized.

These optimizations are more challenging to position on the structure. In the previous case, the connectors could be placed on the structural members and, with the angle of the cut line, avoid damaging the structure. However, with the addition of both voids, on all four sides of the connector, there is a section with a 0 density, the cut line on the top and bottom sides, and the voids, one on each side.

The first case for this optimization, Fig. C.14a, is also the only optimization with the coarse mesh, 60x20 number of elements. One observation is that the optimizer tries to position the connector as one of the structural members of the structure by placing one of the voids out of the design domain and the other into a structural void. This is done by moving the cut line to a desired angle. This is the optimiser's expected behaviour: to place the cut line and the voids on a hole where density is zero and place the connector connecting the structure to avoid its detachment.

Cases 2 (Fig. C.14b) and Case 3 (Fig. C.14c) have the connector's exact positioning and element size as in Case 1. However, as the structure has a finer mesh. The difference between both cases is

the void size. With these examples, the conclusion that the size of the voids affects the final position is obtained. The compliance is 198.89 for Case 2 and slightly higher for Case 3, with a value of 202.98.

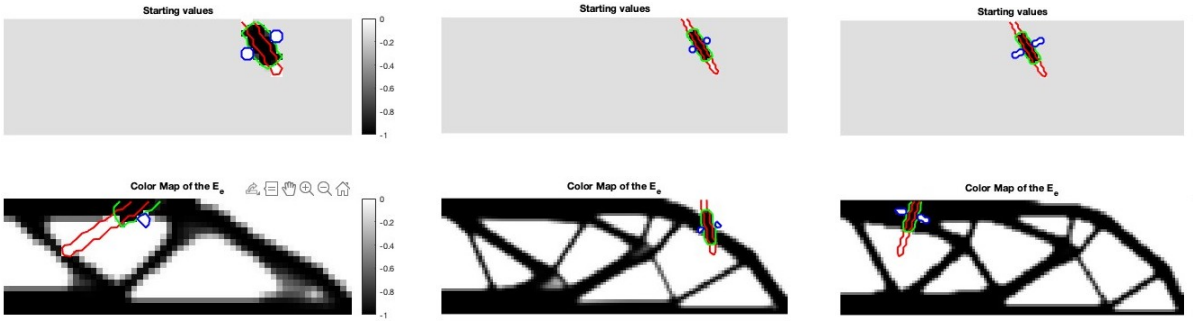

(a) Case 1 - J = 224.79 (b) Case 2 - J = 198.89 (c) Case 3 - J = 202.98

Figure C.14: Optimization of the cut line with the connector and the voids cases 1 to 3

The horizontal dimension of the connector, b_{con}, and the initial position are changed in Case 4 (Fig. C.15a). The initial position is changed to a horizontal line with different y_{cut} values. The optimizer looks to position the connector on an angle and place it where the cut and the voids lie on the structural gap, which is the expected solution. Case 5 (Fig. C.15b) has a different starting position and a larger void side. In this case, the optimiser tried to connect the connector with a member of the structure by the material between the cut line and the void. This case is similar to the previous one, with another dimension and starting position.

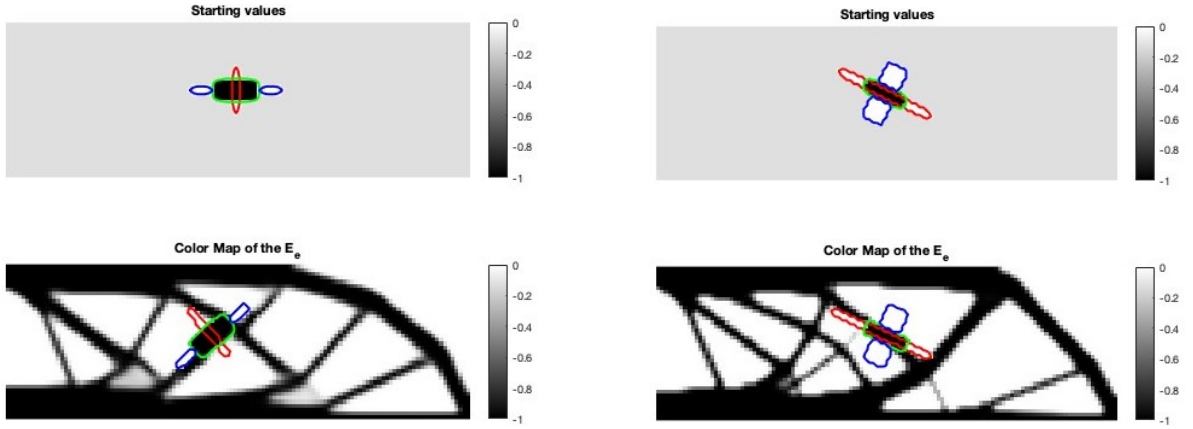

(a) Case 4 - J = 206.5396 (b) Case 5 -J = 209.4513

Figure C.15: Optimization of the cut line with the connector and the voids, cases 4 and 5

The last four cases, Case 6 (Fig. C.16a), Case 7 (Fig. C.16b), Case 8 (Fig. C.16c), and Case 9 (Fig. C.16d), Young's modulus of the component is lower (E_c). Case 6 is similar to Case 2. The cut line's starting x_{cut} values and the $E_c = 0.8$ are different. These changes affect the final optimization as well as compliance. Case 2 has lower compliance, but it is only a 1% difference. Case 7 has a $E_c = 0.8$, which is the same as in the previous case, Case 8 has a $E_c = 0.7$ and Case 9 has a $E_c = 0.5$. In Case 9, the connector's strength is half of the structure's. In cases 7 and 8, the optimizer does what is expected, however, in Case 9, the expected optimized position would have been similar to the one in Case 8, however, this might have differed due to the change of the initial position and the connector's lower Young's modulus.

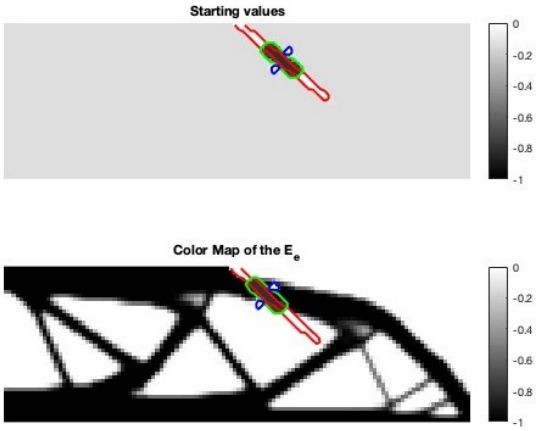

(a) Case 6 - J = 201.7132

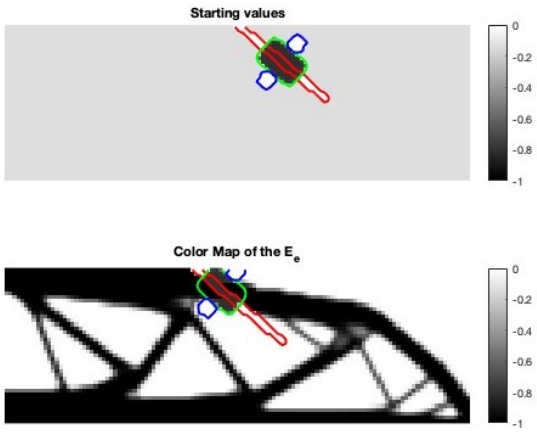

(b) Case 7 -J = 206.7243

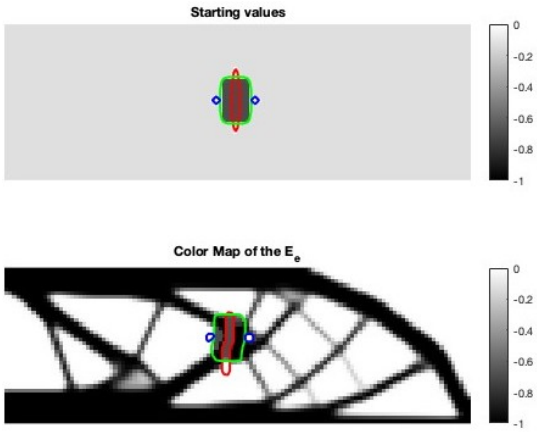

(c) Case 8 - J = 200.6405

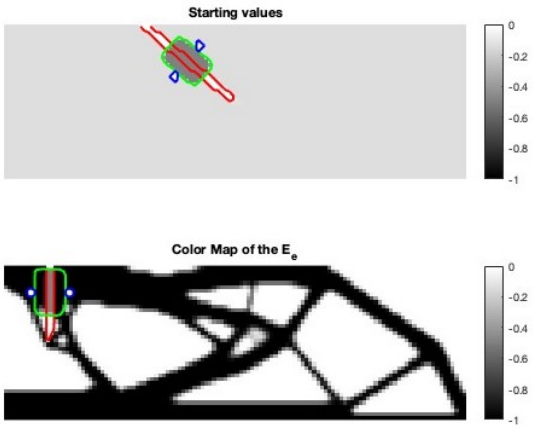

(d) Case 9 - J = 214.4957

Figure C.16: Optimization of the cut line with the connector and the voids, with a lower value for E_c

Tables E.8 and E.9 show the initial and final numerical values for the figures found in Fig. C.14, Fig. C.15, and Fig. C.16.

D

Full parameters studies

In this chapter, the full parameter study is shown.

D.1. Optimization of multiple cut lines and connectors

This section optimises different cases with multiple cut lines and connectors. Fig. C.12b was the only case previously where the entire structure was divided into two different parts joined by the optimization of the connector. From now on, all the cases will fully divide the structure in two. There are multiple starting points for the optimizations and multiple variables which can be changed.

This section aims to see how the variables, which determine the initial conditions and positioning, change the final results. The approach taken in this section is to have a reference case (Case 1 in Fig. D.1a) and start changing the variables, one per case, to observe what consequences have on the optimized structure. There are seventeen cases optimized in this section. The numerical values are in Table E.10, Table. E.11 and Table.E.12. These are divided into three different tables to be easier to read.

Here the comparison of some optimization is shown. The first case in Fig. D.1a, is used as a reference to observe how one change influences the optimization. The initial values for the first case are E_c=1, there are three cut lines which will cut the whole structure, the values for $y_{cut} = 0, 0.3, 0.7, 1$. The starting point of the connector on the cut line s_{con} is 0.5, therefore, it will start in the middle of the cut line. The connector's size is $a_{con} = 6$ x $b_{con} = 3$ elements. The thickness of the cut line, b_{cut}, is set to 1 element.

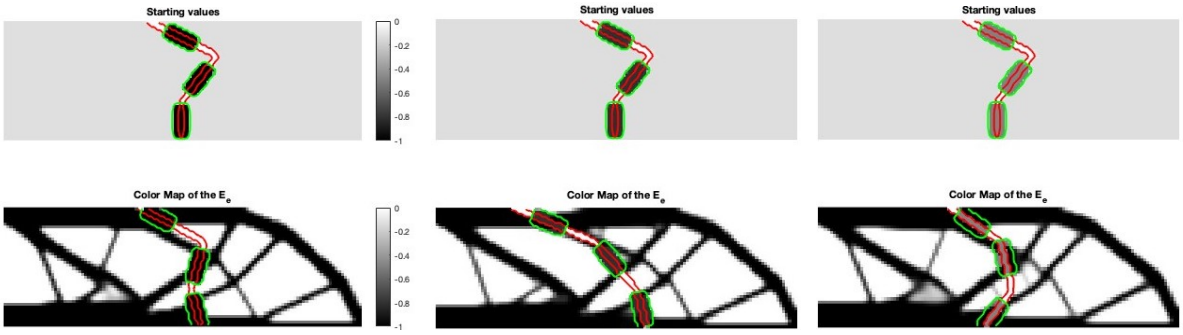

(a) Case 1 - J = 208.92 (b) Case 2 - J = 224.40 (c) Case 3 - J = 210.07

Figure D.1: Optimization of the cut lines with the connectors, Initial case and two cases with lower E_c

In cases 2 and 3 (Fig. D.1), the value of E_c has changed to a lower one, with a value of 0.8 in Case 2 (Fig. D.1b) and 0.5 in Case 3(Fig. D.1c). This means that now, the connector has a lower Young's modulus. As it can be appreciated, the different values of E_c do affect the positioning of the connectors and the cut lines. The final compliance is also affected. The first case has lower compliance, followed by Case 3, then Case 2. The optimiser places the connectors on the outer cut lines in the top and bottom

members of the structure and the middle connector connecting the structure in the middle. This is what is expected to do as the outside part of the structure is the most important and affects compliance.

The initial position of the x_{cut} is changed in the fourth and fifth cases. In Case 4 (Fig. D.2b), the initial position is shifted by adding ten elements in the x direction, and in Case 5 (Fig. D.2c), the initial position is moved by subtracting ten elements in the x direction of the original case. Both changes do have an impact on the positioning of the optimization. When it is shifted to the right, the optimized values are also moved to the right, except for the bottom cut line and connector, which has a lower value than the original case. When the initial positioning is moved to the left, the same happens, the connector is shifted to the left. In both cases, the compliance increases with respect to Case 1. In Case 4, it increases a 6 %, and in Case 5 by a 9.4%. The starting compliance is also higher in both cases than in Case 1. Here it can be observed in these cases that the connectors align with the members of the structure.

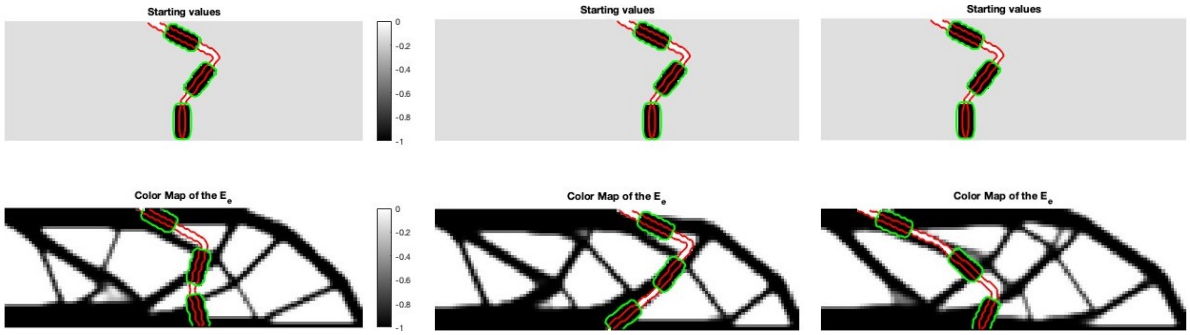

(a) Case 1 - J = 208.92 (b) Case 4 - J = 202.22 (c) Case 5 - J = 222.71

Figure D.2: Optimization of the cut lines with the connectors, moving the x_{cut}

In Case 6 (Fig. D.3b), the position of y_{cut} is modified. The modification is made on the top and middle cut lines. The top line has a larger size, while the middle line is shorter. This change has a more significant influence on the top structural member. In Case 7 (Fig. D.3c), the y_{cut} is also changed. This time, the top and middle cut lines are shorter, and the bottom cut line is larger. The optimization also changes, the shape of the optimized part does not change as in Case 6. Furthermore, the compliance is lower than in Case 6 and Case 1. This is the second lower compliance in this section. Comparing the three images in Fig. D.3, the compliance has improved, and Fig. D.3c has a complex design with finer members.

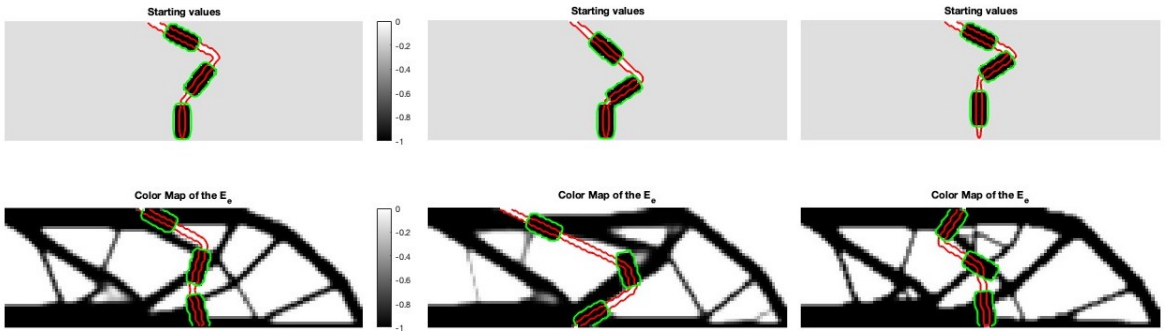

(a) Case 1 - J = 208.92 (b) Case 6 - J = 228.69 (c) Case 7 - J = 205.36

Figure D.3: Optimization of the cut lines with the connectors, different starting values of y_{cut}

Cases 8 (Fig. D.4b) and 9 (Fig. D.4c) show the optimization with a change in s_{con}, the starting position of the connector in their respective cut lines. The optimized positions have changed if compared to each other and Case 1. However, the structure of Case 8 and Case 1 are similar. Case 8 has the lowest compliance of all the different cases. Case 9 also has a lower compliance than Case 1 and higher than Cases 7 and 8. The influence of the starting positioning of the connectors and the cut lines has led to lower compliance in Case 8. Looking at Case 9, it can be observed that the optimiser

creates a member of the structure by aligning two connectors. As the optimizations are now, this will not be a problem, however, the desired idea is to have two voids on the side, which will influence the positioning, as well as the connectors will not have the same strength as the structure.

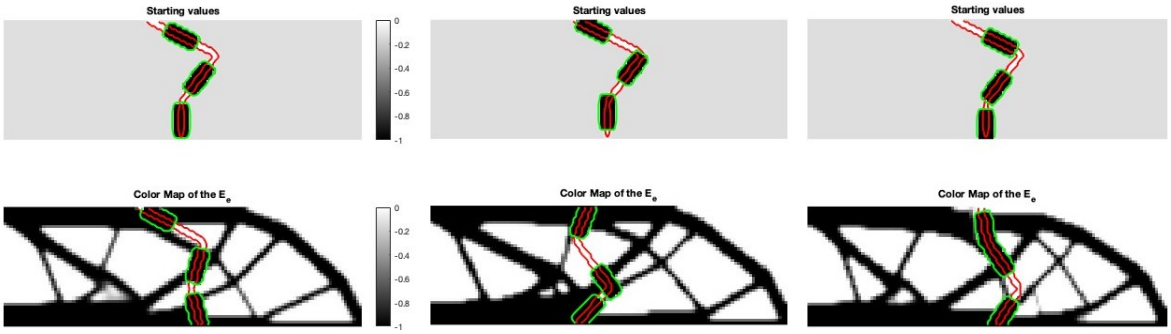

(a) Case 1 - J = 208.92 (b) Case 8 - J = 198.60 (c) Case 9 - J = 207.53

Figure D.4: Optimization of the cut lines with the connectors, different values for s_{con}

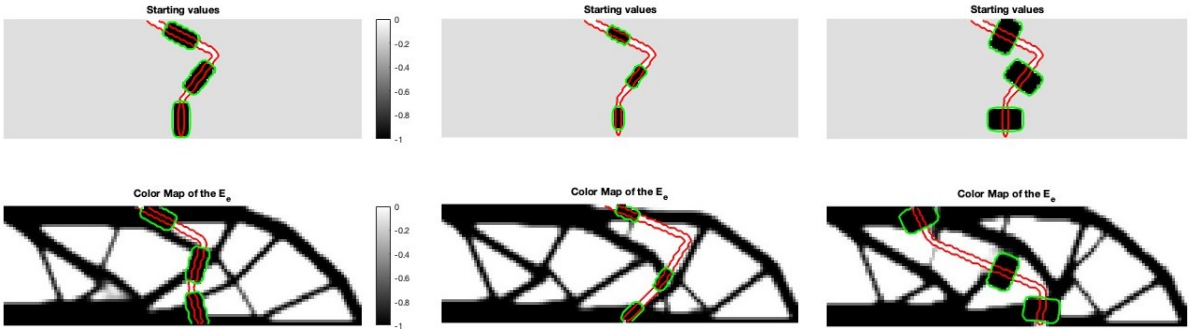

(a) Case 1 - J = 208.92 (b) Case 10 - J = 219.24 (c) Case 11 - J = 213.45

Figure D.5: Optimization of the cut lines with the connectors, changing the connector's size

The connector sizes have changed in Cases 10 (Fig. D.5b) and 11 (Fig. D.5c). Case 10 has smaller connectors in both horizontal and vertical values. However, Case 11 has a larger connector on the horizontal length and the same element length on the vertical as in Case 10. The compliance on both increases respect to the first case. Moreover, the structure also changes to accommodate better the changes on the connector's size. The optimization with larger connectors has lower compliance; however, is still a 1% increase in Case 1.

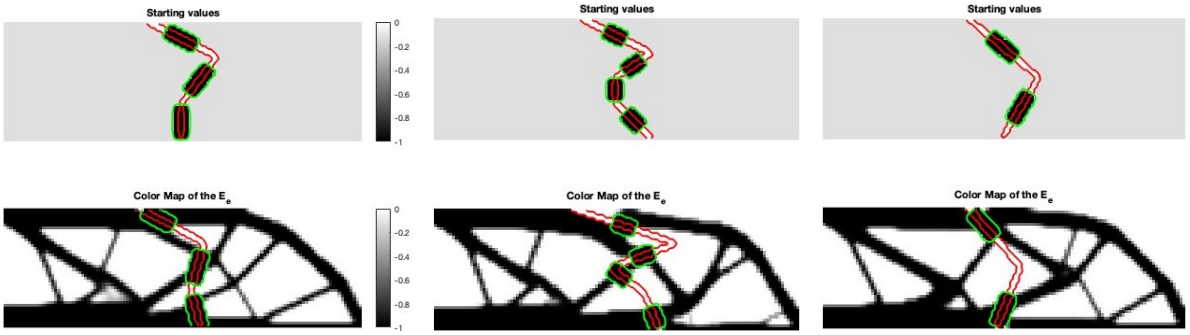

(a) Case 1 - J = 208.92 (b) Case 12 - J = 220.60 (c) Case 13 - J = 204.87

Figure D.6: Optimization of the cut lines with the connectors, with different numbers of connectors and cut lines

The number of cut lines and connectors is increased by 1 in Case 12 (Fig. D.6b). The connector size is also modified to fit the extra connector. The structure changes to accommodate the extra connector

and cut line. The optimizer places all the connectors and tries to make connections between them. The compliance is also higher than in other cases, this can be due to having smaller connectors and more cut lines, which constrain the structure more. In Case 13 (Fig. D.6c), the number of connectors and cut lines is lower; it only has two. This forces the optimizer not to have any solid connection between in the middle, where the cut is, as well as positioning the cut lines at both outer sides. The compliance is lower than in Case 1.

The number of elements has changed in Case 14 (Fig. D.7b). Now it has 180 on the x and 60 on the y. The number of elements has the same x:y ratio as the previous one. Therefore, the structure has the same proportions. As the length of the connectors is determined by element number, they are smaller in this case. The x_{cut} position is the same as the input is not scaled to the number of elements. Looking at the initial figure, the starting position in Case 14 has the same as in Case 10. However, optimising the final positioning is not in the same place or has the same compliance. This can also be affected due to the maximum allowed change for the cut line and connector position. As there are more elements, the maximum change per iteration is smaller.

In Case 15 (Fig. D.7c), the starting position of the cuts and, therefore, the connectors are changed. In the previous cases, they were shifted to both sides but kept the same initial angles and values of a_{cut}. In this case, the starting position is a straight line in the middle of the structure. This leads to a new optimized position with lower compliance of the structure.

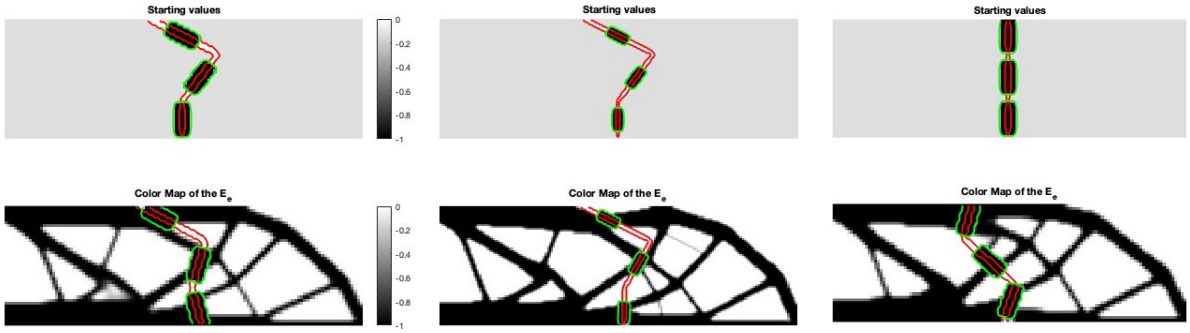

(a) Case 1 - J = 208.92 (b) Case 14 - J = 207.29 (c) Case 15 - J = 205.85

Figure D.7: Optimization of the cut lines with the connectors, with different mesh and the straight line starting point

The thickness of the cut line has been one element in all the optimizations except in Case 16 (Fig. D.8b). Here, the thickness is doubled, as can be seen in the figure. In all the cases until now, even on the previous optimization cases, the r_{min} has been maintained with the same value, 1.5. This value is the most commonly used. But to see the influence on the optimization, the filter radius, which can affect the size of the structural members, is changed to 2, this is in Case 17 (Fig. D.8c). This has changed the optimized value and, as expected, has made the structure blurry.

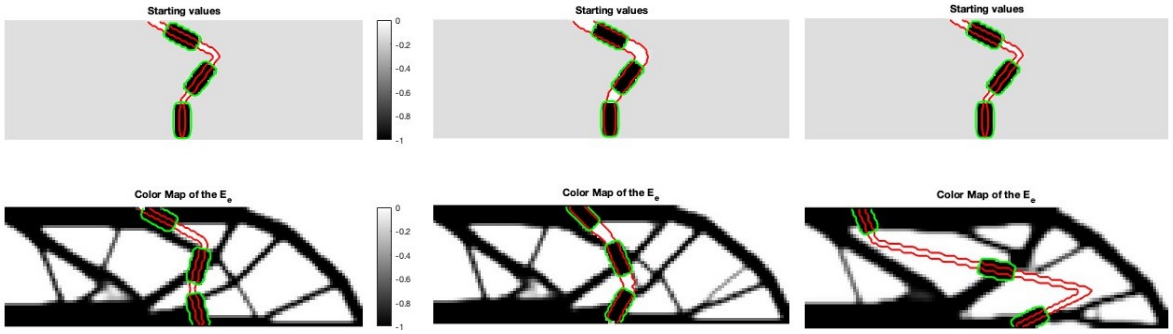

(a) Case 1 - J = 208.92 (b) Case 16 - J = 206.99 (c) Case 17 - J = 207.89

Figure D.8: Optimization of the cut lines with the connectors, change in the b_{cut} and r_{min}

There were only 17 cases tried, and in most of them, only one variable changed per optimization. However, these variables can be changed in multiple ways and obtain different results. For all the

cases on each table, there are their corresponding figures. Table E.10 shows the numerical values for Fig. D.1, Fig. D.2, and Fig. D.3, which shows the cases 1 to 6. Table. E.12 shows the numerical values for the figures in Fig. D.3, Fig. D.4, Fig. D.5, Fig. D.6, Fig. D.7 and Fig. D.8, which shows cases 13 to 17.

D.2. Optimization of multiple cut lines, connectors and voids

The voids are now added to the optimization. This makes the optimizations more challenging. In the previous case, the connectors could be positioned on the structural members of the structure and, with the cut line's angle, avoid breaking the structure. However, with the addition of both voids, there is a zero density area on the four sides of the connector, the cut line on the top and bottom sides, and the voids on the other sides. Making it more challenging to position the connector with a higher dimension of the voids.

This section is divided into two. Firstly, the voids' size is kept constant, and their size changes in the second part. As in the previous comparison, the reference case is the same as the previous one, in Fig. D.1a, but voids are added in these comparisons. This allows the cases to be compared against each other and with the cases without the voids.

D.2.1. Optimizations with the voids size constant

This section shows how the addition of the two holes affects the optimization. This is done by having the same optimization cases as in the previous sections, however, this time with the voids. In this part, the dimensions of the voids are kept constant. Not all the cases in the previous section are also optimized here, only one case per variable changed. The size of the void has the following values: $a_{void} = 1$ and $b_{void} = 2$. In this comparison, there are twelve cases. As in the previous optimization, each case on Table. E.13 and E.14, which show the numerical results for these cases, state what has changed on each optimization. This modification is reversed back to the standard case at the end of the optimization, therefore, from the standard to all cases, there is only one change.

In the first case, Fig D.9a, the final optimization is completely different than in the first case without any holes. The higher compliance is due to the addition of the voids and the different positioning of the connectors and cut lines on the structure. Although the structure is different in the second case, the position of the cut and the connectors are similar to the second case in Fig. D.9b. The main reason for the change is to try to place the voids, not to weaken the structure. This optimization is one where the compliance is lower than the ones without holes. However, it is not one of the lowest on the void optimization. In this case, the E_c is modified to 0.8, making the connector weaker than the structure. Here, it can be observed that the optimizer tries to join both connectors together to create the beam. They are not overlapping due to the non-overlap constraint in Eq. 4.2.

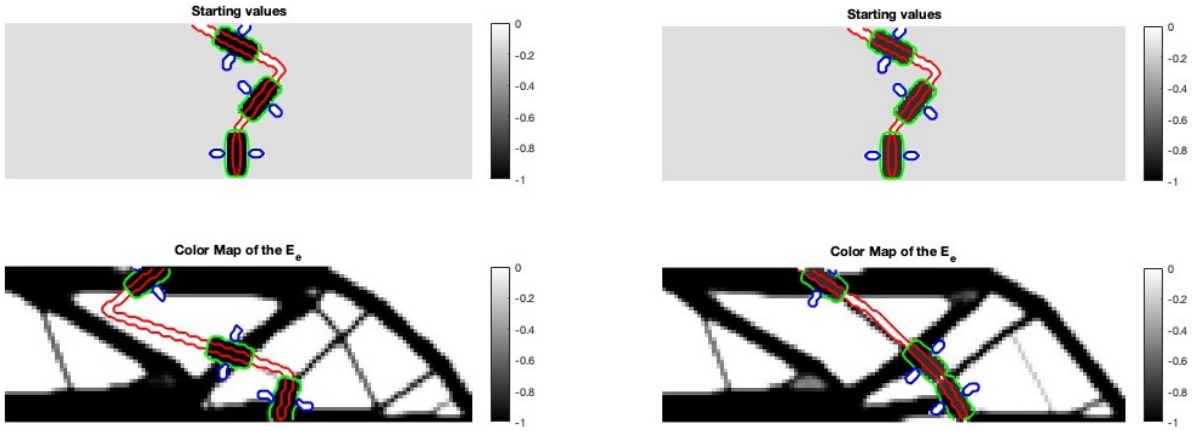

(a) Case 1 - J = 213.89

(b) Case 2 - J = 221.17

Figure D.9: Optimization of the cut lines with the connectors and voids, Initial case and a case with lower E_c

In the third case, in Fig. D.10a, the initial x_{cut} position is shifted to the right, as in Case 4, in Fig. D.10b. The optimized values are different. Also, if compared to the first case with the voids. The

compliance is lower than in the first case of the voids but higher than without them due to their influence.

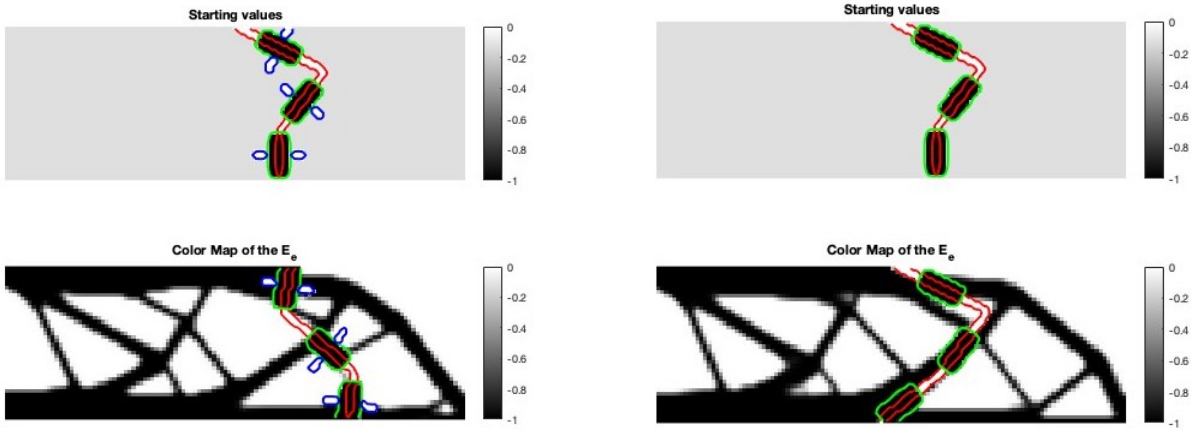

(a) Case 3 - J = 207.46

(b) Case 4- J = 202.22, From previous comparison

Figure D.10: Optimization of the cut lines with the connectors and voids, initial case, changed x_{cut} and Case 4 from the past comparison

The bottom cut line is longer in the fourth case in Fig. D.11a, but the middle cut is shorter. In this optimization, the final position is similar to the initial one. Furthermore, compared to Case 7 in Fig. D.11b, the position of the previous case without holes is similar. It is not the same as if the case without holes includes them, their structure will be disconnected, or it will have a void in the middle of the structural member. This is why the optimizer slightly rotates or moves the connector and the cut line to avoid this. Moreover, there is only a small increase of 2% in compliance.

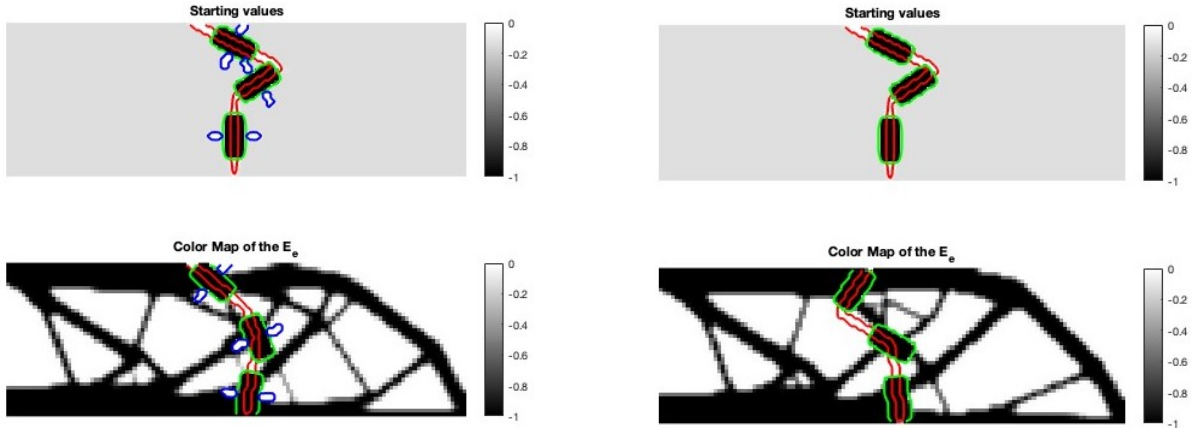

(a) Case 4 - J = 209.51

(b) Case 7 - J = 205.36, From previous comparison

Figure D.11: Optimization of the cut lines with the connectors, with a change of y_{con}, with and without voids from the previous comparison.

In the fifth case in Fig. D.12a, the starting point of the connector on the cut line is changed. It does not start from the middle of the cut, it starts on lower. The compliance has increased by 6%, with final compliance of 210.89. Looking at Fig. D.12a and focusing on the lower connector, it seems like the optimizer is trying to position it outside the design domain to avoid having the voids affect the structure.

In the sixth case (Fig. D.13a), the size of the connector is changed. Now, it has a larger horizontal length than the vertical one. Compared to the case without voids, which has the same change (Case 11, also shown in Fig. D.13b), the position of the cut and connector looks the same. However, the values are not the same if the numerical values are compared from Table E.14 and Table E.12. The final optimizations are different, however, just by a small difference, which also affects the inside structure of the beam. This is due to the voids on each side.

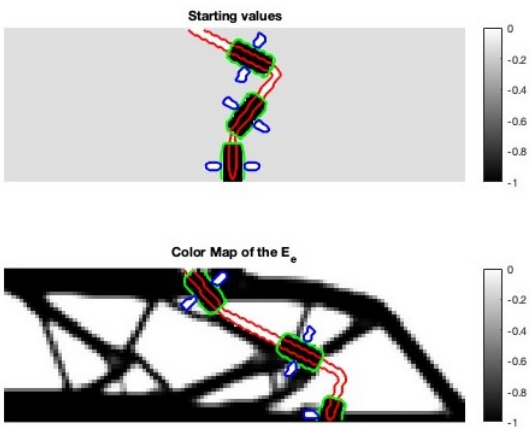

(a) Case 5 - J = 210.89

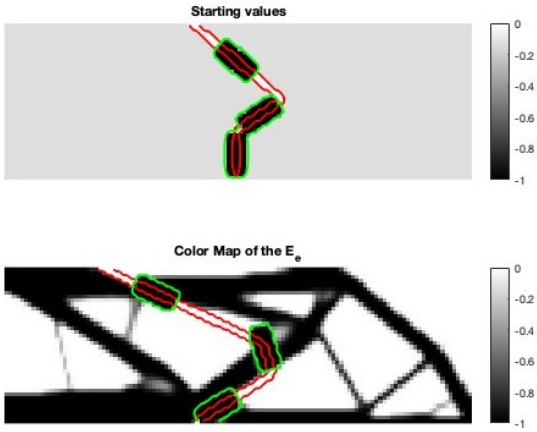

(b) Case 6 - J = 228.69, From previous comparison

Figure D.12: Optimization of the cut lines with the connectors, with a change of s_{con}, with and without voids from the previous comparison.

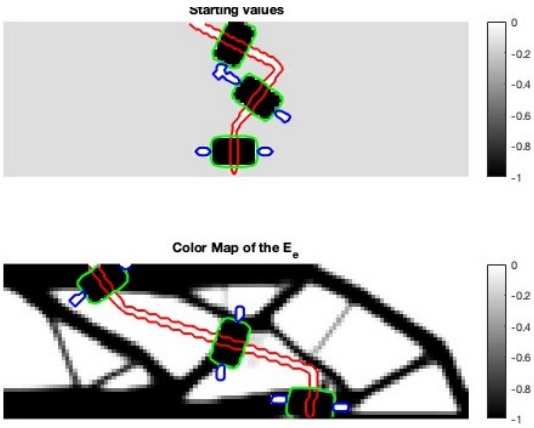

(a) Case 6 - J = 217.35

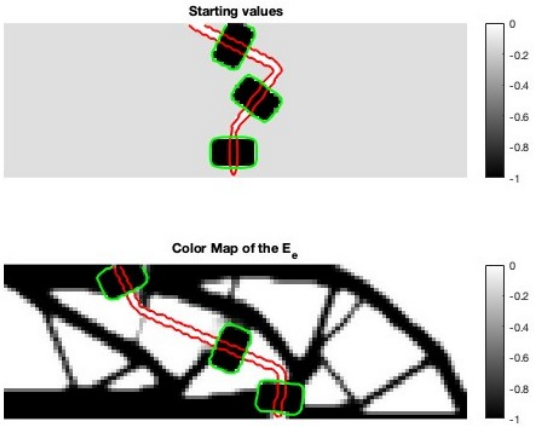

(b) Case 11 - J = 213.45, From previous comparison

Figure D.13: Optimization of the cut lines with the connectors, with a change of a_{con} and b_{con}, a case with and a case without voids from the previous comparison.

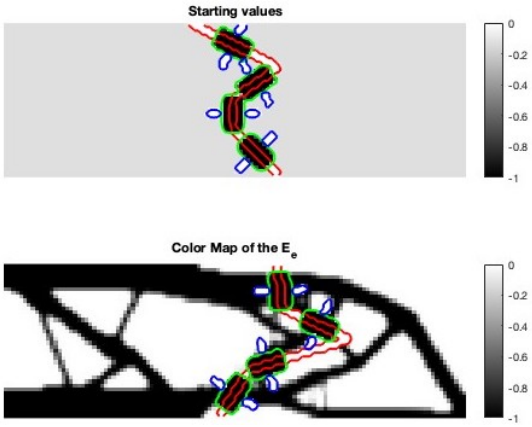

(a) Case 7 - J = 251.84

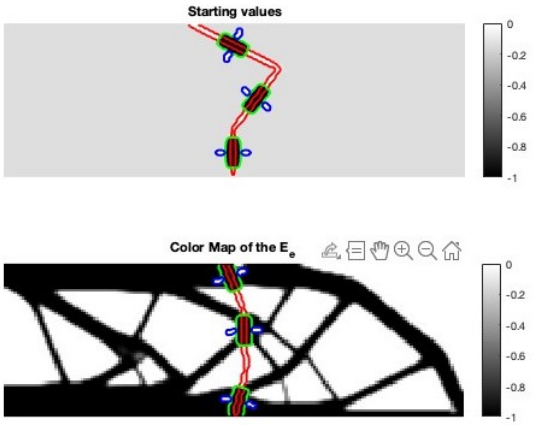

(b) Case 8 - J = 203.45

Figure D.14: Optimization of the cut lines with the connectors, a case with one more connector and a case with finer mesh

The number of connectors has increased in Case 7 in Fig. D.14a, and therefore, the number of

voids. In this case, there is an extra connector and cut line, and as before, when the extra a_{cut} line with its respective connector is added, the size of the connector is changed to a smaller one. However, the size is not as small as in the optimization without the voids. This change influences the final position. The main reason it is not as small is to have more area where the connector can be connected to the structure. This case also has the highest final compliance of all these cases. This can be due to the size of the connectors and the higher number of cut lines and connectors, making it more challenging to place them.

In Case 8 in Fig. D.14b, the number of elements has changed to a finer mesh, with 180x60 elements. As in previous cases, when the mesh is changed, the size of the connector is changed, and in this case, the size of the voids is also changed. As now, the size of the void is smaller, it is easier to place due to the positioning being less affected by the larger sizes of the voids. This case has the lowest compliance, this can be due to the small influence of the voids.

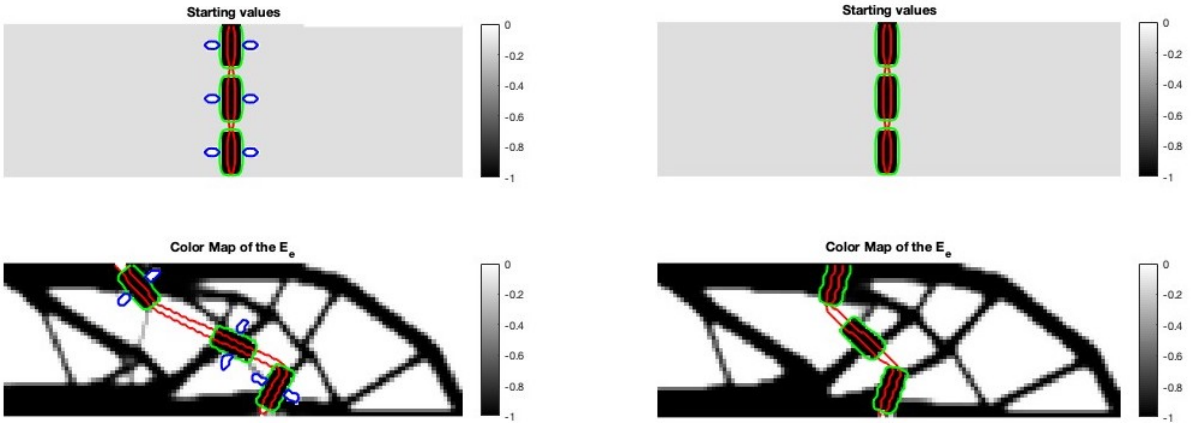

(a) Case 9 - J = 217.33

(b) Case 15 - J = 205.85, from old comparison

Figure D.15: Optimization of the cut lines with the connectors, with a starting position of a straight line, a case with and a case without voids from the previous comparison.

Case 9 starting point is changed to a straight line. The optimization result is similar to the one in Case 5 (Fig. D.12a). The shape of the cut as well as the position of the connectors on the cut line, are similar, however, the main difference is the x position. In this case, the x position is smaller than in Case 5. Due to this shift in the x direction, the internal structure and compliance have changed.

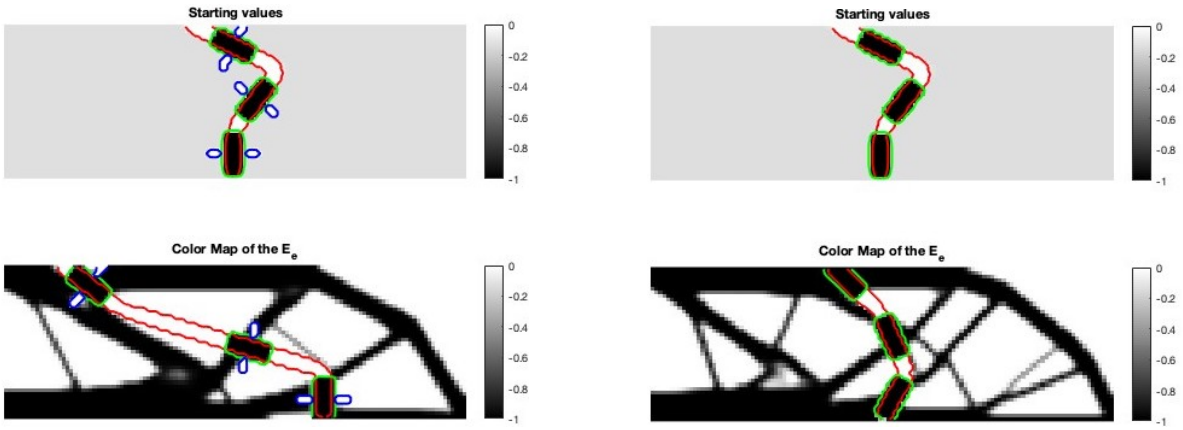

(a) Case 10 - J = 226.57

(b) Case 16 - J = 206.99, From last comparison

Figure D.16: Optimization of the cut lines with the connectors, a case with and a case without voids from the previous comparison

The last case to compare is Case 10. Here, the thickness of the cut line has been modified to double the size of the other cases. In the optimization without the voids, the other sides could still be used to connect the parts, however, as now on those sides there are voids, the area to be able to connect the

connectors with the structure is smaller. Therefore, the optimizer has it more difficult to make those connections, and there are holes inside the structural members on most of the connectors here.

D.2.2. Comparison with voids size changing

Now, in this section, the hole sizes are changed. Different cases are tried with different void sizes to observe the influence. The connector's size is kept constant in some cases, however, in others cases was changed, as in the cases with higher and lower numbers of connectors, or the case less and when $a_{con} = a_{void}$. There are 15 cases in this section. As in other optimizations found in this report, the initial reference case has the same starting conditions for the optimizations as in Fig. D.9a.

Now, different voids sizes are tried in cases where the cut lines and connectors' initial conditions and positions are the same. In this first case, the voids have a 1x1 (a_{void} x b_{void}) element size, which creates a small void. In the second case, the void size is double (2x2 element size), and in the third case, the b_{void} is increased by one element, the voids have a size of 2x3 element. These cases can be appreciated in Fig. D.17. The size of the voids creates a constraint on the optimization, meaning that when the void has larger dimensions, the area where the connector can connect to the structure is limited.

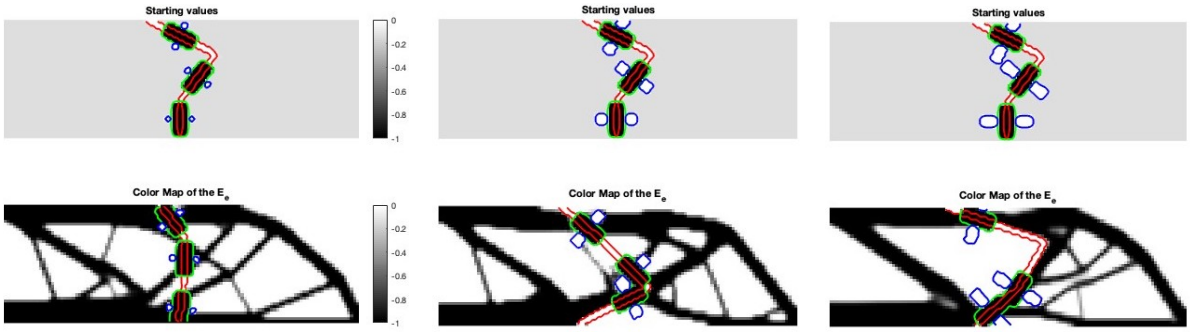

(a) Case 1 - J = 213.14, with a void size = 1x1 element

(b) Case 2 - J = 260.80, void size = 2x2 element

(c) Case 3 - J = 236.76, void size = 2x3 element

Figure D.17: Effect of varying the dimensions of the voids on the initial reference case

In the second and third cases, the optimizer tries to connect the structure and create a structural member with the connectors. This is also observed in one case in the previous optimization. This could be due to the optimizer trying to create a structure member and avoid the cut of the structure while maximising the efficiency of the volume constraint. The numerical results of this optimization can be seen in Table. E.15

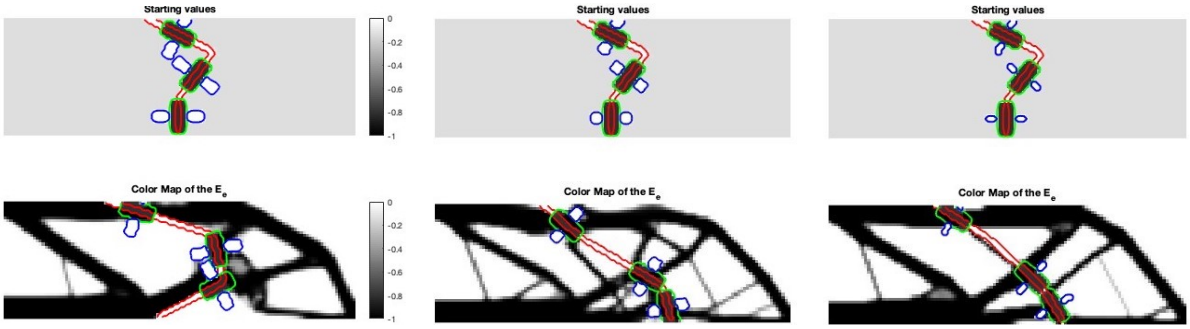

(a) Case 4 - J = 265.29, with a void size = 2x3 element

(b) Case 5 - J = 241.7989, void size = 2x2 element

(c) Case 2 - J = 221.17, from old comparison, void size = 1x2 element

Figure D.18: Effect of varying the dimensions of the voids with a lower E_c than the reference case

One of the design parameters affecting the connector is E_c, the Young's modulus of the connector. In these two cases, Case 4 (Fig. D.18a) and Case 5 (Fig. D.18b), the value for $E_c = 0.8$. As before, larger voids constrain the positioning of the connectors and cut lines, increasing compliance. Comparing these two cases to the one mentioned above in Fig. D.19 with the case with the lower compliance in

the previous comparison also shown in Fig. D.18c. Case 4 has a 16% higher compliance than Case 2 on the last comparison, and Case 5 has an increased compliance of 8%. In both cases, it can be seen the trend the optimizer tends to do, having two connectors close to each other to create a limb.

Table. E.16 shows the numerical results of cases 4 and 5, corresponding to Fig. D.19.

In the following two cases, Case 6 in Fig. D.19a and Case 7 in Fig. D.19b, the starting point is a straight line. This can also be compared to the ninth case of the previous optimization, Which is also shown in Fig. D.19c, this is added for visual comparison. The final compliance is lower when the holes are the smallest and higher when the voids are the highest. This can be due to the voids constraining the connection area between the structure and the connector, weakening the connection point. It can be observed that the optimized position of the cut lines and the connectors are similar. As expected, the two connectors on the sides tend to go to the outer structural member and the middle one is placed on a structural member in the middle of the structure.

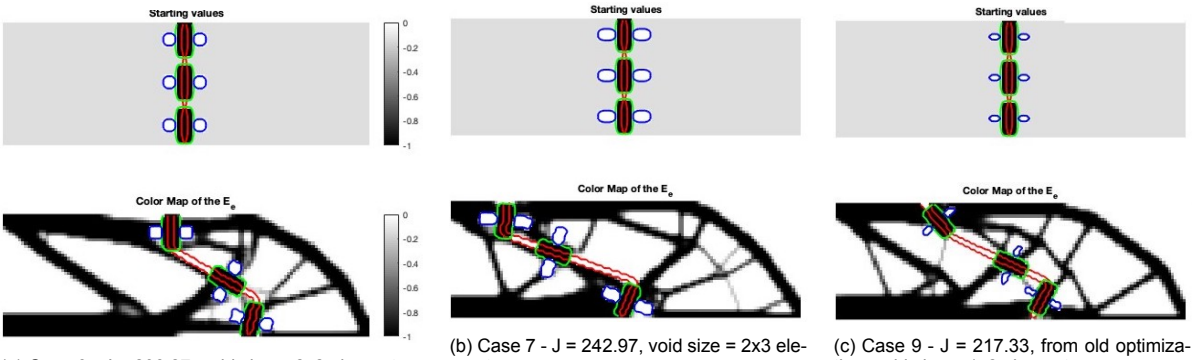

(a) Case 6 - J = 238.27, void size = 2x2 element

(b) Case 7 - J = 242.97, void size = 2x3 element

(c) Case 9 - J = 217.33, from old optimization, void size = 1x2 element

Figure D.19: Effect of varying the dimensions of the voids with the starting position on a straight line

Another parameter to change is the number of connectors. Fig. D.20 shows three cases with an extra cut line and connector than in the reference case (Fig. D.17a). In cases 8 (Fig. D.20a) and 9 (Fig. D.20a), the connectors are the same size as the previous cases, with dimensions of $a_{con} = 6$ and $b_{con} = 3$. By adding one more cut line, consequently, also a connector, and not changing the connector's size, the area occupied by the material due to the connector is larger. As in other cases, the optimizer tries to create a structural member as support by positioning the connectors one after another. In these two cases, three are in a row because the connector and the cut line have similar vertical lengths, a_{cut}. In Case 8, the voids have a size of 2x2, and in Case 9, the vertical direction a_{void} has increased by one element.

To avoid this, the connector's size was minimized in Case 10 (Fig. D.20c). In this case, the value of $a_{con} = b_{con} = 2$. Furthermore, the optimizer tries again to create the connection between the connectors, but this time only the lower two due to the size of the connector.

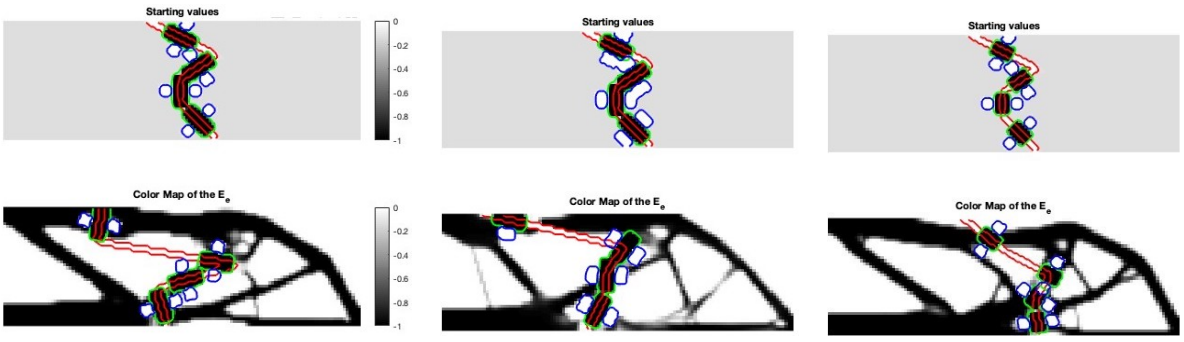

(a) Case 8 - J = 235.49, with a void size = 2x2 element

(b) Case 9 - J = 767.23, void size = 3x2 element

(c) Case 10 - J = 243.82, void size = 2x3 element

Figure D.20: Effect of varying the dimensions of the voids with four connectors and cut lines

Case nine has the highest compliance due to the structure, with a value of 767.23. The optimizer

tried to join the connectors. However, their positioning created a weak structure that does not connect to the outer structural members, which means that the structure is not connected to the top and bottom members, weakening the structure. This is also due to the voids having a larger size, the optimization of them is more difficult due to having less area where they can be connected to the structure, and by connecting them, the area where the cut line breaks the structure is minimised. Table. E.18 shows the numerical values of cases 8,9, and 10, corresponding to the cases in Fig. D.20. Which are the optimizations with four cut lines and connectors.

Table. E.19 shows the numerical values of cases 11 and 12, corresponding to the cases in Fig. D.21. These are the optimizations with five cut lines with their respective connectors.

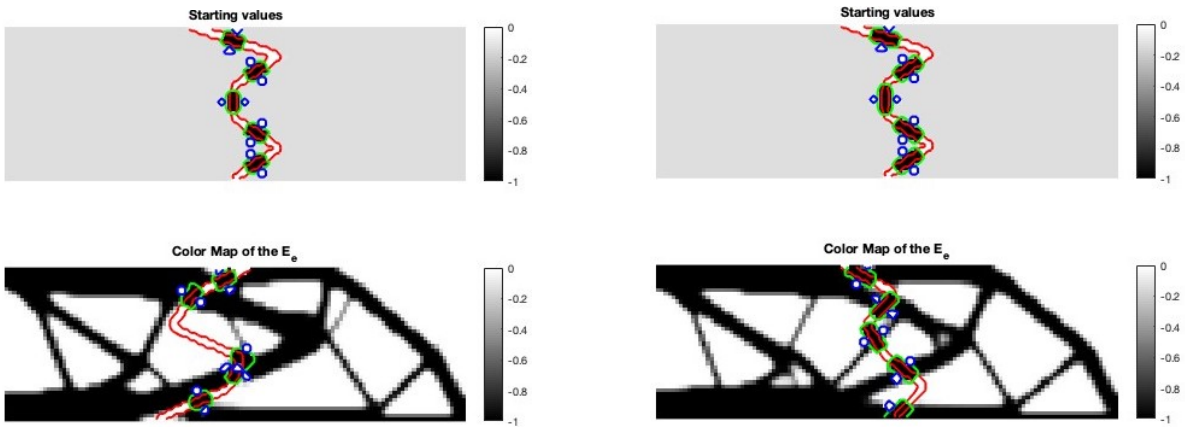

(a) Case 11 - J = 239.37, void size = 1x1 element

(b) Case 12 - J = 210.56, void size = 1x1 element

Figure D.21: Effect of varying the dimensions of the connector with five connectors and cut lines

In the next two cases, Case 11 (Fig. D.21a) and 12 (Fig. D.21b) , there are 5 cut lines and 5 connectors. In both cases, the connector size is reduced to give more space for them to move. As the connector, the size of the voids is also reduced. By comparing both images, it can be guessed that the first case has a more significant compliance by the structure due to the comparison of the connectors and cut lines positioning, which in Case 11 breaks the structure in a few places. This is because both cases have the same voids' size, but the second case has a larger connector, making it less constrained and having a larger area where the connector and the structure can connect. These are the only cases in this comparison where the size of the voids stays constant. In these cases, the relation of the size of the connector with respect to the voids is observed. Moreover, in Fig. D.21a, connectors two and three are joined as in other cases, however, in this case, due to the angles, the void of the third connector is over the second connector. This is not beneficial.

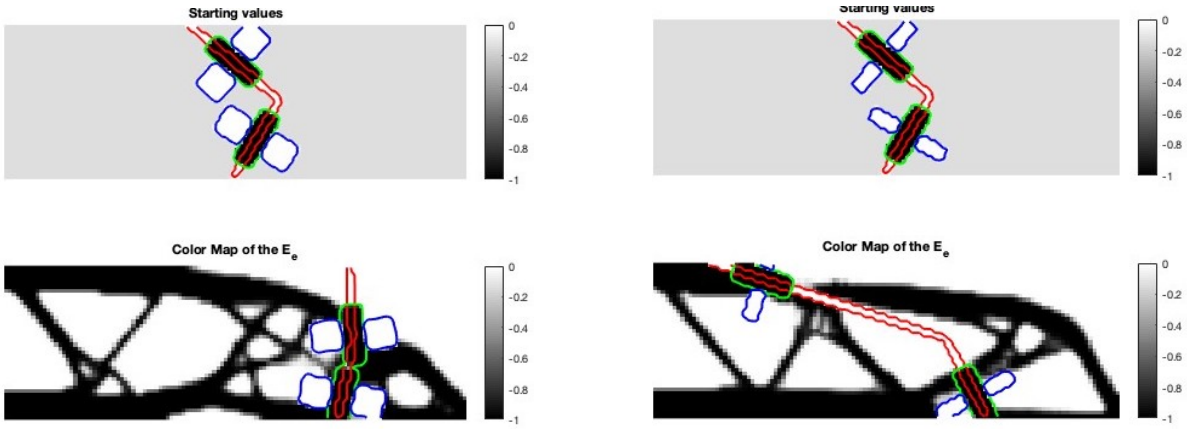

(a) Case 13 - J = 398.71, void size = 3x3 element

(b) Case 14 - J = 344.19, void size = 1x3 element

Figure D.22: Optimization with the same initial variables, only the size of the voids change with 2 connectors

The following two cases are the opposite of the previous five ones, now, the number of connectors is reduced to only two cut lines, meaning two connectors. Case 13 in Fig. D.22a has a larger void size than Case 14 in Fig. D.22a. The connector size is kept constant. As there are only two connectors, the connector's size was increased. In Case 13, the trend of the optimizer is observed again. Tries to create a member or structural member by connecting the connectors. However, in Case 14, the optimizer positions the connectors at opposite ends of the cut lines. This can be due to the position of the cut lines and the connector trying to connect the top and bottom parts of the structure, which are the most relevant for compliance. Case 13 has the highest compliance compared to Case 14, this could be due to the position of the connectors.

From all the previous cases where there were cut lines, connectors and voids to optimize, It was observed that the larger the area the void covers of the connector, the more difficult for the optimizer to position. Leading to trying to optimize a case with the connectors and the voids having the same vertical length in Fig. D.23. This means that the connector is more constrained, as now the only connection it can make to the structure is on the top and bottom part of the connector, next to the cut lines, as the other two sides are forced to be holes due to the voids. Looking at compliance, it is not the highest obtained. But looking at Fig. D.23, the bottom connector is inside the lowermost member of the structure and, with both connectors at the top, tries to join them to make some connection for the top member of the structure.

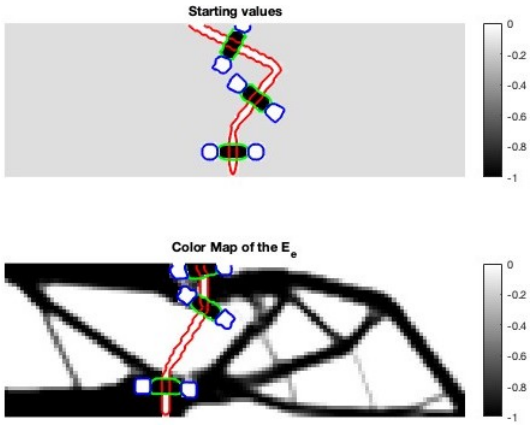

Figure D.23: Optimization with the same initial variables, $a_{con} = a_{void}$ - J = 324.4468

E

Numerical results

This section shows the numerical results of the figures found in 5 and C

E.1. Results for the optimization with a single connector with voids and without voids

The results of the connection optimization are found in Fig. C.1 and Fig. C.2. In the table, x_c, y_c and θ_c are the connector coordinates, Obj is the objective function. These values are shown at the initial iteration and the final one. The number of elements (nelx and nely) are changed for higher resolution.

Cases	Const				Initial				Final				
	nelx	nely	a	b	x_{con}	y_{con}	θ_c	Obj	x_{con}	y_{con}	θ_c	Obj	Iter
1	60	20	3	2	30	10	0	1004.1994	18.1578	2.1446	-3.0036	223.1353	62
2	60	20	3	2	40	6	0	1001.7342	36.3733	2	-3.14097	218.9802	70
3	60	20	5	2	30	10	0	1001.7403	7.0199	0.8999	-3.1416	223.3185	52
4	100	60	5	2	30	10	0	293.9474	25.4412	8.003	1.9487	58.7475	150
5	60	20	5	5	20	8	0	948.6922	7.1811	5.0081	-3.1416	231.3491	155
6	60	20	3	2	20	8	2.5133	996.8572	27.4063	2.2422	3.0938	222.2608	47
7	60	20	3	6	20	8	2.5133	959.3068	21.7993	6.002	3.1416	224.4761	58

Table E.1: Initial and final conditions for the different connection optimisation cases.

The results of the connection optimization with the void are found in Fig. 5.3 and Fig. C.3.

Cases	Constants						Initial				Final				
	nelx	nely	a_{con}	b_{con}	a_{void}	b_{void}	x_{con}	y_{con}	θ_c	Obj	x_{con}	y_{con}	θ_c	Obj	iter
1	60	20	3	2	1	1	30	10	0	1.01E+03	30	11.4998	0.0277	216.8760	57
2	60	20	3	2	2	1	30	10	0	1.01E+03	31	9.4826	0.053	218.3886	39
3	60	20	3	2	2	2	30	10	-2.8274	1.02E+03	31.0759	7.9818	-2.9236	218.5304	101
4	60	20	3	2	2	2	30	10	0	1.02E+03	34.4141	5.4622	-0.0983	225.2292	72
5	120	60	6	3	2	3	30	10	0	437.475	29.2611	21.2088	-1.0927	85.6168	111

Table E.2: Optimization of the connector with the voids

E.2. Results for the optimization of the cut line

A single cut line in Fig. C.4 and Fig. C.5.

Cases	Const					Initial					Final					
	nelx	nely	y_1	y_2	b_{cut}	x_1	x_2	θ_{cut}	a_{cut}	Obj	x_1	x_2	θ_{cut}	a_{cut}	Obj	Iter
1	60	20	0.2	0.5	1	0.4	0.5	0.7854	4.2426	1039.4358	0.2706	0.5255	0.3834	8.0190	222.5602	52
2	60	20	0.5	0.5	1	0.4	0.5	0	3	10123.8387	0.3646	0.5345	0	4.0987	222.4654	52
3	60	20	0.2	0.5	1	0.5	0.5	1.5708	5	1044.1779	0.5194	0.5038	1.6644	5.002	221.0927	53
4	60	20	0	0.2	1	0.5	0.6	0.5880	3.6055	1084.6485	0.4423	0.7523	0.2118	9.5148	222.2679	73
5	60	20	0.2	0.5	0.5	0.2	0.5	0.7854	4.2426	1011.8951	0.7521	0.8759	0.6904	5.7105	224.2951	50
6	100	60	0.2	0.5	1	0.4	0.5	1.6037	10.2956	303.6871	0.3569	0.5115	0.8007	12.5381	59.3146	65

Table E.3: Initial and final conditions for single cut line cases 3 to 5.

Multiple cut lines in Fig. 5.4, Fig. C.6 and Fig. C.7.

Cases	Constant values					Initial				Final				
	nelx	nely	y	nº cuts	b_{cut}	x_{cut}	θ_{cut}	a_{cut}	Obj	x_{cut}	θ_{cut}	a_{cut}	Obj	Iter
1	60	20	0.2 0.4 0.5	2	1	0.4 0.4 0.5	1.5708 0.3218	2 3.1623	1040.3708	0.7530 0.6747 0.3925	2.4365 2.9606	3.0859 5.5546	220.2029	80
2	60	20	0.2 0.4 0.5	2	1	0.6 0.3 0.4	2.9229 0.3218	9.2195 3.1623	1165.1967	0.6448 0.5814 0.4492	2.3316 2.3378	2.7614 1.3890	214.4796	123
3	60	20	0.5 0.7 0.8	2	1	0.5 0.3 0.4	2.8198 0.3218	6.3246 3.1623	1061.0082	0.3973 0.4704 0.3977	0.3669 2.9513	5.5748 5.2876	223.2710	74
4	60	20	0.5 0.7 0.8	2	0.5	0.5 0.3 0.4	2.8198 0.3218	6.3246 3.1623	1021.3343	0.6895 0.5516 0.7697	2.5742 0.1517	3.7211 6.6191	220.9120	106
5	60	20	0.3 0.5 0.7 0.8	3	1	0.5 0.3 0.4 0.6	2.8198 0.5880 0.1651	6.3246 33.6056 6.0828	1223.2730	0.5030 0.3093 0.3351 0.5987	2.7476 1.2020 0.1408	5.2106 2.1442 7.1243	233.3603	50
6	100	60	0.2 0.4 0.5	2	1	0.4 0.4 0.5	1.5708 0.5404	6 5.8310	305.9840	0.3700 0.3881 0.4918	1.5865 0.5247	6.0007 5.9889	59.3214	105

Table E.4: Initial and final conditions for multiple cut line cases

E.3. Results for the complete optimization, optimizing the structure, the cut line and connectors

This section shows the tables with the numerical results of the figures found on C.3.1 for the optimization with the fixed component and in 5 and Cfor the other results.

E.3.1. Optimization of the cut line with a fixed connector

The results here correspond to the ones found in Fig. C.9

Cases	1		2		3		4	
a_{con}	2		2		2		3	
b_{con}	2		2		2		2	
	Initial	Final	Initial	Final	Initial	Final	Initial	Final
x cut	30 30	29.0896 41.4710	18 30	47.9994 46.9459	18 24	24.01397 24.22132	36 24	24.97496 24.00112
a_{cut}	5	7.9577	6.7082	3.0459	4.2426	3.0018	7.8102	5.0237
x_{con}	30	35.2803	24	47.4727	21	24.11765	30	24.48804
y_{con}	9	9	7	7	7	7	9	9
θ_c	1.5708	0.6794	0.4636	1.7446	0.7854	1.5363	2.4469	1.6679
Compliance	1016.3665	220.5124	1027.0603	218.6014	1000.4325	223.7879	1021.8787	222.0232

Table E.5: Optimization of the cut line with a fixed connector

E.3.2. Optimization with movable connector

These results correspond to the figures found in section C.3.2.

Cases	1		2		3		4		5		6	
Nely	60		60		60		120		100		100	
Nex	20		20		20		40		30		30	
y	0.5	0.7	0.3	0.7	0.3	0.7	0.3	0.7	0	0.7	0	0.7
Ec	1		1		1		1		1		1	
b_{cut}	1		1		1		2		2		2	
a_{con}	2		2		2		3		3		3	
b_{con}	2		2		2		6		6		2	
	Initial	Final	Initial	Final	Initial	Final	Initial	Final	Initial	Final	Initial	Final
x_{cut}	30 30	31.3944 32.6852	30 30	28.8237 29.9844	36 18	40.1603 27.6291	60 50	65.0712 50.0935	60 50	58.0706 52.8798	50 50	47 46.0158
a_{cut}	2	2.1015	4	4.0419	9.8489	7.4335	7.8102	9.596	11.6297	10.816	10.5	10.5115
x_{con}	30	31.8981	30	29.3548	27	40.159	55	56.1849	55	56.2227	50	46.8073
y_{con}	12	12.4391	10	9.6604	10	6.0008	15	16.1196	10.5	7.4756	10.5	4.1121
θ_c	-1.5708	-1.2587	1.5708	1.4267	2.7234	2.5734	2.2655	2.4661	2.0152	1.8131	1.5708	1.6176
Compliance	1.01E+03	220.0624	1.01E+03	230.2093	1.03E+03	218.4678	2.69E+03	279.8842	2.73E+03	310.0459	2.95E+03	281.3673

Table E.6: Initial and final conditions for cut line and connector optimization, cases 1 to 6.

Cases	7		8		9		10		11		12	
Nely	180		100		120		120		120		120	
Nelx	60		30		40		40		40		40	
y	0.3	0.5	0	1	0.3	0.7	0	0.5	0	0.5	0.5	1
Ec	1		1		0.7		0.7		0.5		0.5	
b_{cut}	2		2		1		1		1		1	
a_{con}	6		9		6		7		5		5	
b_{con}	3		3		4		2		2		2	
	Initial	Final	Initial	Final	Initial	Final	Initial	Final	Initial	Final	Initial	Final
x_{cut}	54 126	51 125.5163	60 70	62 70	60 36	62.4474 29.9043	60 36	49.1565 32.4471	60 36	49.4273 34.3395	60 36	53.8285 42
a_{cut}	37.108	38.3297	18.6815	18.4391	14.4222	18.1319	15.6205	13.0308	15.6205	12.5264	15.6205	11.618
x_{con}	90	96.9816	65	66	48	46.4999	48	44.7915	48	43.9408	48	45.6901
y_{con}	27	29.1072	15	15	20	19.8407	10	5.2247	10	7.2727	30	33.7606
θ_c	0.245	0.237	1.2998	1.3521	2.5536	2.6846	2.4469	2.2668	2.4469	2.2171	2.4469	2.1049
Compliance	2.11E+03	204.6239	2.87E+03	346.894	1.03E+03	198.2104	1.06E+03	202.5111	1.11E+03	208.7176	1.15E+03	207.1672

Table E.7: Initial and final conditions for cut line and connector optimization, cases 7 to 12.

E.3.3. Optimization with movable connector and voids

These results correspond to the figures found in section C.3.3.

Cases	1		2		3		4		5	
Nely	60		120		120		120		120	
Nex	20		40		40		40		40	
y	0.7	0.8	0.5	1	0.5	1	0.3	0.6	0	0.5
Ec	1		1		1		1		1	
b_{cut}	1		1		1		1		1	
a_{con}	4		6		6		3		6	
b_{con}	2		2		2		6		2	
a_{void}	1		1		1		1		3	
b_{void}	1		1		2		3		3	
	Initial	Final	Initial	Final	Initial	Final	Initial	Final	Initial	Final
x_{cut}	42 48	25.8571 10.7957	84 96	91 95	60 72	27.5385 20.8499	60 60	47.8281 58.1012	48 72	46 72.0469
a_{cut}	5.831	9.0394	11.6619	10.198	11.6619	10.5444	6	7.8984	13.4164	14.3391
x_{con}	45	23.265	90	93.1042	66	25.6032	60	53.8234	60	60.3089
y_{con}	5	1.721	10	10.5208	10	5.787	18	19.0031	18	18.5922
θ_c	1.0304	2.5555	1.0304	1.3734	1.0304	1.8935	1.5708	0.8628	0.4636	0.4317
Compliance	1.00E+03	224.7988	1.03E+03	198.8901	1.05E+03	202.9831	1.03E+03	206.5396	1.04E+03	209.4513

Table E.8: Initial and final conditions for cut line and connector optimization with voids cases 1 to 5

Cases	6		7		8		9	
Nely	120		120		120		120	
Nex	40		40		40		40	
y	0 | 0.5		0 | 0.5		0.3 | 0.7		0 | 0.5	
Ec	0.8		0.8		0.7		0.5	
b_{cut}	1		1		1		1	
a_{con}	6		6		6		6	
b_{con}	2		4		4		4	
a_{void}	1		2		1		2	
b_{void}	1		2		1		2	
	Initial	Final	Initial	Final	Initial	Final	Initial	Final
x_{cut}	60 84	59 81.8569	60 84	49 73	60 60	58.5526 57.4726	36 60	12.4311 12.0002
a_{cut}	15.6205	15.1858	15.6205	15.6205	8	8.0182	15.6205	10.0023
x_{con}	72	68.1428	72	56.485	60	58.1206	48	12.2759
y_{con}	10	8	10	6.2375	20	18.4	10	7.2031
θ_c	0.6947	0.7188	0.6947	0.6947	1.5708	1.6382	0.6947	1.5923
Compliance	1.06E+03	201.7132	1.06E+03	206.7343	1.02E+03	200.6405	1.09E+03	214.4957

Table E.9: Initial and final conditions for cut line and connector optimization with voids cases 6 to 9

E.3.4. Optimization of multiple cut lines and connectors

These results correspond to the figures found in section D.1.

Case	1		2		3		4		5		6	
Changed	Initial case		Ec		Ec		x_{cut} in		x_{cut} in		y cut in	
New value			0.8		0.5		[0.5 0.7 0.6 0.6];		[0.3 0.5 0.4 0.4];		0 0.5 0.7 1	
	Initial	Final	Initial	Final	Initial	Final	Initial	Final	Initial	Final	Initial	Final
x_{cut}	48	45	48	25.4078	48	43.4427	60	60.8708	36	12.1204	48	24
	72	67.7533	72	53.7593	72	61.2487	84	85.3146	60	39.5822	72	66.9993
	60	63.1875	60	67.3577	60	65	72	73	48	58.0605	60	69.3950
	60	66.3920	60	70.4673	60	55.9590	72	57.5786	48	52.7372	60	49.5988
a_{cut}	13.4164	12.8619	13.4164	15.3932	13.4164	10.7361	13.4164	13.6152	13.4164	14.9846	15.6205	23.7115
	10	8.3194	10	10.4990	10	8.2169	10	10.0952	10	12.2214	7.2111	4.1755
	6	6.2103	6	6.1982	6	7.5123	6	9.7701	6	6.5639	6	11.5746
x_{con}	60	52.2741	60	38.0524	60	51.8867	72	73.1822	48	24.5339	60	39.2616
	66	65.4190	66	58.3359	66	62.4682	78	77.6184	54	47.9405	66	67.3196
	60	65.1156	60	68.9588	60	58.4986	72	62.7366	48	54.6228	60	55.1499
y_{con}	6	3.8363	6	5.3519	6	5.6906	6	6.0439	6	5.4243	10	7.0985
	20	20.1802	20	17.3849	20	17.2013	20	21.9994	20	19.2373	24	21.0696
	34	35.2203	34	34.1788	34	36.6293	34	35.9864	34	35.7495	34	36.6351
θ_c	0.4636	0.4853	0.4636	0.4004	0.4636	0.5930	0.4636	0.4564	0.4636	0.4120	0.6947	0.4354
	2.2143	1.8488	2.2143	0.8664	2.2143	1.3405	2.2143	2.2268	2.2143	0.7136	2.5536	1.2798
	1.5708	1.3098	1.5708	1.3172	1.5708	2.2165	1.5708	2.4803	1.5708	1.9883	1.5708	2.5966
Compliance	1019.8978	208.9213	1022.9430	224.4030	1031.1784	210.0731	1022.2576	202.2234	1016.9025	222.7127	1044.7862	228.6962

Table E.10: Cases 1 to 6 of the optimization of the cut lines and connectors

Case	7		8		9		10		11		12	
Changed	y cut in		s comp		s comp		ac and bc		ac abd bc		number of connectors	
New value	0 0.3 0.5 1		0.3		0.7		ac= 4	bc= 2	ac= 4	bc = 6	4, adn ac= 5, bc= 3	
	Initial	Final	Initial	Final	Initial	Final	Initial	Final	Initial	Final	Initial	Final
x_{cut}	48	54.8191	48	53.9864	48	58.2711	48	55.0037	48	29.2699	48	44.9054
	72	46.6339	72	49.2697	72	60.4039	72	83.8333	72	35.0782	72	80.0016
	60	60.4385	60	61.0355	60	71.2861	60	73.8038	60	72.5299	60	58.3782
	60	62.6767	60	49.7947	60	63.5330	60	61.7191	60	71.6647	60	69.4732
											72	74.4382
a_{cut}	13.4164	7.2629	13.4164	6.4469	13.4164	6.0941	13.4164	15.6137	13.4164	6.6659	13.4164	18.5455
	7.2111	7.9776	10	9.9302	10	9.6750	10	9.4418	10	20.3632	7.2111	11.5279
	10	10.0624	6	8.2212	6	7.1434	6	8.5153	6	6.0156	4	6.8392
											8.4853	6.4933
x_{con}	60	50.8667	55.2000	51.8011	64.8000	59.6946	60	63.0806	60	31.2962	60	62.9392
	66	60.4381	68.4000	59.5940	63.6000	64.4867	66	75.1098	66	59.2542	66	69.1531
	60	62.0262	60	53.5666	60	65.8689	60	64.6560	60	72.0295	60	61.4617
											66	72.8935
y_{con}	6	5.7944	3.6000	5.5597	8.4000	8.0094	6	3.3619	6	4.1865	6	6.1660
	16	19.9998	16.8000	26.0398	23.2000	18.0029	20	25.9165	20	22.3284	16	16.0136
	30	34.1874	31.6000	35.9734	36.4000	36.3846	34	37.0837	34	34.9415	24	22.2233
											34	36.2666
θ_c	0.4636	2.1694	0.4636	1.9453	0.4636	1.3949	0.4636	0.3944	0.4636	1.1200	0.4636	0.3295
	2.5536	0.5252	2.2143	0.9367	2.2143	0.9735	2.2143	2.1307	2.2143	0.4037	2.5536	2.7872
	1.5708	1.4593	1.5708	2.3235	1.5708	2.1444	1.5708	2.3597	1.5708	1.6428	1.5708	0.6247
											0.7854	1.1785
Compliance	1030.2305	205.3602	1001.7480	198.6023	1050.8965	207.5314	1066.0353	219.2404	1021.2192	213.4569	1048.3769	220.6015

Table E.11: Cases 7 to 12 of the optimization of the cut lines and connectors

Case	13		14		15		16		17	
Changed	number of connectors		number of elements		startign values of x		b cut		r min	
New value	2,		180x60		all at 0.5		2		2	
	Initial	Final	Initial	Final	Initial	Final	Initial	Final	Initial	Final
x_{cut}	48	48	72	71	60	47.9982	48	47.1965	48	18.7965
	72	66	108	107	60	44.6618	72	60.0085	72	23.6556
	60	58	90	93.3288	60	62.7382	60	67	60	94.8720
			90	93	60	58.5223	60	60.3036	60	70.3843
a_{cut}	15.6205	13.4536	20.1246	20.1246	6	6.2276	13.4164	8.7771	13.4164	6.4733
	11.6619	10.7703	15	13.8103	8	12.0702	10	8.7304	10	36.4958
			9	9.0015	6	6.3595	6	6.8710	6	13.6350
x_{con}	60	53.6058	90	85.4000	60	46.4767	60	50.8940	60	20.1150
	66	60.2245	99	100.5119	60	53.7524	66	62.8784	66	63.8654
			90	93.1067	60	60.8537	60	63.3700	60	74.9131
y_{con}	10	6.2287	9	7.2000	6	5.4723	6	3.4632	6	3.2562
	30	34.4387	30	29.3900	20	20.0464	20	18.5678	20	21.0338
			51	54.1602	34	33.3641	34	34.5051	34	37.7807
θ_c	0.6947	0.8380	0.4636	0.4636	1.5708	1.8420	0.4636	0.7527	0.4636	1.1860
	2.1112	1.9513	2.2143	2.0886	1.5708	0.7245	2.2143	1.1588	2.2143	0.2210
			1.5708	1.5891	1.5708	1.9086	1.5708	2.0798	1.5708	2.6859
Compliance	1079.3000	204.8703	1068.3708	207.2928	1000.7167	204.8578	1035.4539	206.9902	1019.8978	207.8931

Table E.12: Cases 13 to 17 of the optimization of the cut lines and connectors

E.3.5. Optimization of multiple cut lines, connectors and voids

E.3.5.1 Comparison with voids size constant

These results correspond to the figures found in section D.2.1.

Case nº	1		2		3		4		5	
Changed			Ec		x_{cut}		y_{cut}		s_{con}	
New value			0.8		[0.5 0.7 0.6 0.6]		[0 0.3 0.5 1]		0.7	
	Initial	Final	Initial	Final	Initial	Final	Initial	Final	Initial	Final
	48	41.4320	48	35.7362	60	75.3547	48	47.9006	48	47.6426
	72	25.8244	72	54.9222	84	72.8171	72	62.7211	72	57.2045
x_{cut}	60	74.1543	60	72.0952	72	91.5406	60	65.9593	60	88.7088
	60	71.1130	60	79.4539	72	89.8489	60	63	60	85.0338
	13.4164	9.8438	13.4164	11.3149	13.4164	6.1327	13.4164	9.5348	13.4164	7.6719
	10	25.4547	10	11.7357	10	12.3143	7.21110255	4.3153	10	17.6672
a_{cut}	6	6.1897	6	7.0383	6	6.0594	10	10.1089	6	6.2751
	60	36.9939	60	42.5833	72	74.1453	60	54.3829	64.8	52.7292
	66	58.1798	66	68.6804	78	84.8276	66	65.9586	63.6	77.5277
x_{con}	60	72.3874	60	76.0995	72	90.3578	60	63.7573	60	85.0338
	6	3.4123	6	4.2825	6	5.7191	6	5.2487	8.4000	6.3836
	20	22.7115	20	24.8184	20	22.2634	16	19.9984	23.2000	22.3215
y_{con}	34	34.9716	34	34.5299	34	36.3897	30	34.8818	36.4000	39.9999
	0.4636	2.4861	0.4636	0.5589	0.4636	1.7792	0.4636	0.6806	0.4636	0.8980
	2.2143	0.3197	2.2143	0.7501	2.2143	0.7071	2.5536	1.1862	2.2143	0.4699
θ_c	1.5708	1.8190	1.5708	1.0207	1.5708	1.7109	1.5708	1.7177	1.5708	1.8680
Compliance	1034.1928	213.8994	1037.9617	221.1734	1032.0130	207.4672	1044.2011	209.5139	1068.6214	210.8979

Table E.13: Initial and final conditions for multiple cut lines and connectors optimization with voids cases 1 to 5

Case nº	6		7		8		9		10	
Changed	connector's size		number of connectors		number of elements		x_{cut}		b_{cut}	
New value	b_{con}= 6, a_{con}=4		4		180x60		straight line at middle		2	
	Initial	Final	Initial	Final	Initial	Final	Initial	Final	Initial	Final
	48	22.8143	48	71.6370	72	87	60	30.0941	48	15.0814
	72	31.2539	72	72.5273	108	94.1086	60	40.1332	72	30.7094
x_{cut}	60	80.8931	60	90.5693	90	95.2844	60	74.2022	60	83.8105
	60	79.4263	60	64.1625	90	91	60	67.9260	60	83.3374
			72	56.3471						
	13.4164	7.3353	13.4164	6.0165	20.1246	9.6764	6	7.8228	13.4164	9.8519
	10	26.0771	7.2111	9.8680	15	12.0144	8	18.8195	10	27.7296
a_{cut}	6	6.0447	4	13.7960	9	9.2515	6	6.7711	6	6.0047
			8.4853	7.1603						
	60	26.2524	60	72.1882	90	89.1780	60	35.8145	60	22.4759
	66	58.9825	66	82.3887	99	94.5391	60	60.6648	66	64.0791
x_{con}	60	79.8271	60	68.7562	90	92.2493	60	71.5461	60	83.5203
			66	60.2217						
	6	4.8885	6	7.4286	9	5.5149	6	6.8378	6	5.6779
	20	20.9376	16	16.3726	30	26.7874	20	21.6423	20	22.0547
y_{con}	34	36.7209	24	26.6083	51	54.7512	34	33.0784	34	35.3600
			34	34.0508						
	0.4636	0.9579	0.4636	1.4967	0.4636	1.1947	1.5708	0.8741	0.4636	0.6548
	2.2143	0.3118	2.5536	0.4174	2.2143	1.5218	1.5708	0.4391	2.2143	0.2927
θ_c	1.5708	1.6924	1.5708	2.8474	1.5708	1.8045	1.5708	2.0527	1.5708	1.6102
			0.7854	2.1481						
Compliance	1039.1565	217.3544	1047.9121	251.8419	1077.0316	203.4504	1018.0440	217.3388	1051.7760	226.5758

Table E.14: Initial and final conditions for multiple cut lines and connectors optimization with voids cases 6 to 10

E.3.5.2 2. Comparison with voids size changing

These results correspond to the figures found in section D.2.2.

Case number	1		2		3	
void size (a_{void} x b_{void})	1x1		2x2		2x3	
	Initial	Final	Initial	Final	Initial	Final
x_{cut}	48	52.7261	48	40.9408	48	39
	72	61.9697	72	55.0388	72	73
	60	61.2295	60	71	60	63.4996
	60	59.5364	60	47.1524	60	49.5811
a_{cut}	13.4164	7.5737	13.4164	9.2568	13.4164	18.0278
	10	8.0086	10	11.3000	10	9.3040
	6	6.0594	6	13.3483	6	9.1887
x_{con}	60	57.0170	60	50.4591	60	50.3457
	66	61.6542	66	65.5199	66	63.5431
	60	60.1572	60	64.3972	60	54.8482
y_{con}	6	5.5704	6	8.1018	6	4.0043
	20	18.8201	20	22.5065	20	27.9269
	34	35.6000	34	31.3225	34	35.4589
θ_c	0.4636	0.9144	0.4636	0.7052	0.4636	0.3393
	2.2143	1.6170	2.2143	0.7866	2.2143	2.1066
	1.5708	1.7110	1.5708	2.6754	1.5708	2.4301
Compliance	1026.2863	213.1418	1052.4973	260.8097	1064.5106	236.7600

Table E.15: Optimization with the same initial variables, only the size of the voids change

Case number	4		5	
void size (a_{void} x b_{void})	2x3		2x2	
	Initial	Final	Initial	Final
x_{cut}	48	34.5954	48	36.0740
	72	71.8386	72	49.9645
	60	75.6495	60	77.1810
	60	52.8979	60	80.3242
a_{cut}	13.4164	19.5644	13.4164	9.1780
	10	8.2238	10	15.7856
	6	12.8611	6	6.2024
x_{con}	60	46.0893	60	44.9198
	66	73.0072	66	72.1442
	60	73.3743	60	79.1551
y_{con}	6	3.7034	6	7.6419
	20	16.9062	20	25.0390
	34	29.2000	34	35.5366
θ_c	0.4636	0.3117	0.4636	0.7125
	2.2143	1.3370	2.2143	0.5315
	1.5708	2.6562	1.5708	1.3146
Compliance	1069.2610	265.2923	1056.8651	241.7989

Table E.16: Optimization with the same initial variables, only the size of the voids change and both cases have lower Ec

Case number	6		7	
void size (a_{void} x b_{void})	2x2		2x3	
	Initial	Final	Initial	Final
x_{cut}	60	55.6720	60	19.8576
	60	55.7687	60	18.6293
	60	83.8734	60	63.9852
	60	80.7306	60	59.0239
a_{cut}	6	6.0002	6	6.0314
	8	16.1700	8	24.0477
	6	6.2024	6	6.4926
x_{con}	60	55.7231	60	19.1154
	60	73.9375	60	35.7289
	60	81.9995	60	61.1686
y_{con}	6	6.3393	6	7.2513
	20	22.3435	20	18.0322
	34	35.1550	34	34.8126
θ_c	1.5708	1.5627	1.5708	1.6728
	1.5708	0.5175	1.5708	0.3391
	1.5708	1.8269	1.5708	1.9628
Compliance	1045.2787	238.0788	1060.5686	242.9772

Table E.17: Optimization with the same initial variables, only the size of the voids change and starting on a straight line

Case number	8		9		10	
void size (a_{void} x b_{void})	2x2		2x3		2x2	
	Initial	Final	Initial	Final	Initial	Final
x_{cut}	48	34.0842	48	13.3298	48	45.9476
	72	31.6038	72	63	72	61.3143
	60	78.8697	60	57.0052	60	76.3074
	60	51.6818	60	56.6189	60	71.2531
	72	55.6190	72	50.4699	72	72.4625
a_{cut}	13.4164	6.1269	13.4164	25.5496	13.4164	9.7485
	7.2111	23.9691	7.2111	4.9985	7.2111	8.4970
	4	14.1702	4	4.0047	4	4.7314
	8.4853	6.3147	8.4853	6.7419	8.4853	6.0304
x_{con}	60	32.8558	60	23.6292	60	55.7093
	66	71.9870	66	62.9997	66	76.3073
	60	61.8027	60	56.9350	60	71.5554
	66	53.5297	66	53.7731	66	72.0530
y_{con}	6	5.9428	6	2.4882	6	7.6230
	16	18.8351	16	12.0004	16	20
	24	25.0219	24	21.4522	24	27.5215
	34	33.6322	34	33.5537	34	35.9372
θ_c	0.4636	1.7746	0.4636	0.2371	0.4636	0.6630
	2.5536	0.1677	2.5536	2.2139	2.5536	0.4901
	1.5708	2.8554	1.5708	1.6190	1.5708	2.1343
	0.7854	1.2538	0.7854	2.0443	0.7854	1.4704
Compliance	1045.9485	235.4993	1105.73963	767.2398	1089.1732	243.8263

Table E.18: Optimization with the same initial variables, only the size of the voids change with 4 connectors

Case number	11		12	
void size (a_{void} x b_{void})	1x1		1x1	
	Initial	Final	Initial	Final
x_{cut}	48	64.7304	48	48.2452
	72	49.1832	72	62.7819
	60	43.8134	60	55.0512
	60	62.3402	60	60.0544
	72	58.7125	72	70.3512
	60	40.0025	60	62.6359
a_{cut}	12.6491	8.7424	12.6491	8.2963
	7.2111	4.8176	7.2111	5.5625
	4	10.0901	4	4.7179
	7.2111	4.3920	7.2111	6.5197
	7.2111	10.1743	7.2111	5.5571
x_{con}	60	57.8200	60	53.7612
	66	49.1823	66	59.7208
	60	62.3401	60	57.0493
	66	60.6599	66	64.6616
	66	51.4448	66	63.3427
y_{con}	4	3.5558	4	3.0356
	12	8.0013	12	11.1677
	20	24	20	19.1950
	28	27.7054	28	27.5795
	36	35.1075	36	39.2672
θ_c	0.3218	2.6664	0.3218	0.5031
	2.5536	2.1620	2.5536	2.3391
	1.5708	0.4076	1.5708	1.0119
	0.5880	1.9965	0.5880	0.6605
	2.5536	2.7375	2.5536	2.3381
Compliance	1073.4392	239.3779	1049.5337	210.5689

Table E.19: Optimization with the same initial variables, only the size of the voids change with 5 connectors

Case number void size (a_{void} x b_{void})	13		14	
	Initial	Final	Initial	Final
x_{cut}	48 72 60	89.8950 91.1778 87.1074	48 72 60	14.1429 75.8531 86.2304
a_{cut}	15.6205 11.6619	10.0206 10.2050	15.6205 11.6619	32.4351 11.2660
x_{con}	60 66	91.0792 88.2037	60 66	28.6019 83.4315
y_{con}	10 30	18.4630 34.6132	10 30	4.6860 34.6057
θ_c	0.6947 2.1112	1.5067 1.7716	0.6947 2.1112	0.3134 1.0922
Compliance	1177.6721	398.7080	1104.0854	344.1965

Table E.20: Optimization with the same initial variables, only the size of the voids change with 2 connectors

Case number void size (a_{void} x b_{void})	15 2x2	
	Initial	Final
x_{cut}	48 72 60 60	51.6950 52.9867 43 42.3210
a_{cut}	13.4164 10 6	6.0347 9.4304 6.0096
x_{con}	60 66 60	51.9199 52.9818 42.7278
y_{con}	6 20 34	2.0895 12.0078 32.8117
θ_c	0.4636 2.2143 1.5708	1.4636 2.1288 1.6273
Compliance	1182.8097	324.4468

Table E.21: Optimization with the same initial variables, $a_{con} = a_{void}$

Case	1		2		3	
	Initial	Final	Initial	Final	Initial	Final
x_{cut}	48 72 60 60	26 51.9657 72.4123 77.3270	48 72 60 60	18.8651 55.7311 51.1854 54.2754	16 24 20 20	15.5701 20.1167 25.2251 9.4629
a_{cut}	13.416 10 6	14.3023 12.9814 6.4837	13.4164 10 6	19.3849 8.3166 6.1957	18.4391 24.0832 18.0001	18.1430 24.1355 19.6498
x_{con}	60 66 60	35.9463 68.0209 75.1725	60 66 60	33.9486 52.4263 53.1451	20 22 20	18.4850 24.2762 17.6480
y_{con}	6 20 34	4.5966 24.5636 34.7395	6 20 34	4.9097 23.6320 35.6105	17.9999 60 102	23.0803 75.0837 101.3058
θ_c	0.4636 2.2143 1.5708	0.4329 0.6640 1.1821	0.4636 2.2143 1.5708	0.3147 1.8476 1.3188	1.3521 1.6539 1.5708	1.4452 1.4648 1.9835
Compliance	1095.7352	242.8818	1125.374	315.5179	1092.1605	224.9645

Table E.22: Table showing the results for the optimization with the bolt requirements

In table E.22, the last case is the values of the horizontal cut.